ANALYSIS OF THE ELECTROMAGNETIC SCATTERING FROM AN INLET GEOMETRY WITH LOSSY WALLS

N. H. MYUNG, P. H. PATHAK AND C. D. CHUANG

Progress Report 715723 prepared by

April 1985

NASA Lewis Research Center
21000 Brookpark Rd.
Cleveland, Ohio 44135

Grant NAG 3-476

TABLE OF CONTENTS

		PAGE
LIST OF FIGURES		iii
CHAPTERS		
I	INTRODUCTION	1
II	ANALYSIS OF A PARALLEL PLATE WAVEGUIDE WITH LOSSY WALLS	7
III	ANALYSIS OF ELECTROMAGNETIC SCATTERING FROM A SEMI-INFINITE PARALLEL PLATE WAVEGUIDE WITH LOSSY WALLS	39
IV	SUMMARY AND DISCUSSION	75
REFERENCES		77
APPENDICES		
A	NUMERICAL SOLUTION OF MODAL EIGENVALUES	78
B	REFLECTION COEFFICIENT FOR AN IMPEDANCE BOUNDARY	80
C	MAGNITUDE AND PHASE OF THE TRANSITION FUNCTION	82

LIST OF FIGURES

Figure		Page
1	Diffraction by an open ended semi-infinite parallel plate waveguide with inner impedance walls and perfectly-conducting outer walls.	2
2	Infinitely long (in±z) parallel plate waveguide excited by an interior line source.	3
3	Dominant ray paths for the problem in Figure 2.	5
4	Integration path in complex α plane.	12
5	|G| for an electric line source excited infinite parallel plate waveguide as a function of normalized distance KZ.	14
6	|G| for an electric line source excited infinite parallel plate waveguide as a function of normalized distance KZ.	16
7	|G| for an electric line source excited infinite parallel plate waveguide as a function of normalized distance KZ.	17
8	|G| for an electric line source excited infinite parallel plate waveguide as a function of normalized distance KZ.	18
9	|G| for an electric line source excited infinite parallel plate waveguide as a function of normalized distance KZ.	19
10	|G| for a magnetic line source excited infinite parallel plate waveguide as a function of normalized distance KZ.	20
11	|G| for a magnetic line source excited infinite parallel plate waveguide as a function of normalized distance KZ.	21
12	|G| for a magnetic line source excited infinite parallel plate waveguide as a function of normalized distance KZ.	22
13	|G| for a magnetic line source excited infinite parallel plate waveguide as a function of normalized distance KZ.	23
14	|G| for a magnetic line source when both source and field points are near the lower wall and transition function is not included in the ray solution.	25

Figure		Page
15	|G| for the case of Figure 14 except that the transition function is included in the ray solution.	27
16	|G| for a magnetic line source when a source point is near the lower wall and a field point is near the upper wall.	28
17	|G| for a magnetic line source when both source and field points are on the lower wall.	29
18	Convergence of model and ray solution for an electric line source at fixed KZ.	31
19	Convergence of model and ray solution for an electric line source at fixed KZ.	32
20	Convergence of model and ray solution for an electric line source at fixed KZ.	33
21	Convergence of model and ray solution for an electric line source at fixed KZ.	34
22	Convergence of modal and ray solution for a magnetic line source at fixed KZ.	35
23	Convergence of modal and ray solution for a magnetic line source at fixed KZ.	36
24	Convergence of modal and ray solution for a magnetic line source at fixed KZ.	37
25	Convergence of modal and ray solution for a magnetic line source at fixed KZ.	38
26	Dominant ray paths for the problem in Figure 1.	39
27	Rays associated with the problem of line source excitation of an impenetrable half plane with two face impedances.	41
28	A half plane geometry with perfectly-conducting on one side and impedance surface on the other side.	47
29	Incident, reflected, diffracted and total fields for a plane wave of unit strength which is polarized such that $\bar{E}^i = \hat{y}E^i_y$.	48

Figure		Page
30	Incident, reflected, diffracted and total fields for a plane wave of unit strength which is polarized such that $\bar{E}^i = \hat{y}E_y^i$.	49
31	Incident, reflected, diffracted and total fields for a plane wave of unit strength which is polarized such that $\bar{E}^i = \hat{y}E_y^i$.	50
32	Incident, reflected, diffracted and total fields for a plane wave of unit strength which is polarized such that $\bar{E}^i = \hat{y}E_y^i$.	51
33	Incident, reflected, diffracted and total fields for a plane wave of unit strength which is polarized such that $\bar{E}^i = \hat{y}E_y^i$.	52
34	Incident, reflected, diffracted and total field for a plane wave of unit strength which is polarized such that $\bar{H}^i = \hat{y}H_y^i$.	53
35	Incident, reflected, diffracted and total field for a plane wave of unit strength which is polarized such that $\bar{H}^i = \hat{y}H_y^i$.	54
36	Incident, reflected, diffracted and total field for a plane wave of unit strength which is polarized such that $\bar{H}^i = \hat{y}H_y^i$.	55
37	Incident, reflected, diffracted and total field for a plane wave of unit strength which is polarized such that $\bar{H}^i = \hat{y}H_y^i$.	56
38	Incident, reflected, diffracted and total field for a plane wave of unit strength which is polarized such that $\bar{H}^i = \hat{y}H_y^i$.	57
39	Semi-infinite parallel plate waveguide geometry showing the incident plane wave and the angle of incident.	58
40	Semi-infinite parallel plate wave guide showing different combinations of geometrical optical, direct, singly and multiply reflected rays in each region of the waveguide.	60
41	Incident, reflected, diffracted and total fields as a function of the axial distance form open end to the field point for the plane wave with a parallel polarization (TM_y) case.	61

Figure		Page
42	Incident, reflected, diffracted and total fields as a function of the axial distance form open end to the field point for the plane wave with a parallel polarization (TM_y) case.	62
43	Incident, reflected, diffracted and total fields as a function of the axial distance form open end to the field point for the plane wave with a parallel polarization (TM_y) case.	63
44	Incident, reflected, diffracted and total fields as a function of the axial distance from open end to the field point for the plane wave with a perpendicular polarization (TE_y) case.	64
45	Incident, reflected, diffracted and total fields as a function of the axial distance from open end to the field point for the plane wave with a perpendicular polarization (TE_y) case.	65
46	Incident, reflected, diffracted and total fields as a function of the axial distance from open end to the field point for the plane wave with a perpendicular polarization (TE_y) case.	66
47	Incident, reflected, diffracted and total fields as a function of the axial distance from open end to the field point for the plane wave with a parallel polarization (TM_y) case.	67
48	Incident, reflected, diffracted and total fields as a function of the axial distance from open end to the field point for the plane wave with a parallel polarization (TM_y) case.	68
49	Incident, reflected, diffracted and total fields as a function of the axial distance from open end to the field point for the plane wave with a parallel polarization (TM_y) case.	69
50	Incident, reflected, diffracted and total fields as a function of the axial distance from open end to the field point for the plane wave with a perpendicular polarization (TE_y) case.	70

Figure		Page
51	Incident, reflected, diffracted and total fields as a function of the axial distance from open end to the field point for the plane wave with a perpendicular polarization (TE_y) case.	71
52	Incident, reflected, diffracted and total fields as a function of the axial distance from open end to the field point for the plane wave with a perpendicular polarization (TE_y) case.	72
53	Backscattered field as a function of incident angle for a parallel polarization case.	73
54	Backscattered field as a function of incident angle for a perpendicular polarization case.	74
55	Backscattered field as a function of waveguide width for a parallel polarization case.	75
56	Backscattered field as a function of waveguide width for a perpendicular polarization case.	76
B.1	A plane wave (TEy) obliquely incident on a surface impedance boundary.	82
C.1	The magnitude and phase of transition function.	84

I. INTRODUCTION

One of the primary goals of this study is to develop an approximate but sufficiently accurate analysis for the problem of electromagnetic (EM) plane wave scattering by an open ended, perfectly-conducting, semi-infinite hollow circular waveguide (or duct) with a thin, uniform layer of lossy or absorbing material on its inner wall, and with a simple termination inside. While the analysis of the EM scattering by such a configuration is in general a difficult task, this difficulty can hopefully be substantially reduced if one proceeds from relatively simple to more complex duct geometries and develops an understanding of the basic scattering mechanisms involved in such geometries.

With the above view in mind, the less difficult but useful problem of the EM scattering by a two-dimensional (2-D), semi-infinite parallel plate waveguide with an impedance boundary condition on the inner walls was chosen initially for analysis. The impedance boundary condition in this problem serves to model a thin layer of lossy dielectric/ferrite coating on the otherwise perfectly-conducting interior waveguide walls. An approximate but efficient and accurate ray solution was obtained recently for this problem. That solution is presently being extended to the case of a moderately thick dielectric/ferrite coating on the walls so as to be valid for situations where the impedance boundary condition may not remain sufficiently accurate. These solutions will provide the

background for the development of an analogous three-dimensional (3-D) solution for analyzing the EM scattering by a semi-infinite circular duct with an absorber (lossy dielectric/ferrite) coating on its inner wall and with a simple termination inside.

It was mentioned above that as a first step, the simple problem of the EM scattering by a semi-infinite open ended parallel plate waveguide was chosen for analysis. This semi-infinite parallel plate geometry is excited by an EM plane wave which is incident from the exterior region as shown in Figure 1. The reason for initially choosing this simpler parallel plate problem was to examine the efficiency and utility of an approximate ray method of analysis while retaining the essential features of the absorber coated circular duct geometry but without the added complexity of the latter. The approximate ray method of analysis was selected here because of its conceptual simplicity.

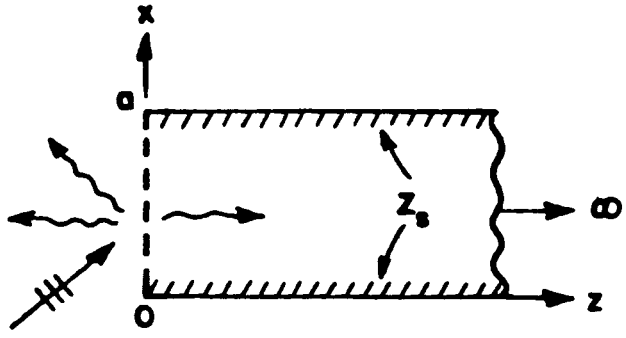

Figure 1. Diffraction by an open ended semi-infinite parallel plate waveguide with inner impedance walls and perfectly-conducting outer walls.

While the fields scattered into the exterior region by the edges of the semi-infinite parallel plate waveguide of Figure 1 as well as the fields coupled into the interior waveguide region are described here in terms of rays diffracted by the edges and by the rays which propagates inside the waveguide, respectively, one can also employ modes to describe the fields within the interior waveguide region. It is noted, of course, that at high frequencies where the width of the parallel plate waveguide becomes large in terms of the wavelength, one "generally" requires many modes, and likewise many rays, to represent the fields within the waveguide so that neither the modal nor the ray approach is expected to remain efficient at high frequencies to describe the interior waveguide fields. On the other hand, one might anticipate that the modal and the ray procedures might become more efficient if the impedance surface was lossy (i.e. if the real part of the surface impedance was non-zero) as is true for inlets with absorber coating on the inner walls.

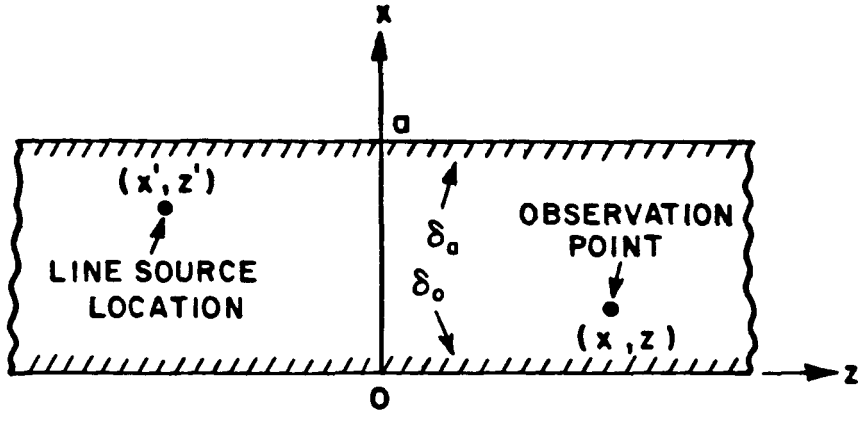

Figure 2. Infinitely long (in±z) parallel plate waveguide excited by an interior line source.

Clearly, in order to study the utility and relative efficiencies of the ray and modal approaches for describing the fields within the lossy walled parallel plate waveguide region, it became necessary to study a second problem directly related to the first one in Figure 1. The configuration of the second related problem consists of an inteiror line source exciting a parallel plate waveguide with an impedance boundary condition on its inner walls as shown in Figure 2. It is important to note that the geometry in Figure 2 is infinitely long; whereas, that in Figure 1 is semi-infinite.

An exact modal solution can be constructed for this source excited infinite waveguide problem in Figure 2. Basically, an integral representation for the waveguide Green's function can be developed first from which a formal modal expansion is readily obtained via Cauchy's residue theorem applied to the abovementioned integral representation. Due to the surface impedance boundary condition the modal eigenvalues cannot be determined analytically and must therefore have to be determined numerically in this problem from the resonant denominator of the integrand (pertaining to the integral representation of the waveguide Green's function). Once the roots of the resonant denominator are found numerically, the modal (eigenfunction) expansion for the impedance walled parallel plate waveguide Green's function can also be computed numerically. Furthermore, an asymptotic approximation of the integral representation for the waveguide Green's function (after the resonant denominator is expressed as a geometric series) yields the approximate ray series solution for the same waveguide Green's function.

The latter ray solution is the one which is of major interest in this study. Some of the dominant ray paths in the ray solution for this problem in Figure 2 are shown in Figure 3.

In the ray method, the field from a source point to an observation point is tracked along ray paths that obey the rules of geometrical optics. Such an approach can also suffer the limitations of the exact modal solution in that a large number of rays can contribute to the field point if the guide width is large in terms of the wavelength.

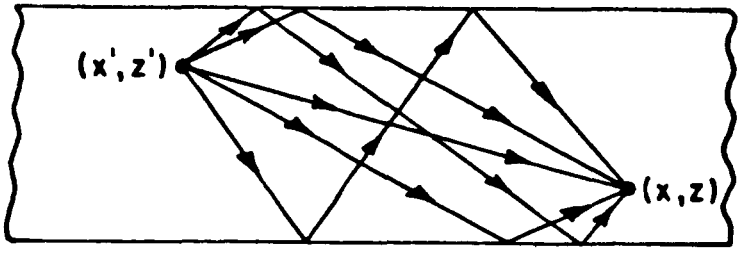

Figure 3. Dominant ray paths for the problem in Figure 2.

However, some of the advantages of the purely ray approach are that it does afford some physical insight into the scattering mechanisms particularly in connection with the coupling of the fields from the exterior to the interior regions in the case of the semi-infinite waveguide configuration, as well as into the effect of the wall impedance on the fields in the interior waveguide region. Also, the ray solution does not require one to evaluate the eigenvalues which are essential for the construction of the modal solution. This eigenvalue

evaluation must be done numerically for different impedance values and for each mode making the modal approach more inefficient as compared to the ray approach. Furthermore, as will be indicated later in this report, it was found from the numerical study of the modal and ray solutions that, in general, the ray solution converged much faster than the modal solution for the case of interest, namely, when the wall surface impedance contained loss; furthermore, it was also found in this work that, in general, the rate of convergence of the modal solution did not improve significantly even with the presence of loss in the wall surface impedance. Thus, the ray solution is being pursued with a view toward gaining an insight into the utility and accuracy of such a field representation.

The format of the present report is as follows. In section II, the exact modal and the approximate ray solution for the fields inside an infinitely long parallel plate waveguide with impedance walls is analyzed for the case of electric (or magnetic) line source excitation. Numerical results based on these two representations are also indicated together with a comparison of these modal and ray solutions. An analysis of the EM scattering and coulping problems by open ended semi-infinite parallel plate waveguide are presented in section III together with some numerical results.

II. ANALYSIS OF A PARALLEL PLATE WAVEGUIDE WITH LOSSY WALLS

The problem of a line source excited 2-D parallel plate waveguide with impedance walls is analyzed in this section. An $\exp(+j\omega t)$ time dependence is assumed and suppressed in this analytical development. The 2-D time harmonic wave equation for the parallel plate Green's function G due to a line source at $x = x'$ and $z = z'$ in the waveguide geometry of Figure 2 is given by

$$\left[\frac{\partial^2}{\partial x^2} + \frac{\partial^2}{\partial z^2} + k^2\right] G = -\delta(x-x')\ \delta(z-z') \quad , \tag{1}$$

where k is the free-space wavenumber. In this 2-D problem, the EM fields can be simply related to the Green's function G because one can scalarize the solution into the TEy and TMy cases. One notes that the magnetic field has only a $\hat{y}$ component for the TEy case and likewise, the electric field has only a $\hat{y}$ component for the TMy case. Thus, let $\bar{H} = \hat{y}Hy$ represent the magnetic field in the TEy case; likewise let $\bar{E} = \hat{y}\,Ey$ represent the electric field in the TMy case. The excitation in the TEy case can be a magnetic line source of a strength M at (x',z'); likewise, an electric line source of strength I at (x',z') generates the TMy fields. These line sources are of infinite extent in the $\pm\hat{y}$ direction. It can be shown that $Hy = -jkYMG$ and $Ey = -jkZIG$ where Z (or Y) is the free-space impedance (or admittance), provided G satisfies the following boundary conditions:

$$\frac{\partial G}{\partial x} - jk\delta_o G = 0 \qquad \text{at } x = 0$$

$$\frac{\partial G}{\partial x} + jk\delta_a G = 0 \qquad \text{at } x = a \quad , \tag{2}$$

where

$$\delta_{o,a} = \begin{cases} Z_{o,a} & \text{for TEy case} \\ Y_{o,a} & \text{for TMy case} \end{cases}$$

and $Z_{o,a}$ (or $Y_{o,a}$) is the surface impedance (or admittance) at $x = 0$ and $x = a$ which is normalized to the free-space wave impedance (or admittance). (See Figure 2.) Using separation of variables, the Green's function $G(x,x';z,z')$ is represented in terms of the one dimensional Green's functions $G_x(x,x')$ and $G_z(z,z')$ as [1,2]

$$G(x,x';z,z') = -\frac{1}{2\pi j} \int_{C_z} G_x \cdot G_z \, d\lambda_z \quad , \tag{3}$$

where the integration contour C_z in the above equation encloses only the singularities of G_z. Solving (1) for G_x subject to the boundary conditions in (2), $G_x(x,x')$ is found to be:

$$G_x(x,x') = \frac{(e^{j\sqrt{\lambda_x}x_<} + R_o e^{-j\sqrt{\lambda_x}x_<})(e^{-j\sqrt{\lambda_x}x_>} + R_a e^{j\sqrt{\lambda_x}x_>})}{2j\sqrt{\lambda_x}\,(1-R_o R_a)} \quad , \tag{4}$$

where $x_>$ and $x_<$ denote the values of x which satisfy $x < x'$ and $x > x'$, respectively and

$$R_o = \frac{\sqrt{\lambda_x} + k\delta_o}{\sqrt{\lambda_x} - k\delta_o}$$

$$R_a = \frac{\sqrt{\lambda_x} + k\delta_a}{\sqrt{\lambda_x} - k\delta_a} e^{-j2\sqrt{\lambda_x}a} \quad .$$

In addition

$$\lambda_x + \lambda_z = k^2$$

Now $G_z(z,z')$ which satisfies the radiation condition for $|z| \to \infty$ is likewise given by:

$$G_z(z,z') = \frac{e^{-j\sqrt{\lambda_z}|z-z'|}}{2j\sqrt{\lambda_z}} \quad . \tag{5}$$

Therefore, $G(x,x';z,z')$ becomes via (3),(4) and (5), the following:

$$G(x,x';z,z') = -\frac{1}{2\pi j} \int_{c_z} \frac{(e^{j\sqrt{\lambda_x}x_<} + R_o e^{-j\sqrt{\lambda_x}x_<})(e^{-j\sqrt{\lambda_x}x_>} + R_a e^{j\sqrt{\lambda_x}x_>})}{2j\sqrt{\lambda_x}\,(1-R_oR_a)}$$

$$\cdot \frac{e^{-j\sqrt{\lambda_z}|z-z'|}}{2j\sqrt{\lambda_z}} d\lambda_z$$

$$= \frac{1}{2\pi j} \int_{-\infty}^{\infty} \frac{(e^{jk_x x_<} + R_o e^{-jk_x x_<})(e^{-jk_x x_>} + R_a e^{jk_x x_>})}{2k_x(1-R_oR_a)}$$

$$\cdot e^{-jk_z|z-z'|} dk_z \quad , \tag{6}$$

where $\sqrt{\lambda_x} = k_x$, and $\sqrt{\lambda_z} = k_z$ transformations are used. An evaluation

of the above integral in (6) via the residue theorem yields a representation for G in terms of a summation of guided modes propagating along the z direction; namely:

$$G = \sum_{n=0}^{\infty} \frac{1}{2\sqrt{k^2-k_{z_n}^2}} \cdot \frac{(e^{jk_{x_n}x_<} + R_o e^{-jk_{x_n}x_<})(e^{-jk_{x_n}x_>} + R_a e^{jk_{x_n}x_>})}{\frac{\partial(R_o R_a)}{\partial k_z}}$$

$$\cdot e^{-jk_{z_n}|z-z'|} \quad . \tag{7}$$

It is noted that the modes arise from the residues of the poles in the integrand of (6). The zeros of the denominator of the integrand in (6) yield the required poles. Also these zeros yield the eigenvalues of the modes. These eigenvalues are obtained by solving the zeros of the the integrand in (6) via a numerical 'Newton-Raphson' iteration method which is described in Appendix A.

An altenative ray series representation for G is obtained by expanding the resonant denominator of the integral in (6) into a partial power series,

$$\frac{1}{1-R_o R_a} = \sum_{n=0}^{\infty} (R_o R_a)^n \quad . \tag{8}$$

Then,

$$G = -\frac{j}{4\pi} \int_{-\infty}^{\infty} \sum_{n=0}^{\infty} \frac{(e^{jk_x x_<} + R_o e^{-jk_x x_<})(e^{-jk_x x_>} + R_a e^{jk_x x_>})}{k_x}$$

$$\cdot e^{-jk_z|z-z'|} (R_o R_a)^n dk_x \quad . \tag{9}$$

It is convenient for subsequent evaluation of (9) to introduce further transformations

$$k_x = k \cos \alpha$$
$$k_z = k \sin \alpha \quad . \tag{10}$$

The Green's function $G(x,x';z,z')$ of (9) is now expressed in the complex α plane as

$$G = -\frac{j}{4\pi} \int_{C_n} \sum_{n=0}^{\infty} (e^{jk\cos\alpha \cdot x_<} + R_0 e^{-jk\cos\alpha \cdot x_<})(e^{-jk\cos\alpha \cdot x_>} + R_a e^{jk\cos\alpha \cdot x_>})$$
$$\cdot e^{-jk\sin\alpha \cdot |z-z'|} \cdot (R_0 R_a)^n d\alpha \quad . \tag{11}$$

After interchanging the orders of summation and integration, each of the integrals in the sum is evaluated asymptotically for large $k\sqrt{(x-x')^2+(z-z')^2}$ term by term via the method of steepest descent to arrive at the ray series. The integration path and a saddle point in the above equation are shown in Figure 4.

It is noted that the ray series could also be constructed directly from geometrical optics considerations. To assess the accuracy of the ray field representation which was mentioned above, the magnitude of the ray series approximation to the Green's function in (11) has been examined by comparing this with the magnitude of the exact guided mode series in (7) which is used as a reference solution. The magnitude of

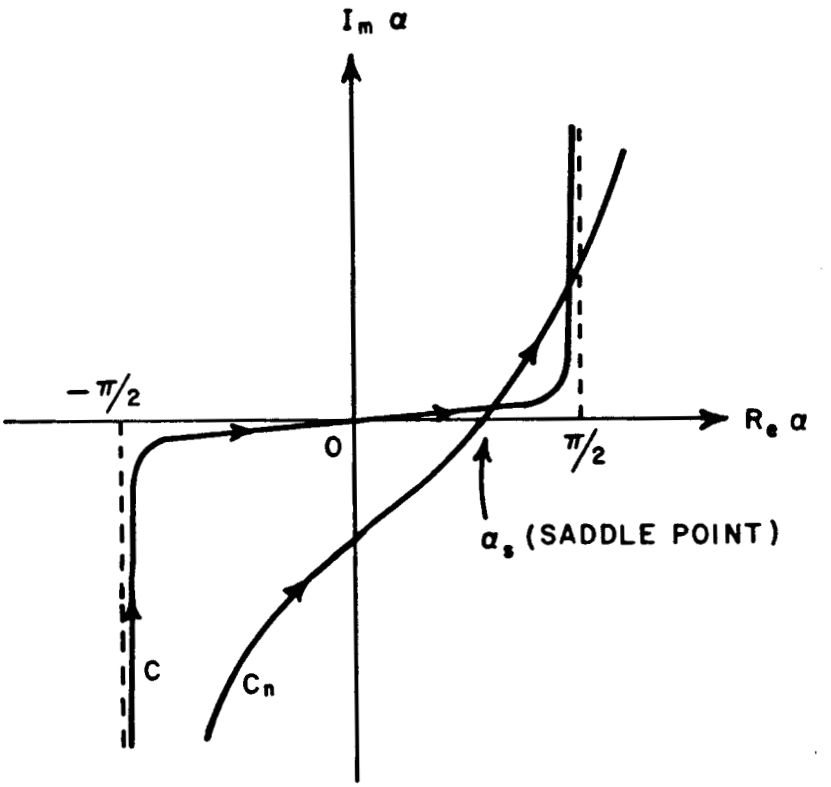

Figure 4. Integration path in complex α plane.

the Green's function in terms of the exact modal solution is plotted against the normalized distance KZ as a solid line in each of the figures, while that of the ray solution is plotted as a dashed line. For the sake of convenience, the various parameters which appear in these figures are defined below.

KA - normalized waveguide height

KX' - normalized x-coordinate of source point

KX - normalized x-coordinate of observation point

KZ - normalized z-coordinate of observation point

PM - no. of propagating modes inside the waveguide

EM - no. of evanescent modes included in a figure

N - terms which have been included in the summation of the ray series of (11)

Ro - resistance of lower waveguide wall

Xo - reactance of lower waveguide wall

Ra - resistance of upper waveguide wall

Xa - reactance of upper waveguide wall

K - wave number in the medium given by $K = 2\pi/\lambda$

λ - wavelength

For KA = 50.0, there are 16 propagating modes for an electric line source and the modal solution is plotted as a solid line in Figure 5 for the range $1.0 < KZ < 41.0$ which is examined here. The source and observation points are both equidistant from the waveguide walls in this case. The corresponding ray field is shown as a dashed line for the same range. Only N = 3 is used in the ray solution in contrast with 16 modes in the modal summation. As seen from the figure, there is a good agreement between modal and ray solutions for the range $KZ > 15.0$. The discrepancy for $KZ < 15.0$ is due to the fact that the first three evanescent modes are close to cutoff and the observation point is near the source point. When this evanescent field contribution is included in the modal solution, it is then found to agree with the ray

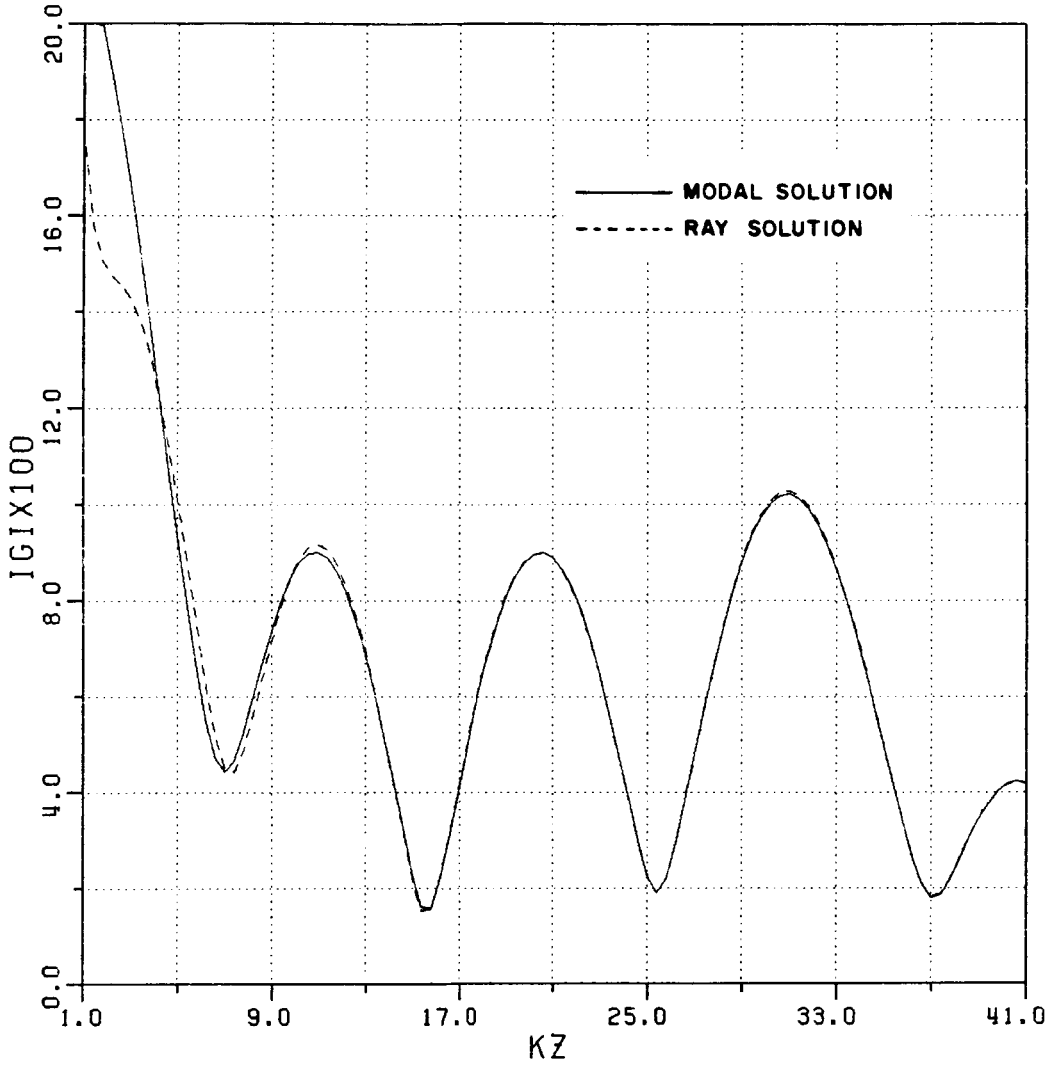

KA = 50.0	N= 3.0	R0= 0.1
KX'= 25.0	PM= 16.0	X0= 0.3
KX = 25.0	EM= 0.0	RA= 0.1
		XA= 0.3

Figure 5 |G| for an electric line source excited infinite parallel plate waveguide as a function of normalized distance KZ.

solution very well except in the region where the observation point is very near the source point ($KZ < 3.0$) as shown in Figure 6. Hence, the first three evanescent modes are included in the modal solution shown in all the other figures. In Figures 7-9, the ray solutions are compared again with the modal solutions for different impedance values of the waveguide walls. As shown in the figures, the ray solutions show very good agreement with the corresponding modal solutions. The magnitude of G is again plotted for a magnetic line source in Figures 10-13. From the Figures 6-13, it may be concluded that the ray solution converges faster than the modal solution. This convergence of the two solutions is examined in detail later in this section.

Another interesting phenomenon which can take place in the case of a waveguide with impedance walls is that pertaining to the excitation of surface wave type fields. In the modal expression for the configuration in Figure 2, there are two surface wave type modes in addition to the usual waveguide type modes which are excited if the impedance is inductively (or capacitively) reactive when the excitation is due to a magnetic (or electric) line source within the waveguide. These surface wave modes are distinct from the other waveguide modes because, in contrast to the other modes, these modes disappear when the walls become perfectly-conducting (as the impedance tends to zero); secondly, these particular modes exhibit the behaviour of the usual bound surface wave fields that can exist on a single impedance surface excited by a line source if the wall spacing is made sufficiently large.

An important characteristic of these surface wave type fields is that the energy associated with these fields is guided very close to

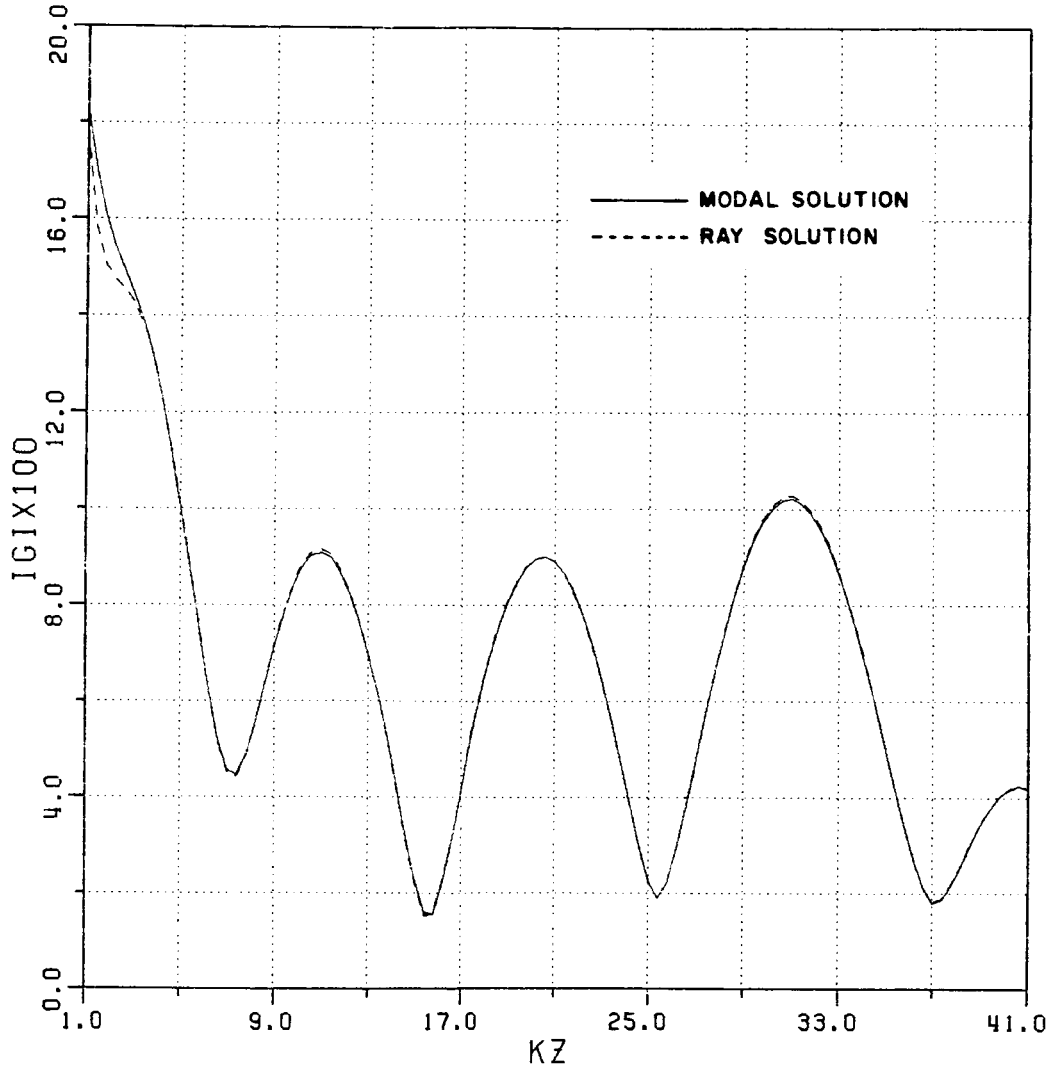

KA = 50.0 N= 3.0 R0= 0.1
KX'= 25.0 PM= 16.0 X0= 0.3
KX = 25.0 EM= 3.0 RA= 0.1
XA= 0.3

Figure 6 |G| for an electric line source excited infinite parallel plate waveguide as a function of normalized distance KZ.

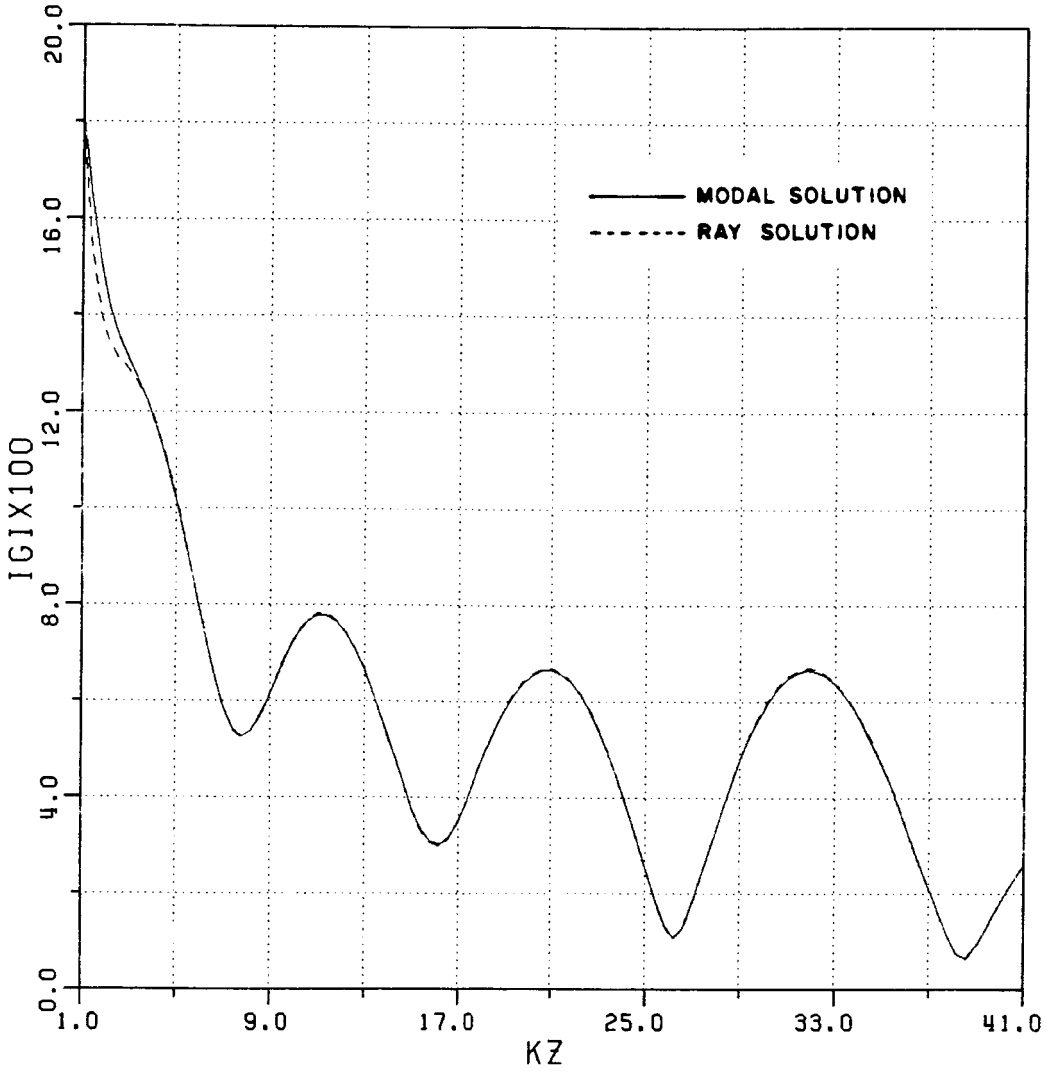

KA = 50.0	N= 3.0	RO= 0.5
KX'= 25.0	PM= 16.0	XO= 0.5
KX = 25.0	EM= 3.0	RA= 0.5
		XA= 0.5

Figure 7 |G| for an electric line source excited infinite parallel plate waveguide as a function of normalized distance KZ.

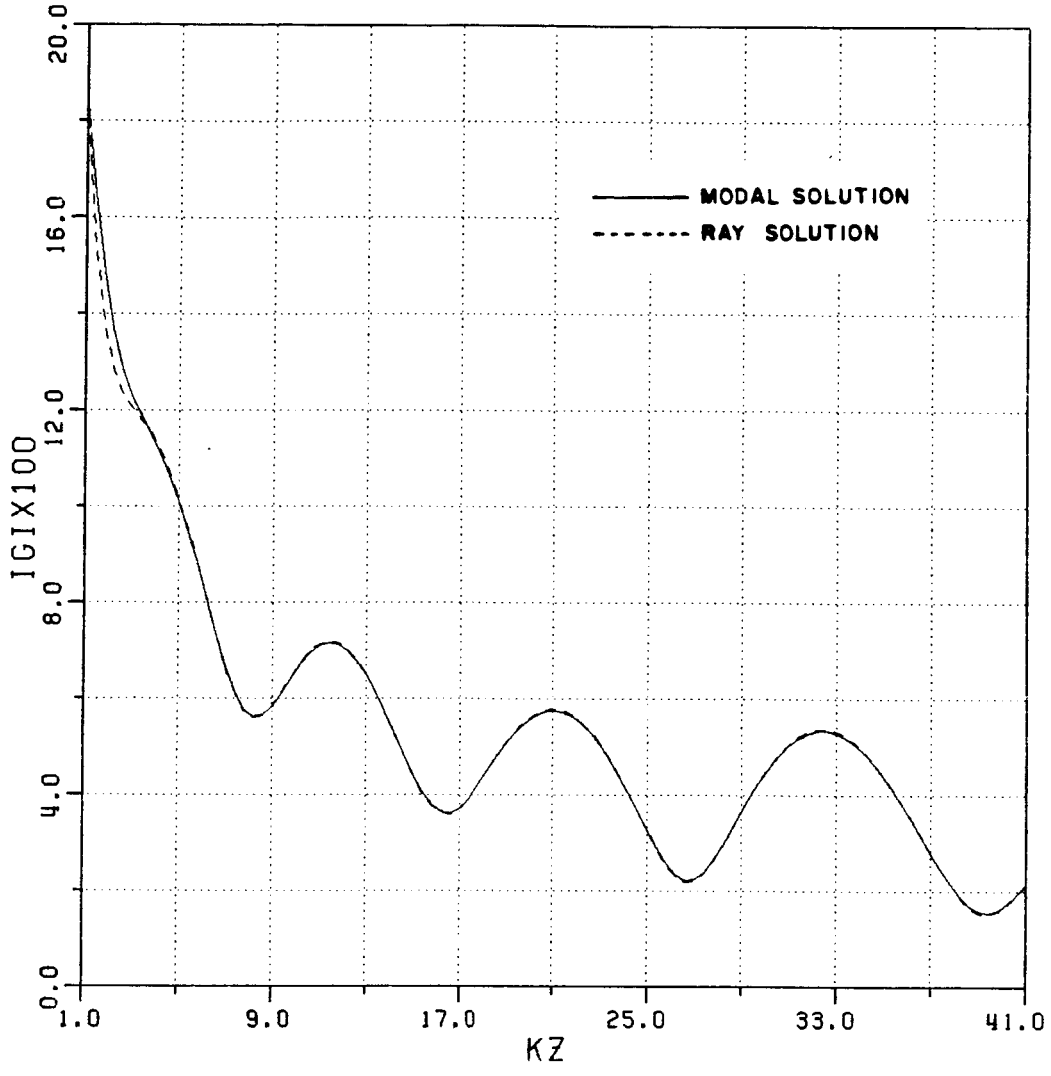

KA = 50.0	N= 3.0	RO= 0.8
KX'= 25.0	PM= 16.0	XO= 0.5
KX = 25.0	EM= 3.0	RA= 0.8
		XA= 0.5

Figure 8 |G| for an electric line source excited infinite parallel plate waveguide as a function of normalized distance KZ.

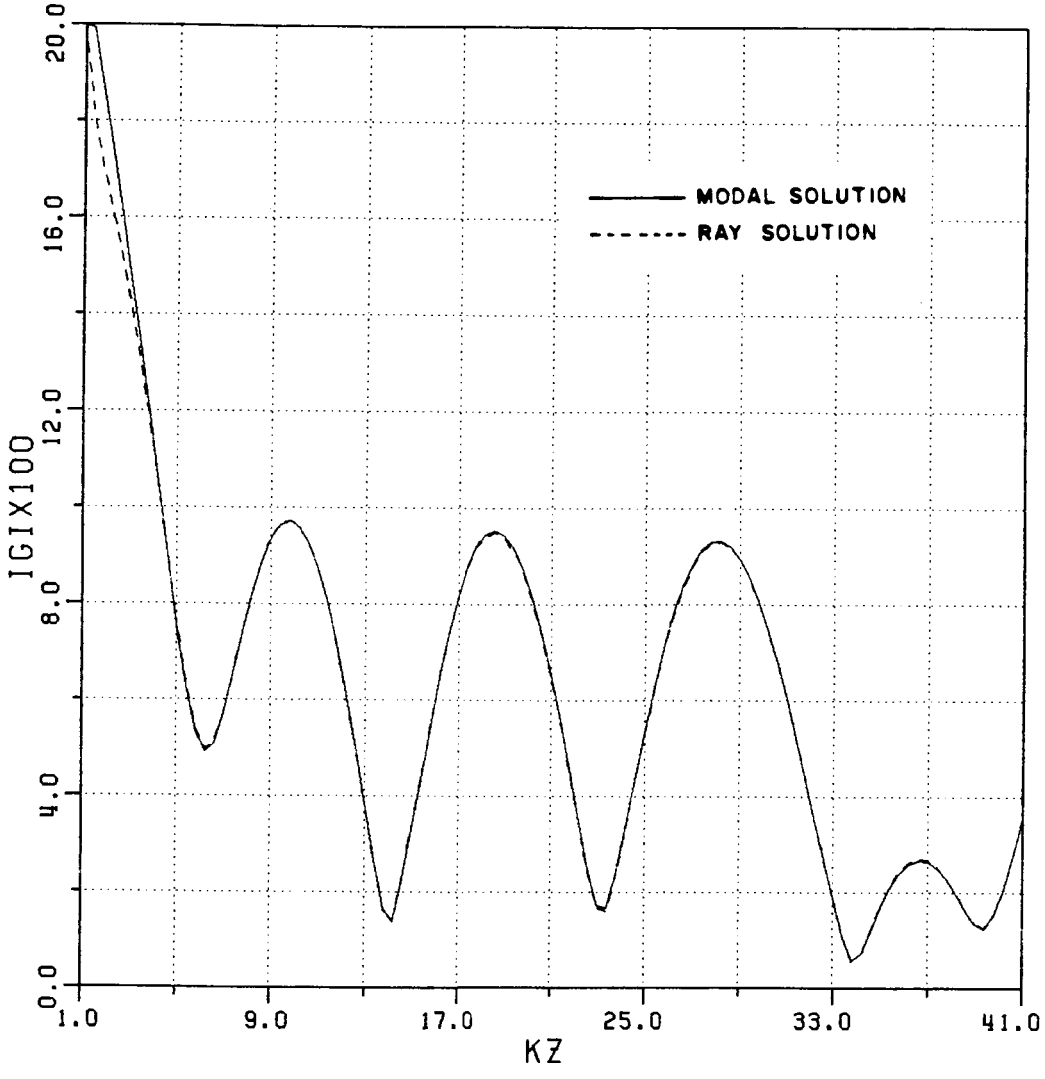

KA = 50.0 N= 3.0 RO= 0.2
KX'= 25.0 PM= 15.0 XO= -0.3
KX = 25.0 EM= 3.0 RA= 0.2
XA= -0.3

Figure 9 |G| for an electric line source excited infinite parallel plate waveguide as a function of normalized distance KZ.

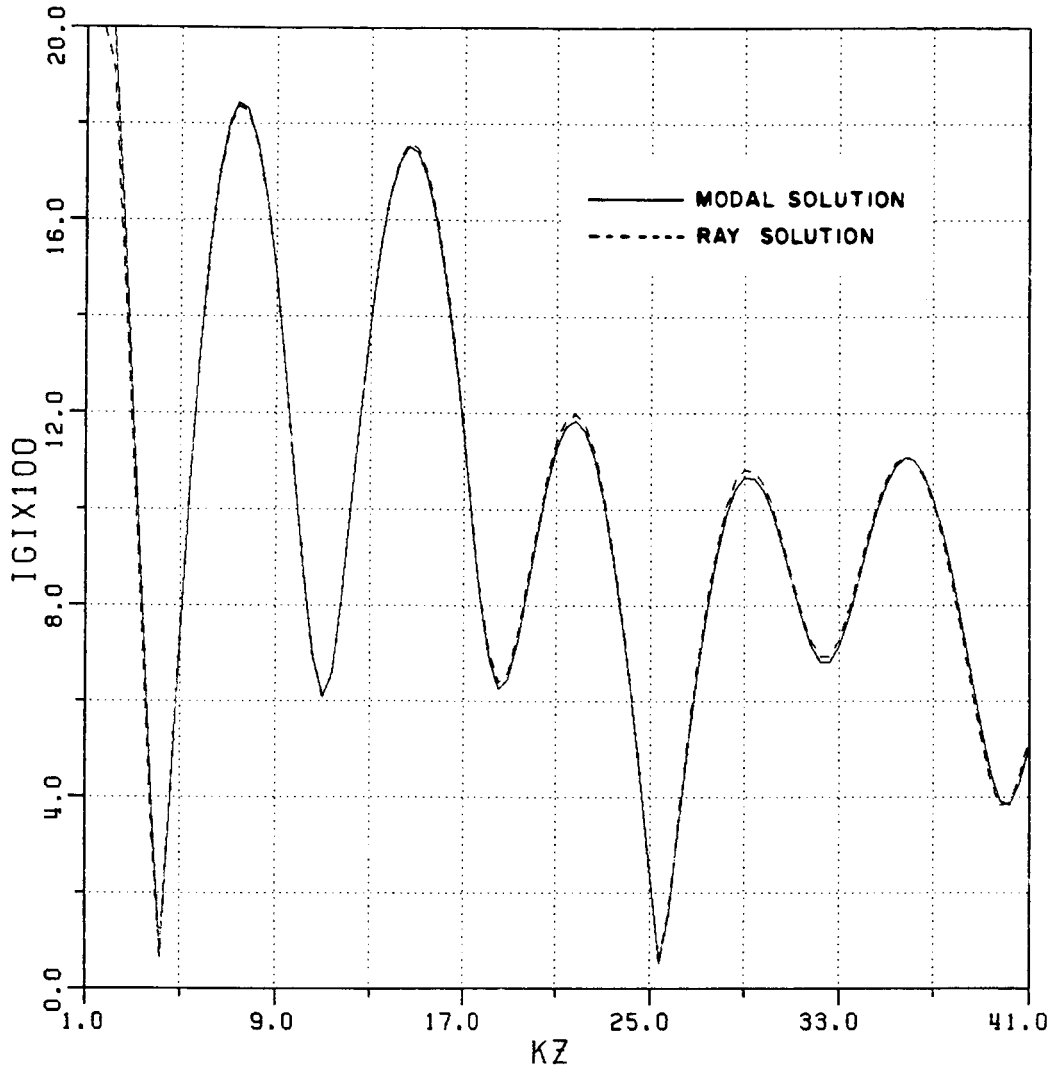

KA = 50.0	N= 7.0	RO= 0.1
KX'= 25.0	PM= 15.0	XO= 0.3
KX = 25.0	EM= 3.0	RA= 0.1
		XA= 0.3

Figure 10 |G| for a magnetic line source excited infinite parallel plate waveguide as a function of normalized distance KZ.

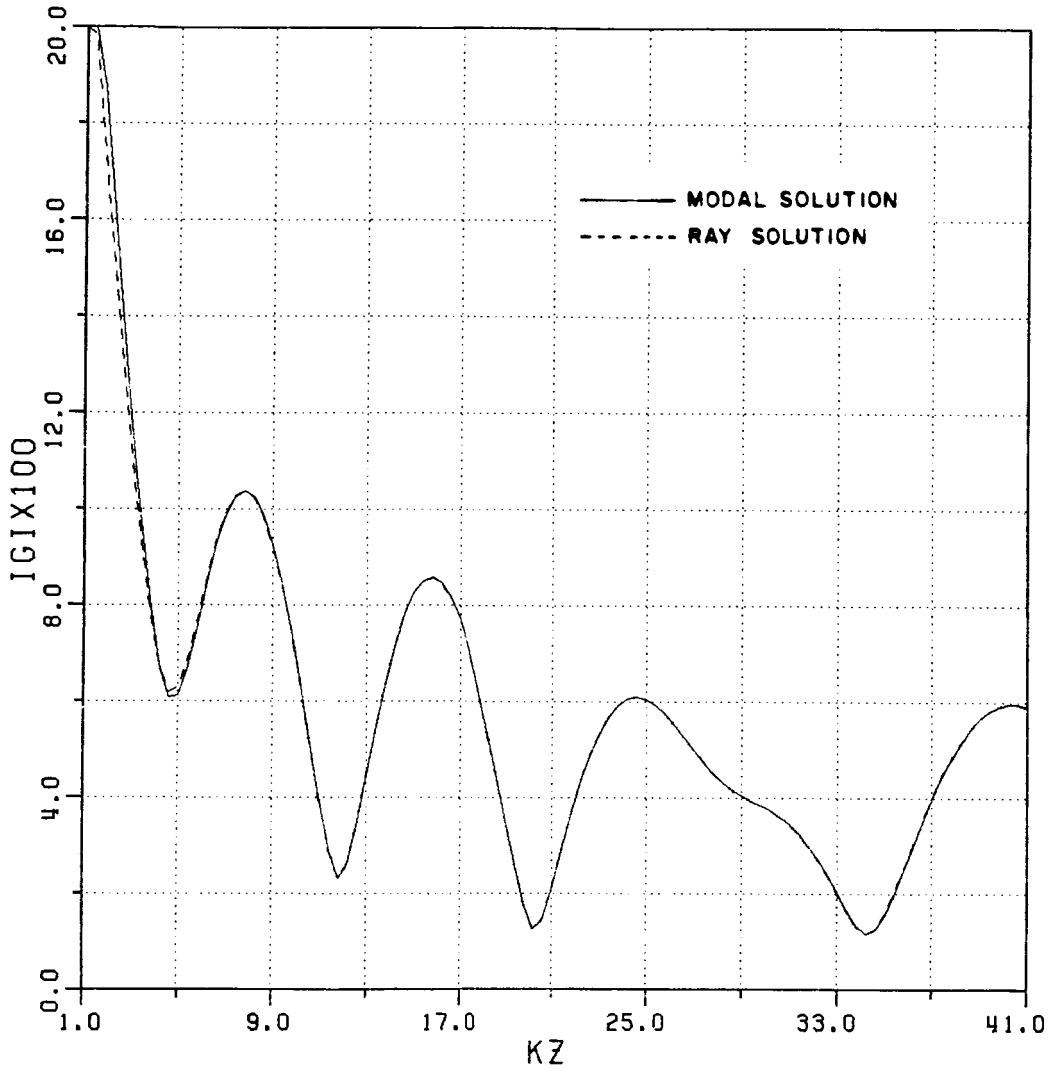

KA = 50.0	N= 3.0	RO= 0.5
KX'= 25.0	PM= 15.0	XO= 0.5
KX = 25.0	EM= 3.0	RA= 0.5
		XA= 0.5

Figure 11 |G| for a magnetic line source excited infinite parallel plate waveguide as a function of normalized distance KZ.

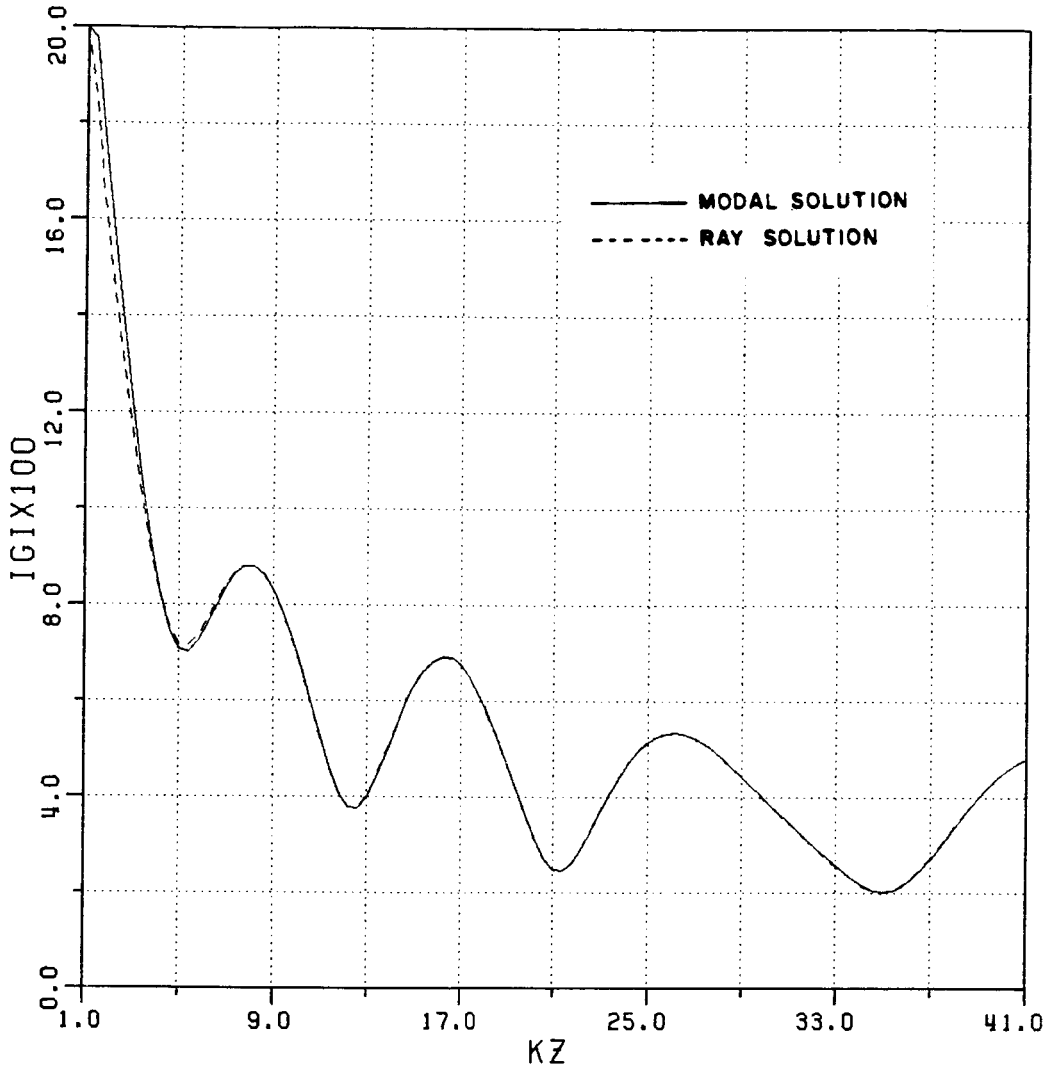

KA = 50.0	N= 3.0	RO= 0.8
KX'= 25.0	PM= 15.0	XO= 0.5
KX = 25.0	EM= 3.0	RA= 0.8
		XA= 0.5

Figure 12 |G| for a magnetic line source excited infinite parallel plate waveguide as a function of normalized distance KZ.

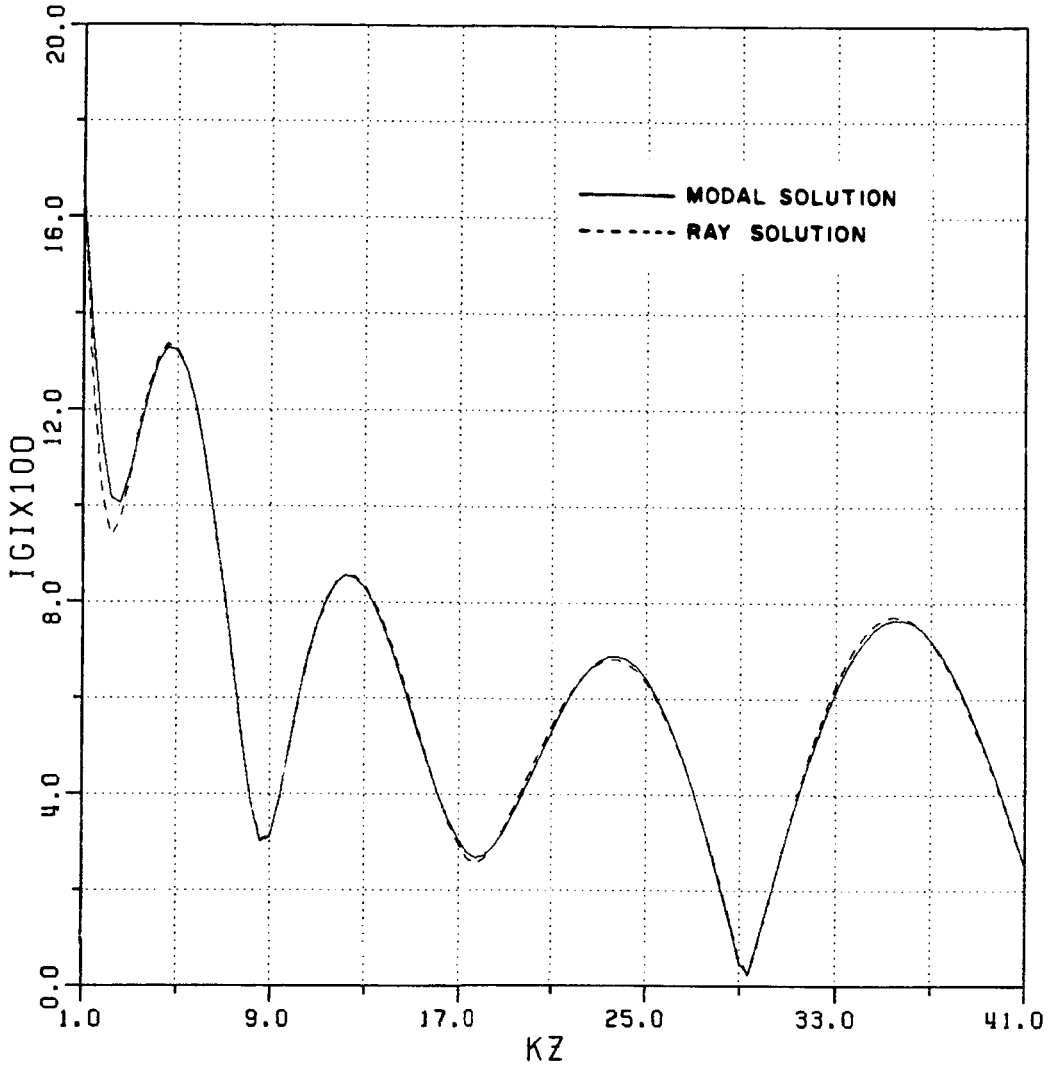

KA = 50.0	N= 3.0	R0= 0.2
KX'= 25.0	PM= 16.0	X0= -0.3
KX = 25.0	EM= 3.0	RA= 0.2
		XA= -0.3

Figure 13 |G| for a magnetic line source excited infinite parallel plate waveguide as a function of normalized distance KZ.

the impedance surface. It is noted that in the case of an inductively reactive impedance boundary one can excite a surface wave on this boundary only if the line source is magnetic. Likewise an electric line source excites a surface wave on an impedance boundary only if the impedance is capacitively reactive. Figure 14 shows the fields inside the waveguide of Figure 2 when the source and observation points are both located close to one of the impedance walls of the waveguide, and the impedance is chosen to be inductively reactive for a magnetic line source excitation so that surface wave modes can exist. The surface wave modes are included in the results obtained via the modal expansion solution in this figure; likewise, the corresponding effect of the surface wave ray fields is also included in the ray solution in this figure. Despite the inclusion of the surface wave effects, the agreement between the exact modal and the approximate ray solution is not so good in Figure 14, unless the distance from the source to the observer is sufficiently large. It was found that the reason for this discrepancy between the two solutions could be traced to the need for an increased accuracy in the asymptotic approximation of the ray solution near the surface when the observation point lies within the surface wave "transition region". This transition region extends over a certain distance from the source depending on the value of the impedance; e.g., it becomes larger for the magnetic line source excitation of an inductively reactive impedance boundary as the inductive reactance becomes smaller. This transition region may be viewed as a launching or peel out distance required to establish the surface wave. A uniform

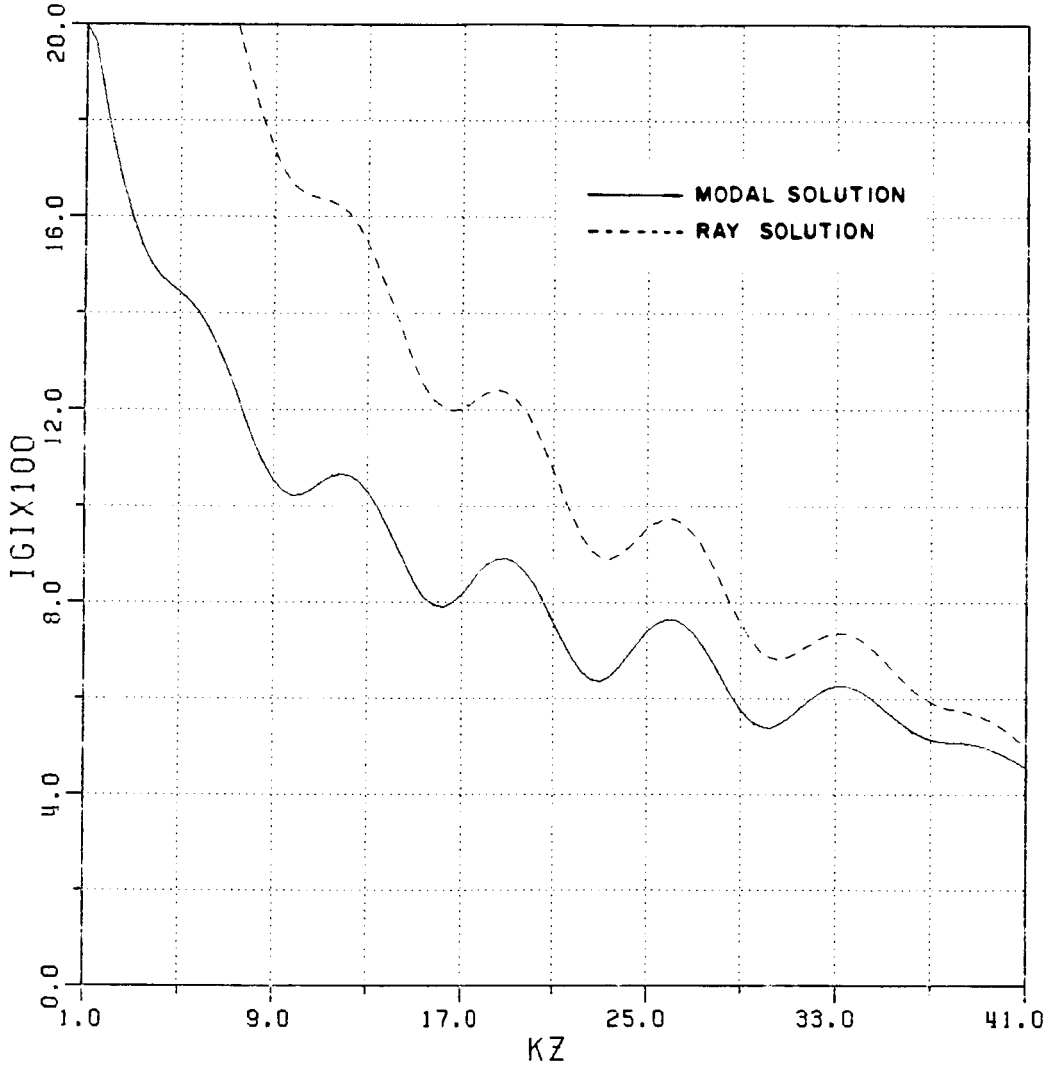

KA = 50.0	N= 7.0	R0= 0.1
KX'= 1.0	PM= 15.0	X0= 0.3
KX = 1.0	EM= 3.0	RA= 0.1
		XA= 0.3

Figure 14 |G| for a magnetic line source when both source and field points are near the lower wall and transition function is not included in the ray solution.

asymptotic treatment of the integral representation of the waveguide Green's function which yields the ray series provides a simple transition function correction to the surface ray solution in terms of a Fresnel integral. The ordinary ray series solution including the surface wave (or ray) contribution results from a non-uniform asymptotic treatment of the integral for the waveguide Green's function; this ordinary ray solution is accurate only outside the surface wave transition region. A comparison of the improved or uniform ray solution with the exact modal solution shown in Figure 15 now indicates that they are in excellent agreement. Note that the modal solution in Figure 14 is unchanged as compared to that in Figure 15; only the ray solution has been improved in Figure 15 by including the uniform surface wave transition function. It is indeed gratifying to see that the uniform ray solution predicts the proper surface wave transition effects. Since surface wave effects are dominant only in the vicinity of the surface on which the source is located, these surface wave effects are thus small whenever the observation point is located far from the surface near which the source is placed as shown in Figure 16. A particulary interesting result is observed when the source and observation points lie on the same impedance wall of the parallel plate waveguide as in Figure 17. In Figure 17, the ray solution composed of the direct ray contribution from the source together with the contribution from rays singly and multiply reflected from the walls interferes strongly with the surface wave field plus the term containing the surface wave transition effects, since all of the latter surface wave effects are particulary significant at and near the surface containing the source.

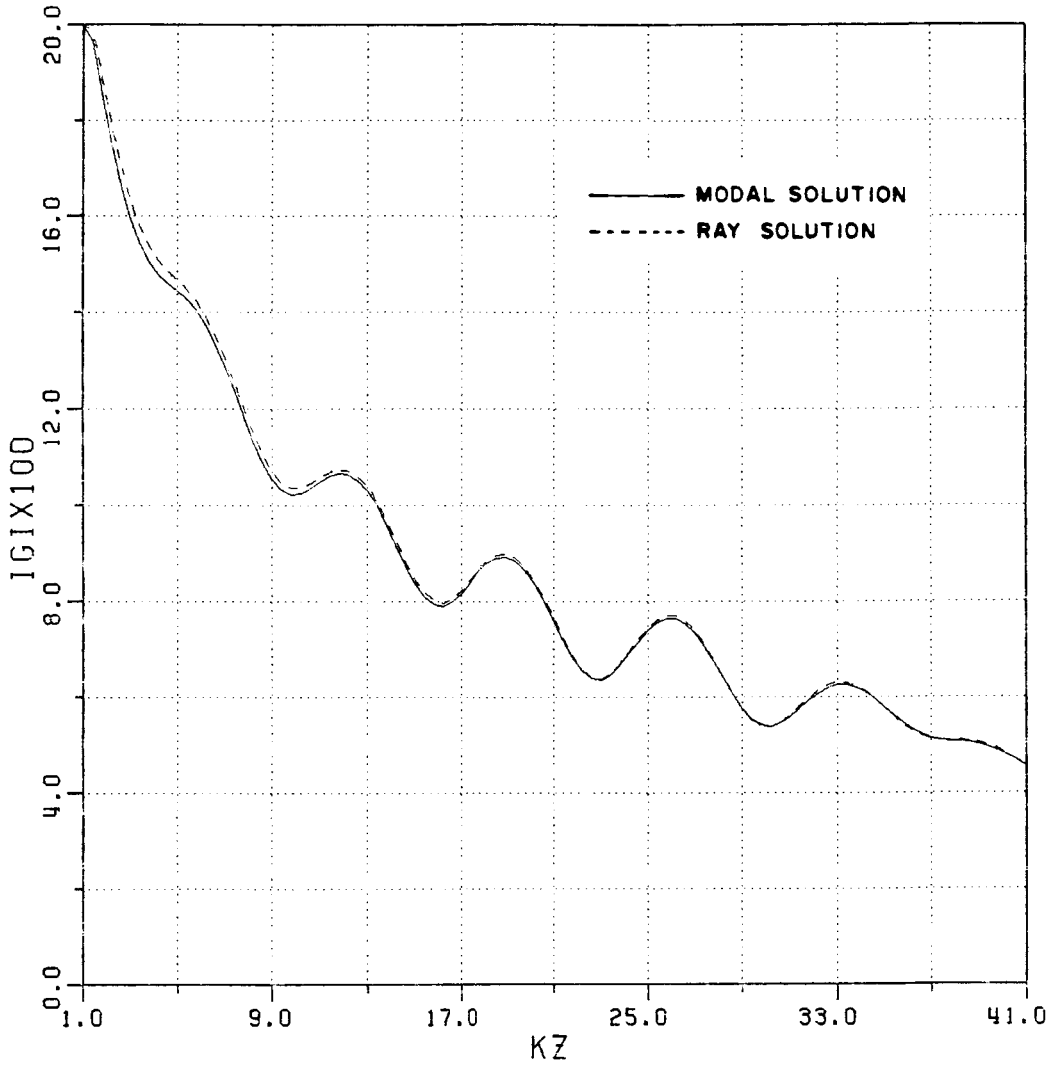

KA = 50.0	N= 7.0	RO= 0.1
KX'= 1.0	PM= 15.0	XO= 0.3
KX = 1.0	EM= 3.0	RA= 0.1
		XA= 0.3

Figure 15 |G| for the case of Figure 14 except that the transition function is included in the ray solution.

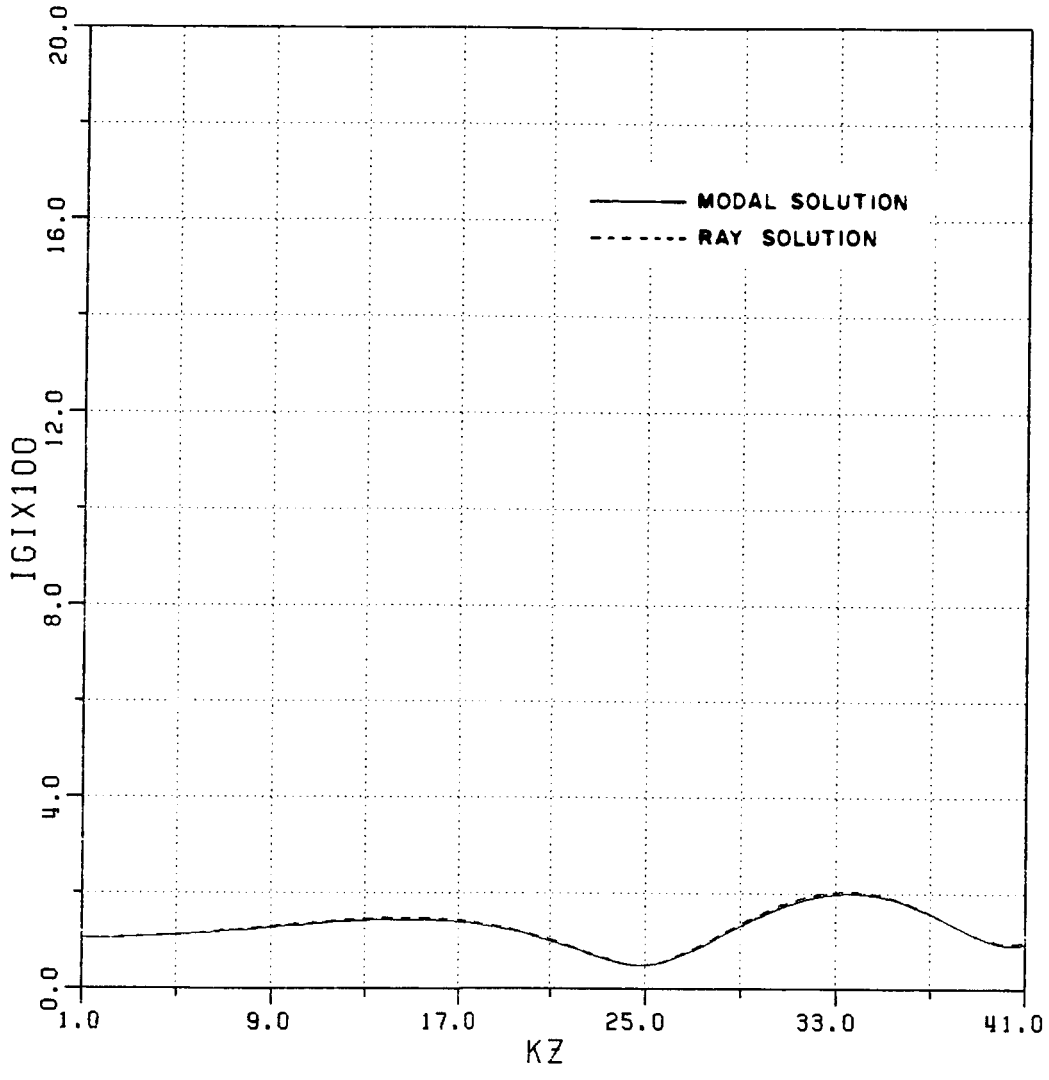

KA = 50.0	N= 7.0	RO= 0.1
KX'= 1.0	PM= 15.0	XO= 0.3
KX = 49.0	EM= 3.0	RA= 0.1
		XA= 0.3

Figure 16 |G| for a magnetic line source when a source point is near the lower wall and a field point is near the upper wall.

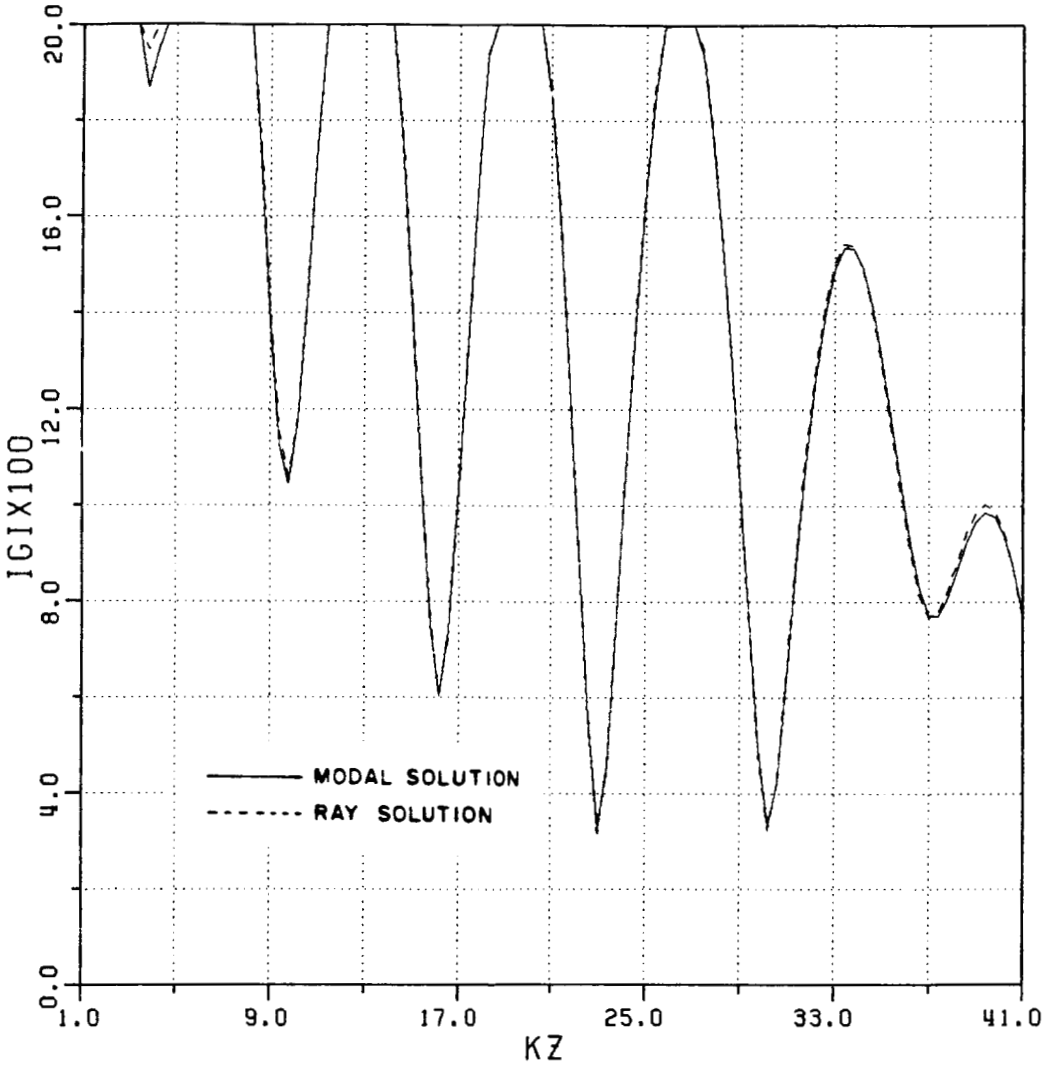

KA = 50.0	N= 7.0	R0= 0.1
KX'= 0.0	PM= 15.0	X0= 0.3
KX = 0.0	EM= 3.0	RA= 0.1
		XA= 0.3

Figure 17 |G| for a magnetic line source when both source and field points are on the lower wall.

The result in Figure 17 indicates that the surface wave launched by the incident wave at the edges in Figure 1 may reflect strongly from any discontinuity placed close to the walls of an absorber lined duct; the reflected surface wave could then radiate outside the inlet geometry in Figure 1 again via diffraction from the edges at the inlet opening. On the other hand, the effect of the surface wave field could be controlled to exhibit a greater attenuation along the direction of propagation with the inclusion of greater loss in the impedance surface characterizing the thin absorber lined waveguide (or inlet) walls.

To check the nature of the convergence of the modal and ray solutions, the magnitude of G is plotted against the number of modes and rays for a fixed KZ in Figures 18-21 for an electric line source, and 22-25 for a magnetic line source for various impedance values. It is observed from the figures that modal solution reaches a stable field value after summing all the propagating modes for KZ = 20.0. On the other hand, at most N = 3 terms are needed in the ray series to arrive at the same result.

As pointed out above, it is observed from Figures 18-25 that the convergence of the ray solution is faster than the modal solution, and secondly, the convergence of the modal solution is not significantly improved by the presence of loss in the walls since all the propagating modes in this case (plus one evanescent mode near the source region) are required for convergence. On the other hand, the convergence of the ray solution is improved much as the impedance value becomes bigger (for the TE_y case) as shown in the figures.

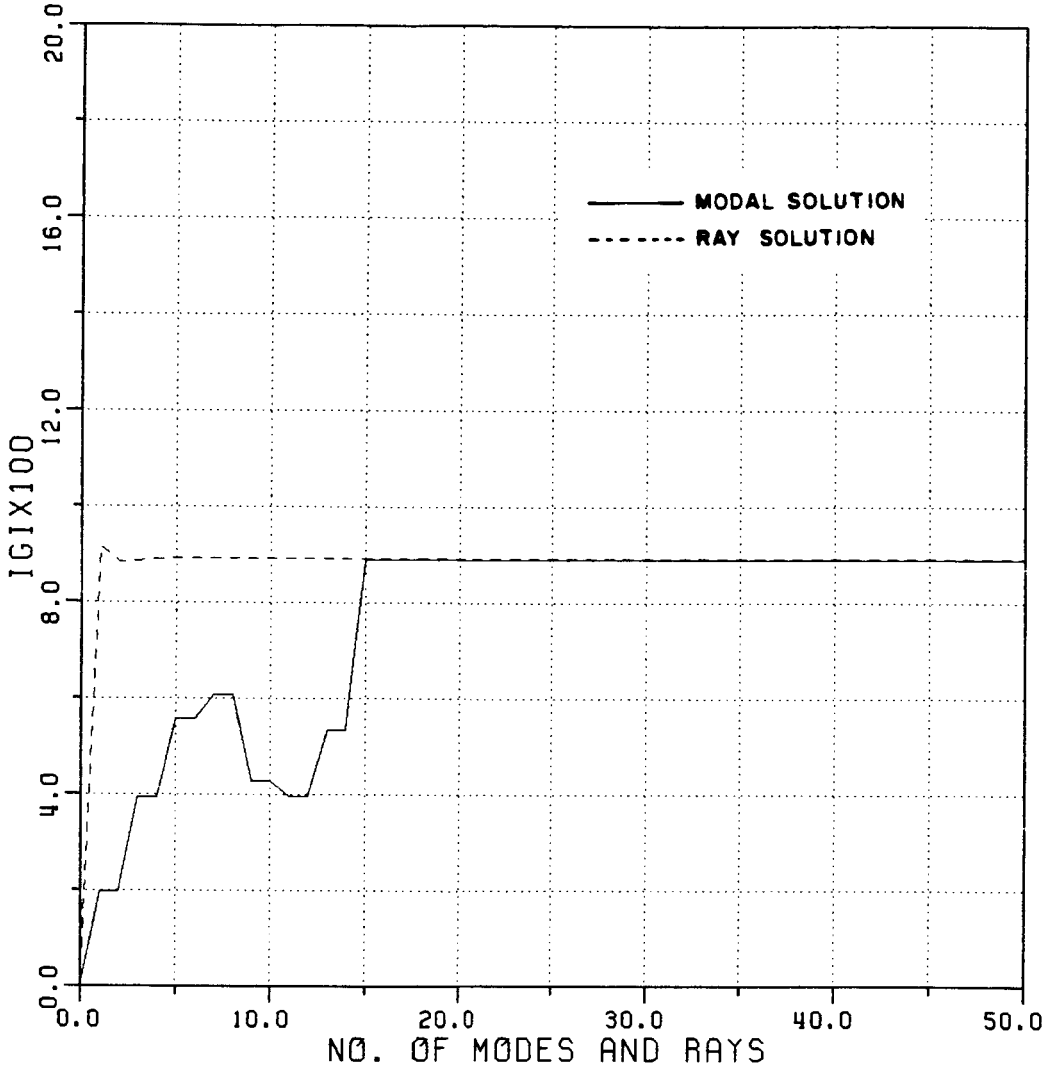

KA = 50.0 KZ= 20.0 RO= 0.1
PM = 16.0 XO= 0.3
KX'= 25.0 RA= 0.1
KX = 25.0 XA= 0.3

Figure 18 Convergence of model and ray solution for an electric line source at fixed KZ.

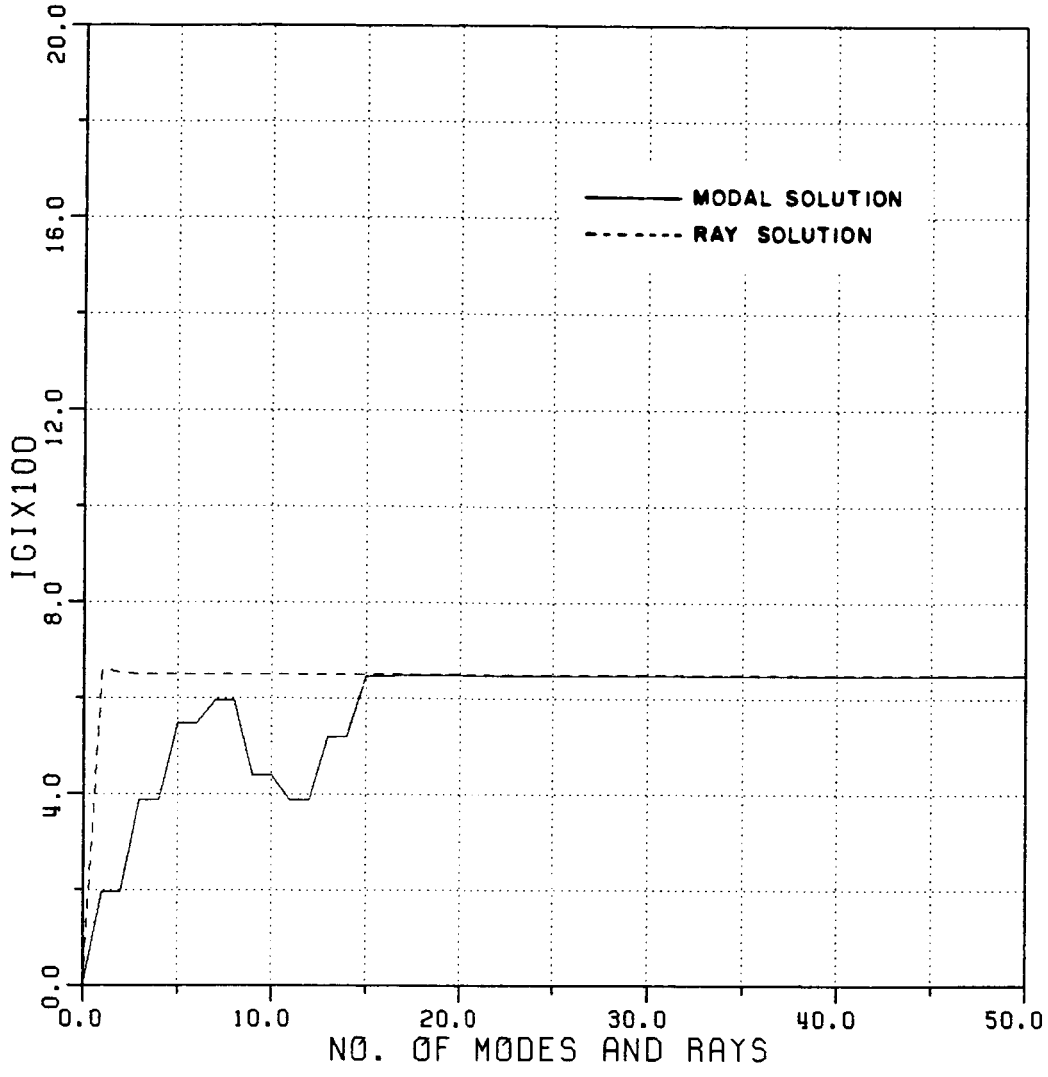

KA = 50.0	KZ= 20.0	RØ= 0.5
PM = 16.0		XØ= 0.5
KX'= 25.0		RA= 0.5
KX = 25.0		XA= 0.5

Figure 19 Convergence of model and ray solution for an electric line source at fixed KZ.

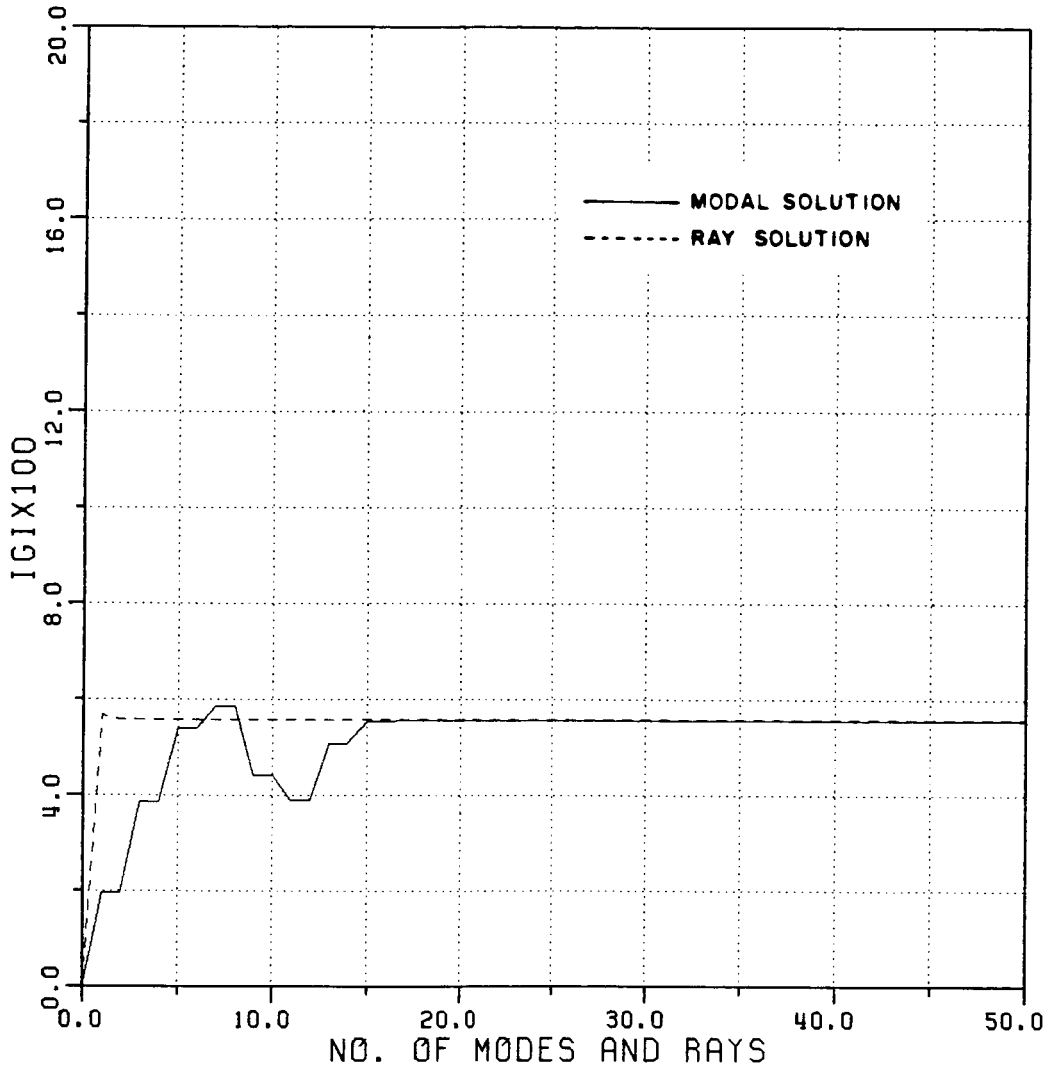

KA = 50.0	KZ= 20.0	RO= 0.8
PM = 16.0		XO= 0.5
KX'= 25.0		RA= 0.8
KX = 25.0		XA= 0.5

Figure 20 Convergence of model and ray solution for an electric line source at fixed KZ.

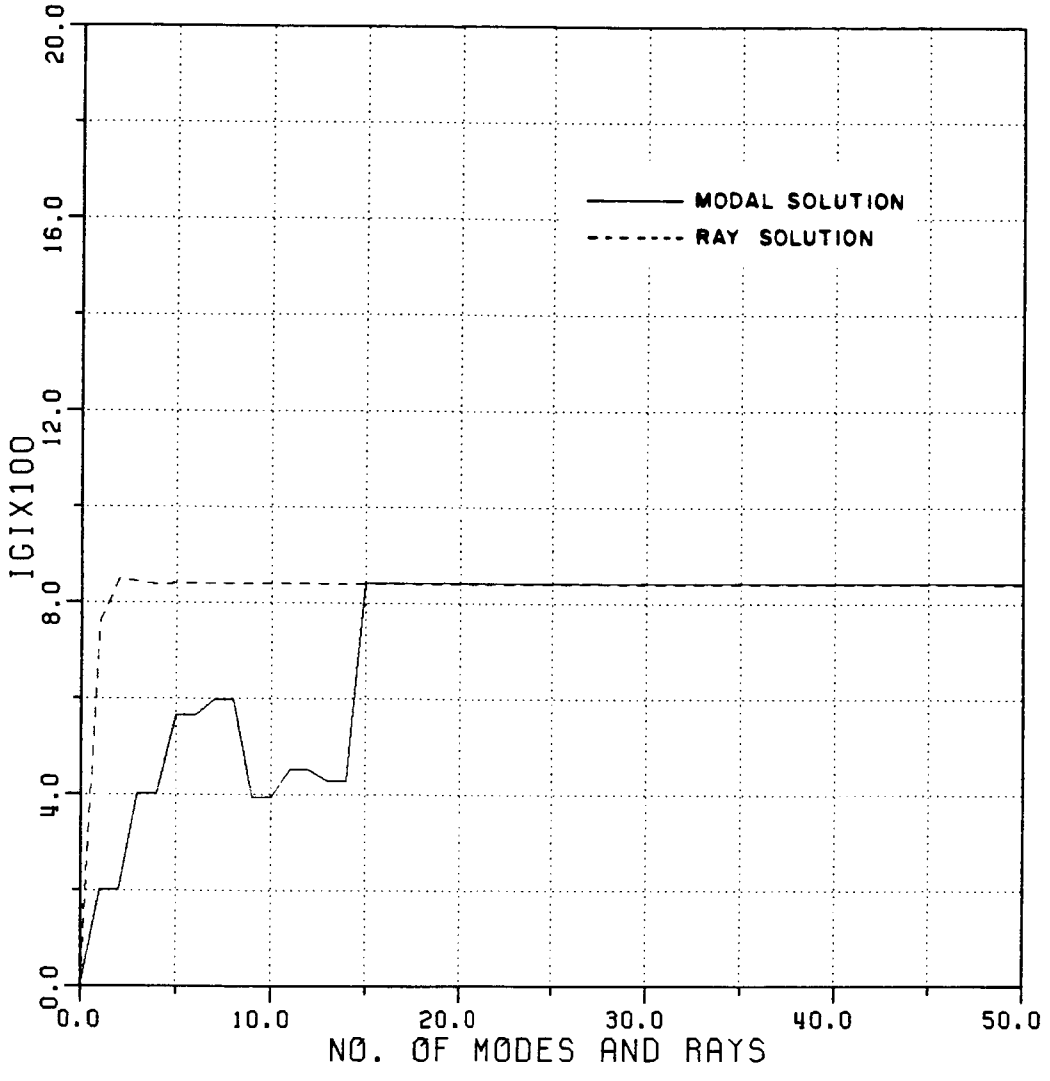

KA = 50.0 KZ= 20.0 RO= 0.2
PM = 15.0 XO= -0.3
KX'= 25.0 RA= 0.2
KX = 25.0 XA= -0.3

Figure 21 Convergence of model and ray solution for an electric line source at fixed KZ.

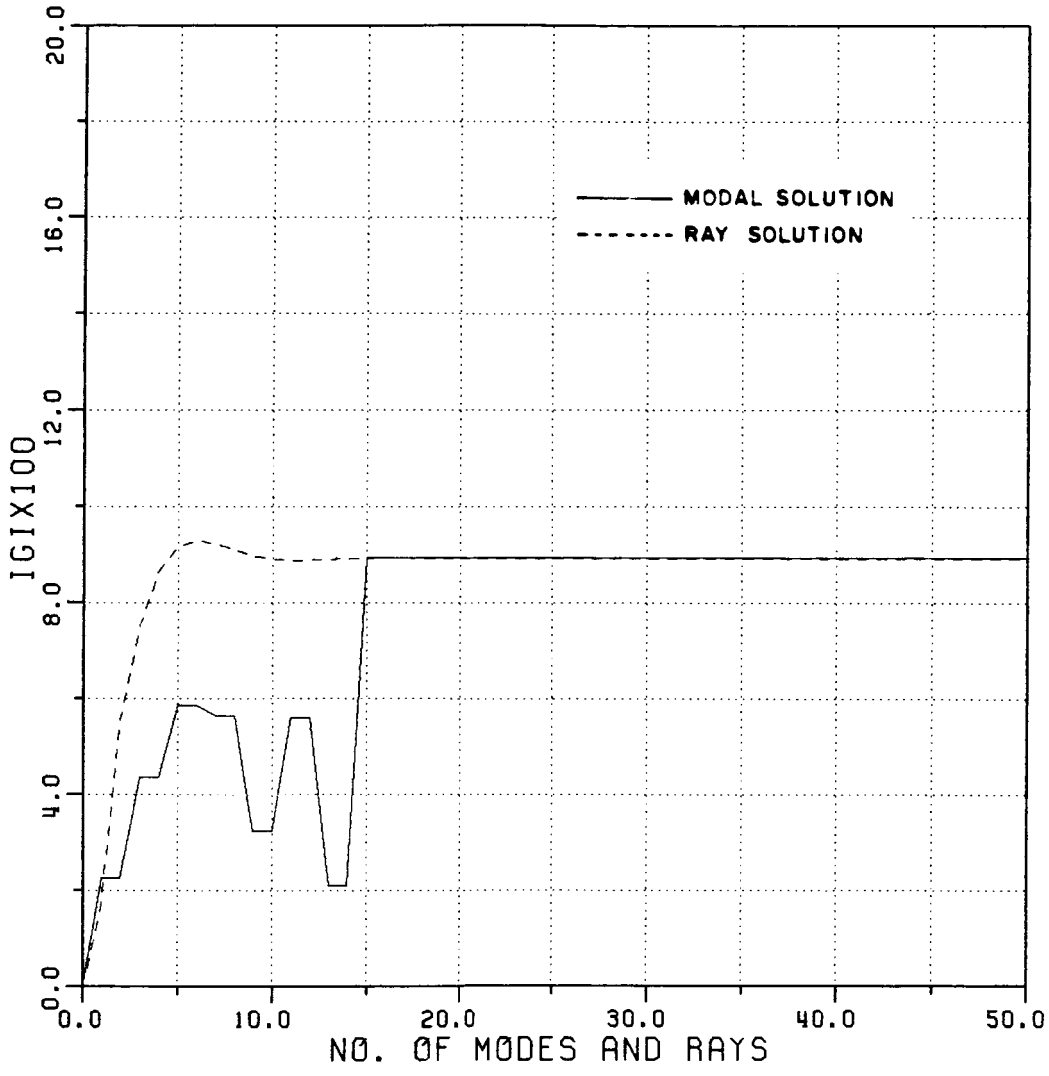

KA = 50.0	KZ= 20.0	RØ= 0.1
PM = 15.0		XØ= 0.3
KX'= 25.0		RA= 0.1
KX = 25.0		XA= 0.3

Figure 22 Convergence of modal and ray solution for a magnetic line source at fixed KZ.

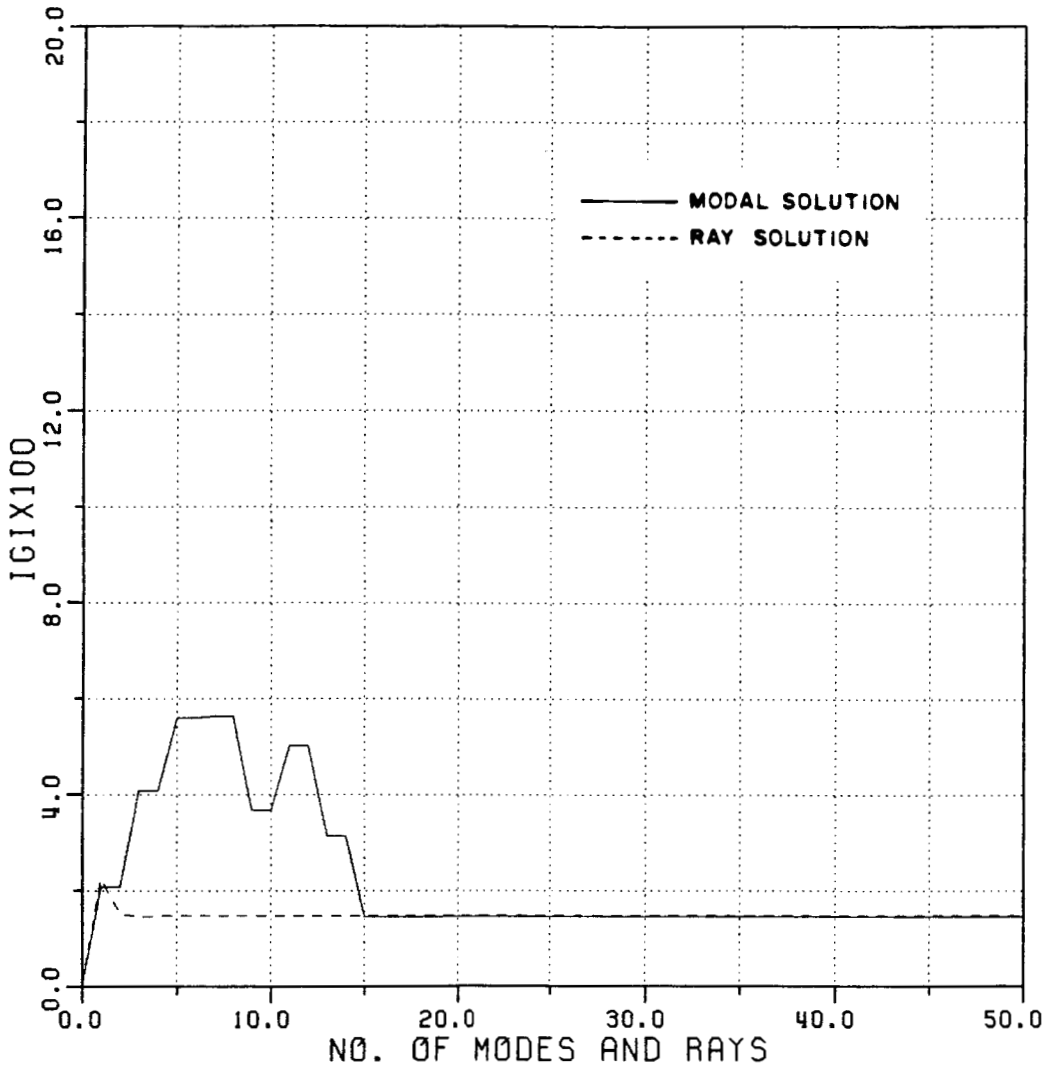

KA = 50.0	KZ= 20.0	RØ= 0.5
PM = 15.0		XØ= 0.5
KX'= 25.0		RA= 0.5
KX = 25.0		XA= 0.5

Figure 23 Convergence of modal and ray solution for a magnetic line source at fixed KZ.

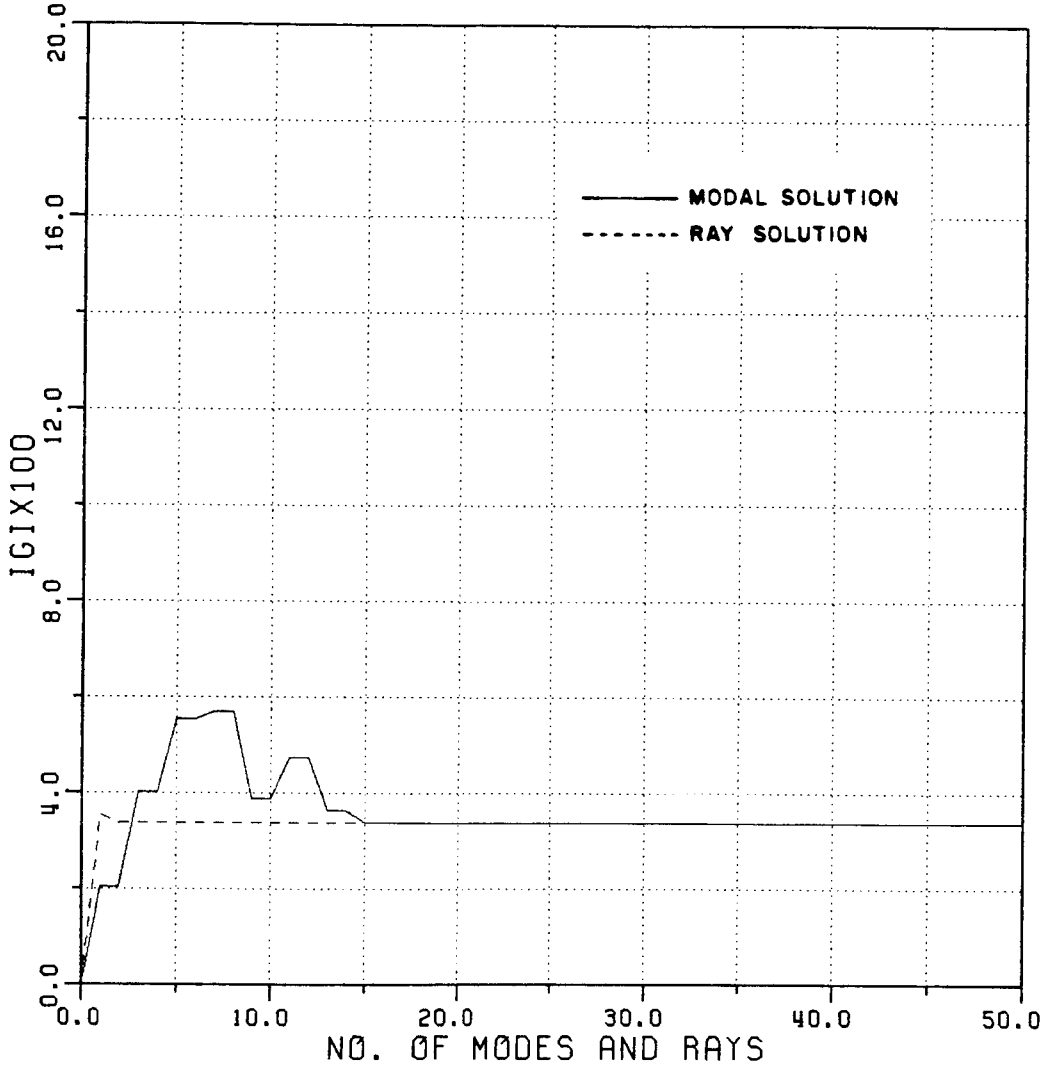

KA = 50.0 KZ= 20.0 RO= 0.8
PM = 15.0 XO= 0.5
KX'= 25.0 RA= 0.8
KX = 25.0 XA= 0.5

Figure 24 Convergence of modal and ray solution for a magnetic line source at fixed KZ.

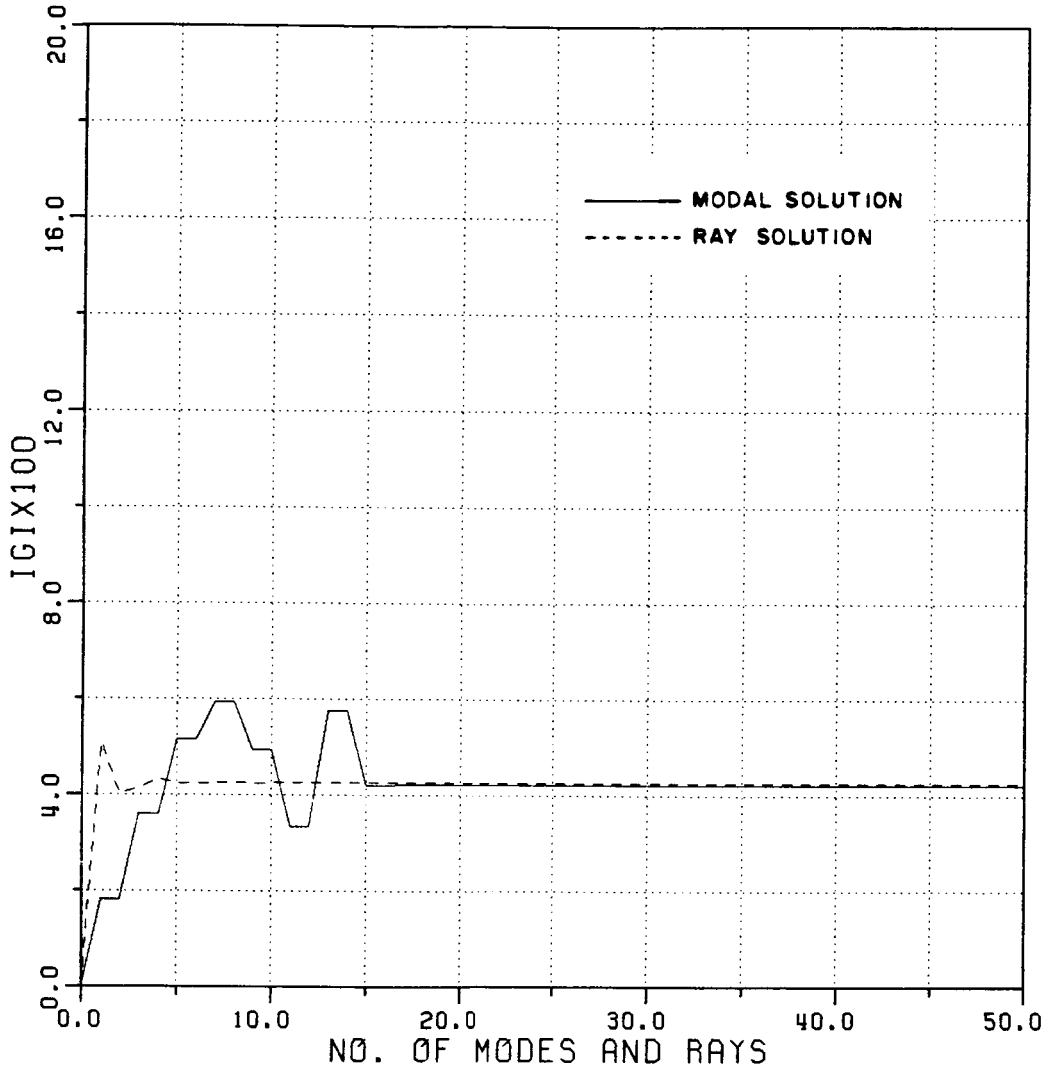

KA = 50.0	KZ= 20.0	RO= 0.2
PM = 16.0		XO= -0.3
KX'= 25.0		RA= 0.2
KX = 25.0		XA= -0.3

Figure 25 Convergence of modal and ray solution for a magnetic line source at fixed KZ.

III. ANALYSIS OF AN ELECTROMAGNETIC SCATTERING FROM AN SEMI-INFINITE PARALLEL PLATE WAVEGUIDE WITH LOSSY WALLS

Returning to the problem in Figure 1, the field at some observation point inside the semi-infinite duct are due to the direct and reflected rays which would result from the incident plane wave when it directly enters the duct, as well as due to the rays diffracted from the edges which enter the duct after diffracting from the edges as shown in Figure 26.

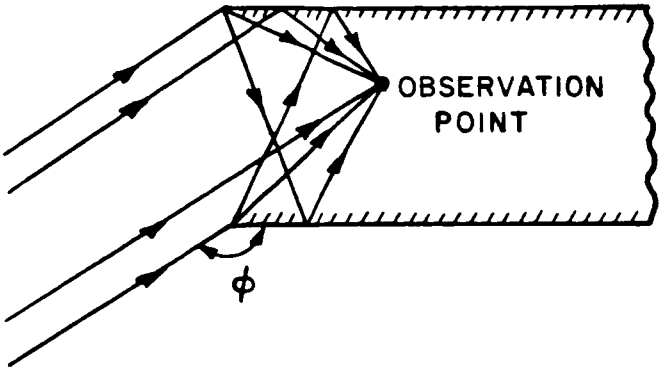

Figure 26. Dominant ray paths for the problem in Figure 1.

The incident field impinging on the edges at the open end produces diffracted rays which can be calculated via Maliuzhinets' edge diffraction coefficient [3] that is valid for the problem of plane wave diffraction by a wedge with two face impedances. Here the Maliuzhinets' result [3] is specialized to the configuration in Figure 1 corresponding

to the case of a half plane pertaining to each of the semi-infinite waveguide walls; In particular, the half plane here is a special case of a wedge with a zero internal angle and with a non-zero impedance on one face (corresponding to the inner waveguide wall) and with a zero impedance on the other face (corresponding to the outer perfectly-conducting waveguide wall) of the half plane. An alternative, more approximate but simpler method [4] for computing the diffracted rays by the edges at open end is to modify the diffraction coefficient which is based on the Uniform geometrical Theory of Diffraction (UTD) solution for a perfectly-conducting half plane [5,6]. In this report, the modified diffraction coefficent [4] is used for its simplicity. In the very near future, that diffraction coefficient will be replaced by the diffraction coefficient available from Maliuzhinets' work. The simpler solution in [4] is discussed below for completeness.

BASIC 2-D EDGE DIFFRACTION SOLUTION

Consider a plane wave incident on a half plane whose one side is perfectly-conducting and the other side is an impedance surface as shown in Figure 27. The total UTD ray field U^{tot} at an observation point (P) for this problem may be expressed as the sum of the fields associated with the incident, reflected and diffracted rays such that

$$U^{tot} = U^{i} + U^{r} + U^{d} \tag{12}$$

Note that U^{tot} represents the total $\hat{y}$-directed electric field if an

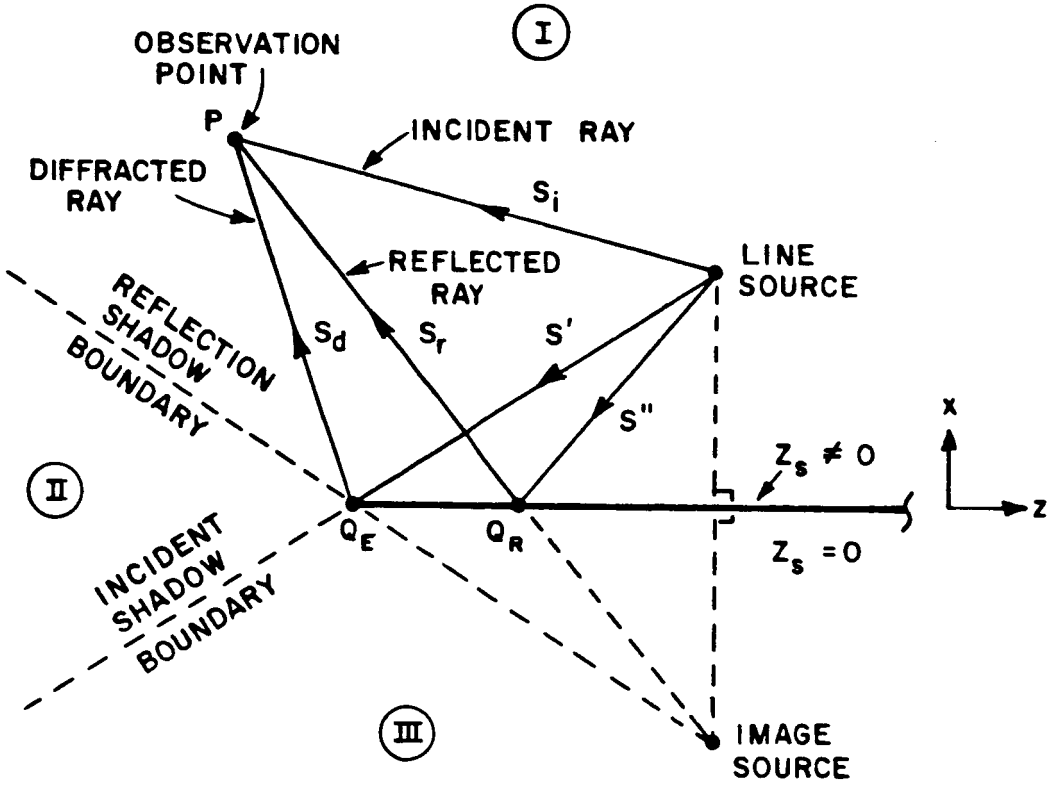

Q_R = point of reflection

Q_E = point of edge diffraction

Figure 27 Rays associated with the problem of line source excitation of an impenetrable half plane with two face impedances.

electric line source is used, whereas, it represents the total $\hat{y}$-directed magnetic field if a magnetic line source is present. The fields U^i and U^r are associated with the usual geometrical optics (GO) incident and reflected rays; whereas, the field U^d is associated with the edge diffracted ray as shown in Figure 27.

According to the regions where the observation point P is located, the individual terms may be expressed in the following forms

$$U^i(P) = \begin{cases} A_o \dfrac{e^{-jks_i}}{\sqrt{s_i}}, & \text{in regions I and II, and } A_o \text{ is some known complex constant related to the strength of the line source.} \\ 0, & \text{in Region III} \end{cases} \tag{13}$$

$$U^r(P) = \begin{cases} U^i(Q_R)R \dfrac{e^{-jks_r}}{\sqrt{s_r}}, & \text{in Region I with } U^i(Q_R) = A_o \dfrac{e^{-jks''}}{\sqrt{s''}} \\ 0, & \text{in Regions II and III} \end{cases} \tag{14}$$

$$U^d(P) = U^i(Q_E)\cdot D_{\substack{M \\ E}} \frac{e^{-jks_d}}{\sqrt{s_d}}, \quad ; \quad u^i(Q_E) = A_o \frac{e^{-jks'}}{\sqrt{s'}} \tag{15}$$

where s_i (or s_r) is the distance from the source (or point of reflection Q_R) to the observation point P and s_d is the distance from the edge (Q_E) to the observation point. Also $\tilde{R}$ is a reflection coefficient for the surface which is illuminated and is derived in Appendix B.

For a half plane considered here, the diffraction coefficient $D_{\substack{M \\ E}}$ for the $\binom{TEy}{TMy}$ case is given by [4,6]

$$D_{\substack{M \\ E}}(\phi,\phi') = \frac{-e^{-j\,\pi/4}}{2\sqrt{2\pi k}} \cdot \left\{ \frac{F[kLa(\phi-\phi')]}{\cos(\phi-\phi')/2} + \tilde{R}\,\frac{F[kLa(\phi+\phi')]}{\cos(\phi+\phi')/2} \right\} \qquad (16)$$

where

$$L = \frac{s's_d}{s'+s_d} \quad ; \quad a(\beta) = 2\cos^2(\beta/2) \quad ; \quad \beta = \phi \mp \phi' \quad ,$$

and

$$F(x) = 2j\sqrt{x}e^{jx}\int_{\sqrt{x}}^{\infty} e^{-j\tau^2}\,dt \quad .$$

F(x) is called transition function and involves a Fresnel integral. The magnitude and phase of the transition function is shown in Appendix C. Note that in (16), if the magnetic (or electric) field vector is parallel to the edge, the positive (or negative) sign is used.

The diffraction coefficient in (16) is often expressed by

$$D_{\substack{M \\ E}}(\phi,\phi') = D(\phi-\phi') \pm D(\phi+\phi') \qquad (17)$$

with

$$D(\phi \mp \phi') = \frac{-e^{-j\,\pi/4}}{2\sqrt{2\pi k}} \frac{F[kLa(\phi \mp \phi')]}{\cos(\phi \mp \phi')/2} \tag{18}$$

This diffraction coefficient provides a continuity in the total field across the incident and reflection shadow boundary transition regions. It is noted from Equations (13) and (14) that the geometrical optics (GO) field is discontinuous at these shadow boundaries; thus the diffracted field must properly compensate the discontinuities in the incident and reflected fields there. In particular, the $D(\phi-\phi')$ type term in the $D_{\substack{M \\ E}}$ keeps the total field bounded at the incident shadow boundary (ISB); likewise, the $D(\phi+\phi')$ term does the same thing at the reflection shadow boundary (RSB).

Using the diffraction coefficient developed above, the incident, reflected, diffracted and total fields are examined for this geometry as shown in Figure 28. The difference between Figure 27 and 28 is that the line source is allowed to recede to infinity in Figure 28 giving rise to a plane wave illumination. In the above figure, R is the distance from the edge of half plane to the field point, and ϕ' and ϕ are incident and observation angle, respectively. In addition, R_S and X_S correspond to the surface resistance and reactance of the impedance wall, respectively. For an incident TM plane wave of unit strength (and zero phase at Q_E) which is polarized such that $E^i = \hat{y}\, E^i_y$, the corresponding GO (incident and reflected) and diffracted fields are

plotted against the observation angle Figure 29. The incident and observation angles are measured from the perfectly-conducting face in this case. The reflected field is plotted as a dashed line; whereas the total GO (incident plus reflected) field is shown as a solid line in the figure with vertical axis marked GO. The oscillation in the GO field results from an interference between incident and reflected fields. Note also that the dicontinuities in the GO field are compensated by the corresponding discontinuities in the diffracted field as shown in the figures with vertical axis marked DIFFRACTED and TOTAL fields, respectively. The total field is thus continuous for all observation angles including the ISB (ϕ = 210°) and RSB (ϕ = 150°) directions. Similiar plots are shown in Figures 30-33 for different incident angles. In all the figures (29-33), the total fields are continuous for all observation angles. Additional calculations are also shown in Figures 34 -38 for the TEy or perpendicularly polarized plane wave case with different impedance values on the half plane. The incident and observation angles are measured from the impedance wall side in Figures 34-38. Note that the ripples in the total fields are getting smaller as the loss in the impedance wall becomes higher because the magnitude of reflected field decreases with higher loss.

The analysis developed above can be employed to treat the scattering and coupling problems associated with the semi-infinite parallel plate waveguide illuminated by a plane wave as shown in Figure 1 because the waveguide can be formed by two parallel half planes; one half plane corresponds to the lower wall, and the other one corresponds to the upper wall as shown in Figure 39.

Then according to the location of the field point inside the waveguide, different combinations of rays such as direct, reflected, diffracted,and also multiply reflected rays reach the field point as shown in Figure 40. Of course, the edge diffracted rays also reach the field point via direct and multiply reflected ray paths. If the spacing between the walls is sufficiently large in terms of the wavelength, then the effect of the rays multiply diffracted across the aperture (at the open end) before they enter the waveguide can be neglected. Such rays which undergo multiple diffractions across the aperture are ignored in the present work.

As an illustration, each type of ray field is plotted against the axial distance from open end to the field point in Figures 41-43 for a plane wave with TMy or parallel polarization, and in Figures 44-46 for a TE_y or perpendicularly polarized plane wave for various incident angles, respectively. Note that the observation point in all these plots is located off the walls; hence, the surface wave effects are not expected to be strong in this case. As shown in these plots, the total fields are continuous for all the boundaries designated in Figure 40. Similar plots are shown for different impedance values in Figures 47-49 for a TMy incident plane wave, and in Figures 50-52 for a TEy incident plane wave.

Using the same diffraction coefficient as in (16) the far zone, fields backscattered from the inlet are computed and shown in Figures 53 and 54 as a function of incident angle for parallel and perpendicular polarization cases, respectively. R_d represents the far zone distance

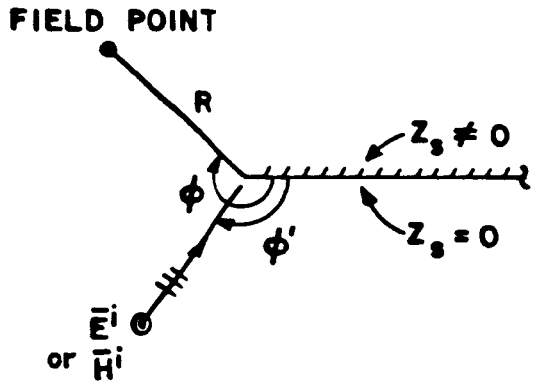

Figure 28. A half plane geometry with perfectly-conducting on one side and impedance surface on the other side.

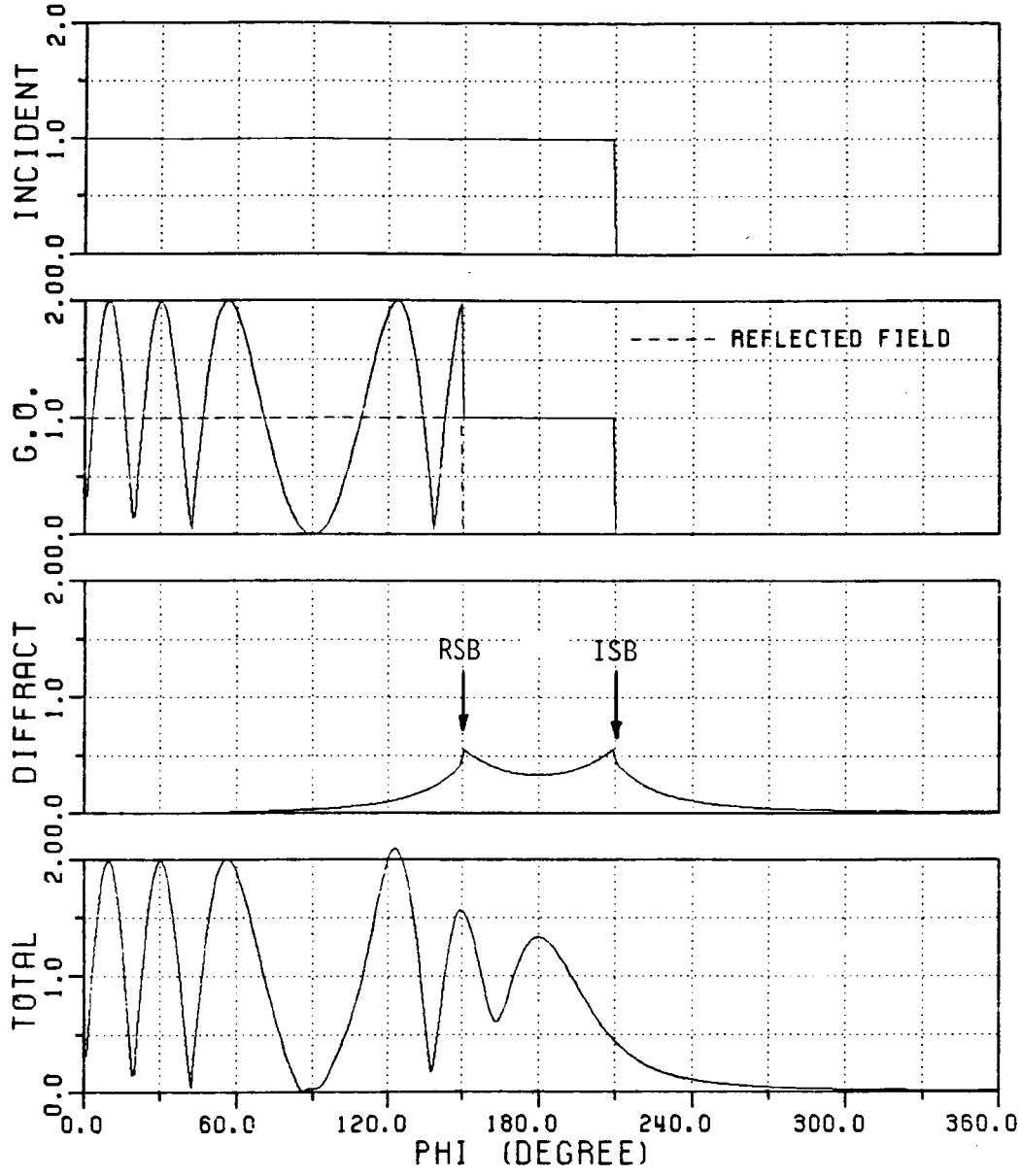

RS= 0.5 ϕ' = 30.0 (DEGREE)
XS= 0.5 R = 3.0 (LAMBDA)

Figure 29 Incident, reflected, diffracted and total fields for a plane wave of unit strength which is polarized such that $\bar{E}^i = \hat{y}E_y^i$.

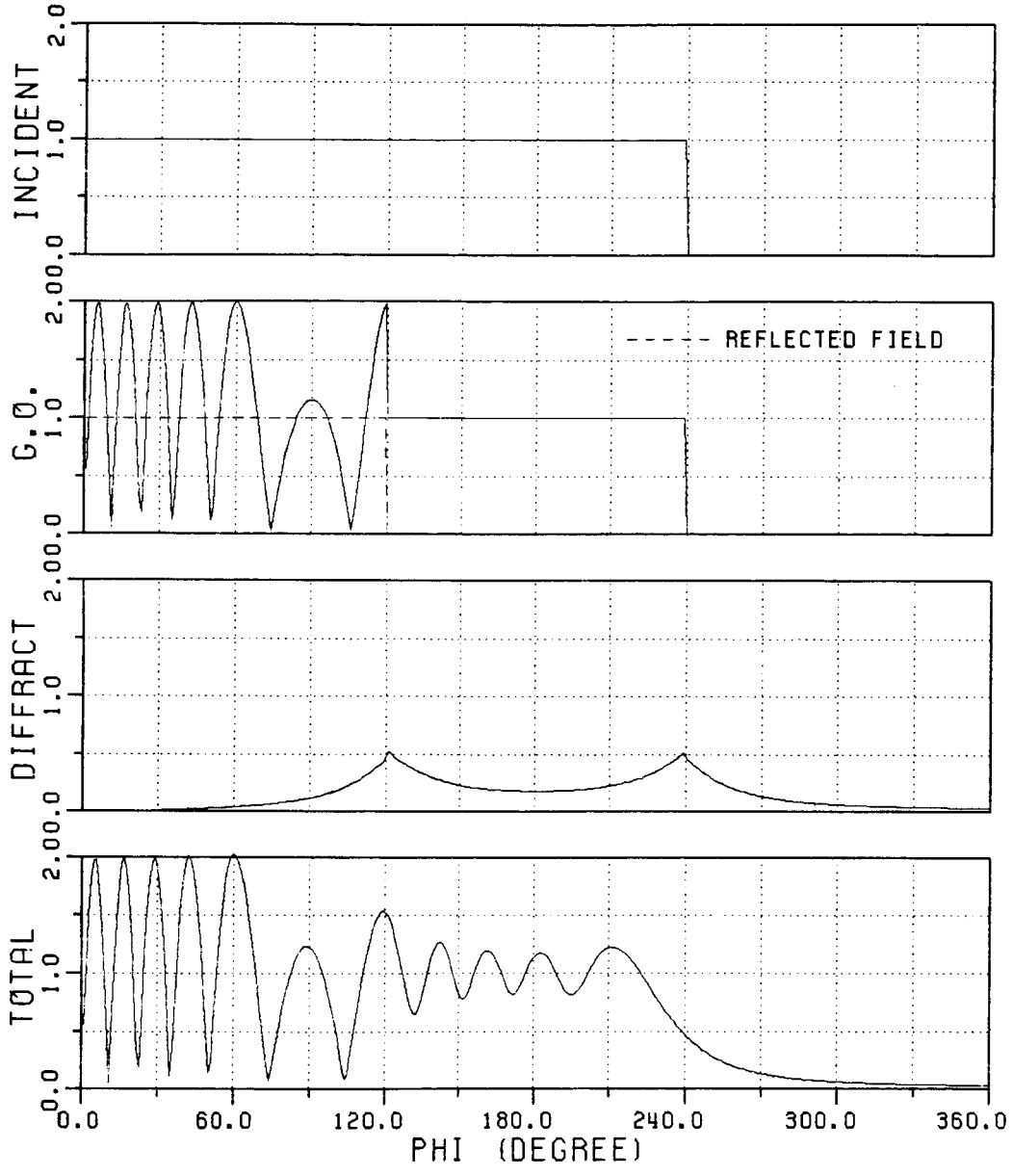

RS= 0.5 ϕ' = 60.0 (DEGREE)
XS= 0.5 R = 3.0 (LAMBDA)

Figure 30 Incident, reflected, diffracted and total fields for a plane wave of unit strength which is polarized such that $\bar{E}^{i} = \hat{y}E^{i}_{y}$.

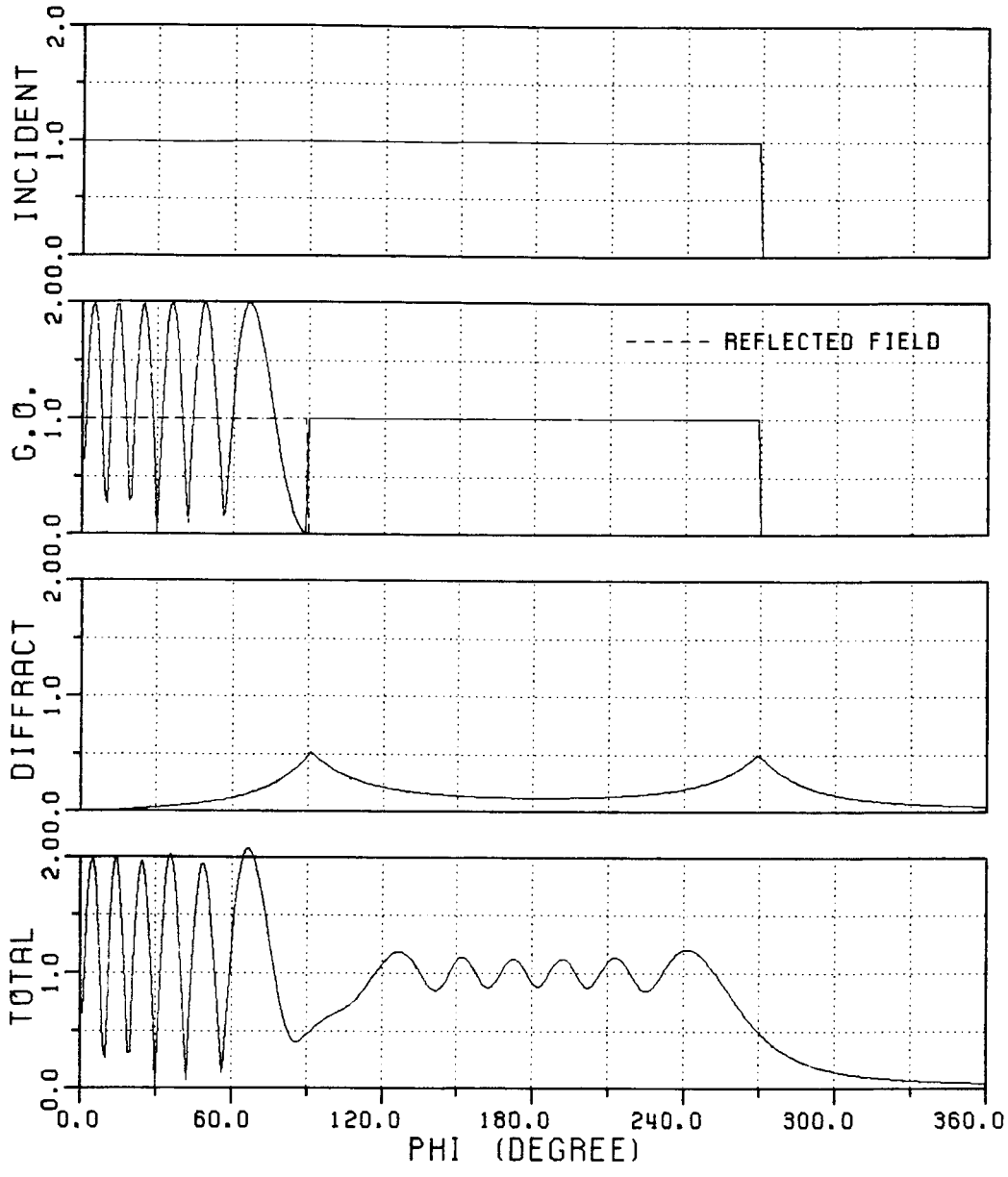

RS= 0.5 ϕ' = 90.0 (DEGREE)
XS= 0.5 R = 3.0 (LAMBDA)

Figure 31 Incident, reflected, diffracted and total fields for a plane wave of unit strength which is polarized such that $\bar{E}^i = \hat{y}E^i_y$.

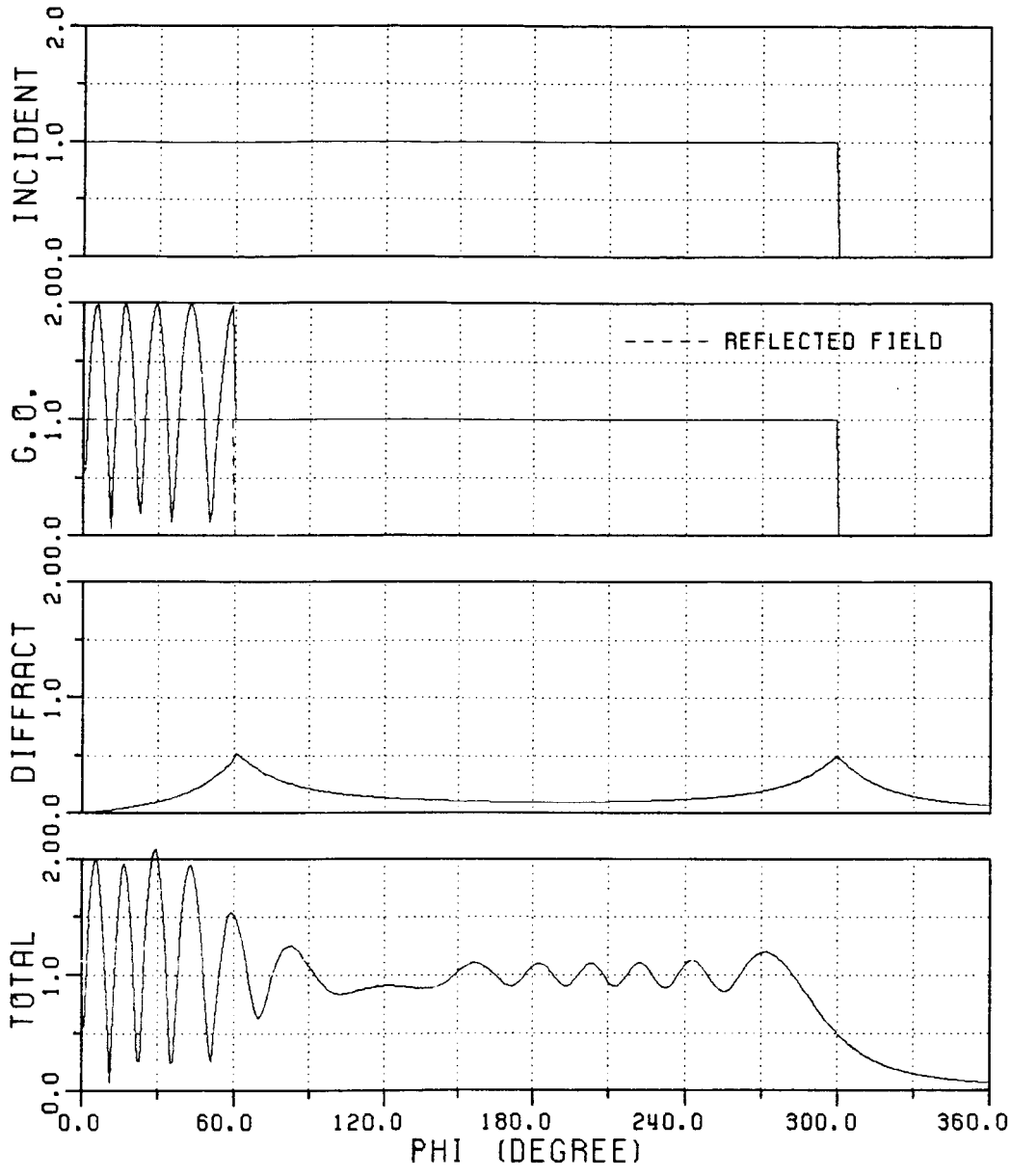

RS= 0.5 ϕ' = 120.0 (DEGREE)
XS= 0.5 R = 3.0 (LAMBDA)

Figure 32 Incident, reflected, diffracted and total fields for a plane wave of unit strength which is polarized such that $\bar{E}^i = \hat{y}E^i_y$.

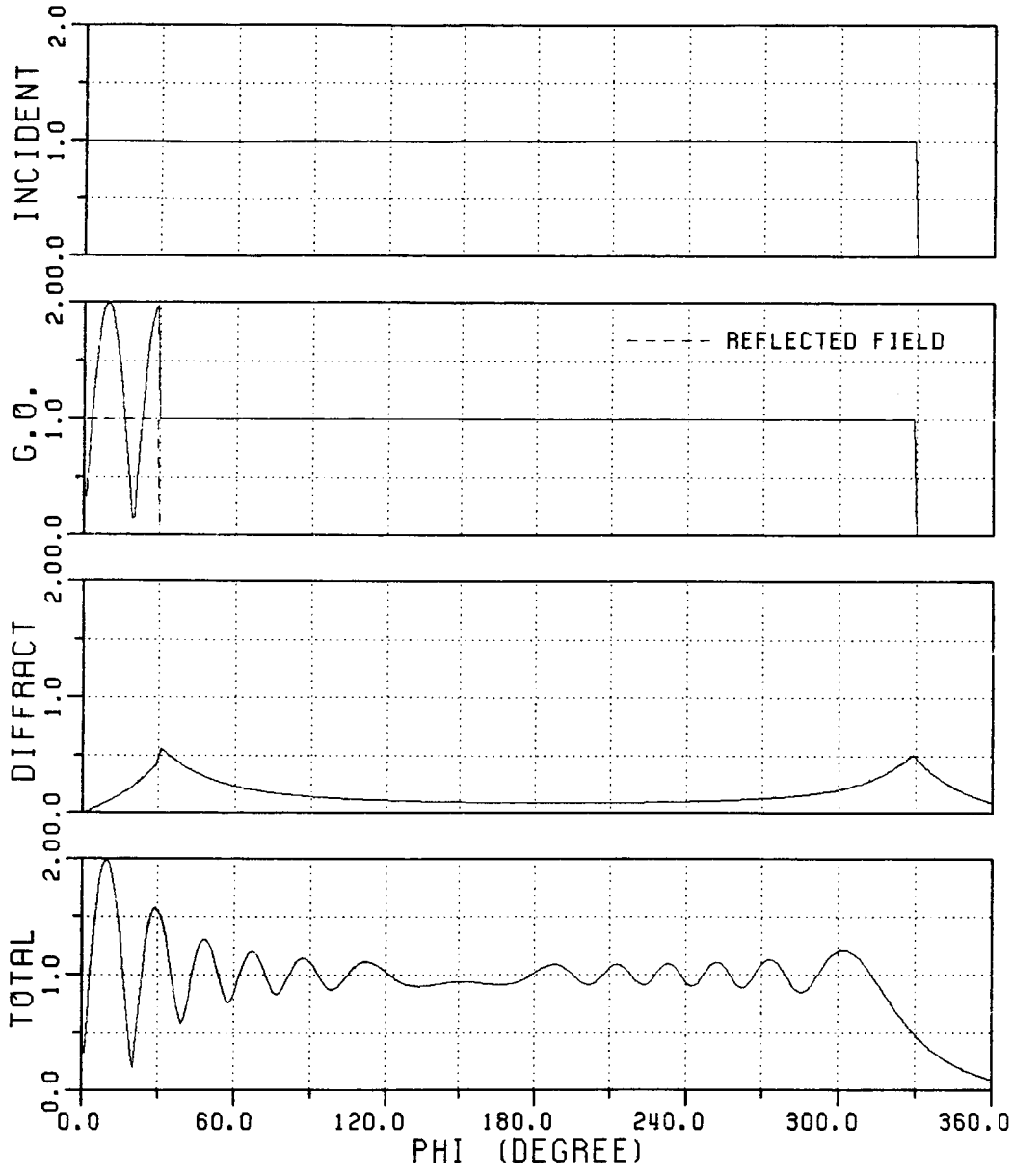

RS= 0.5 ϕ' = 150.0 (DEGREE)
XS= 0.5 R = 3.0 (LAMBDA)

Figure 33 Incident, reflected, diffracted and total fields for a plane wave of unit strength which is polarized such that $\bar{E}^i = \hat{y}E_y^i$.

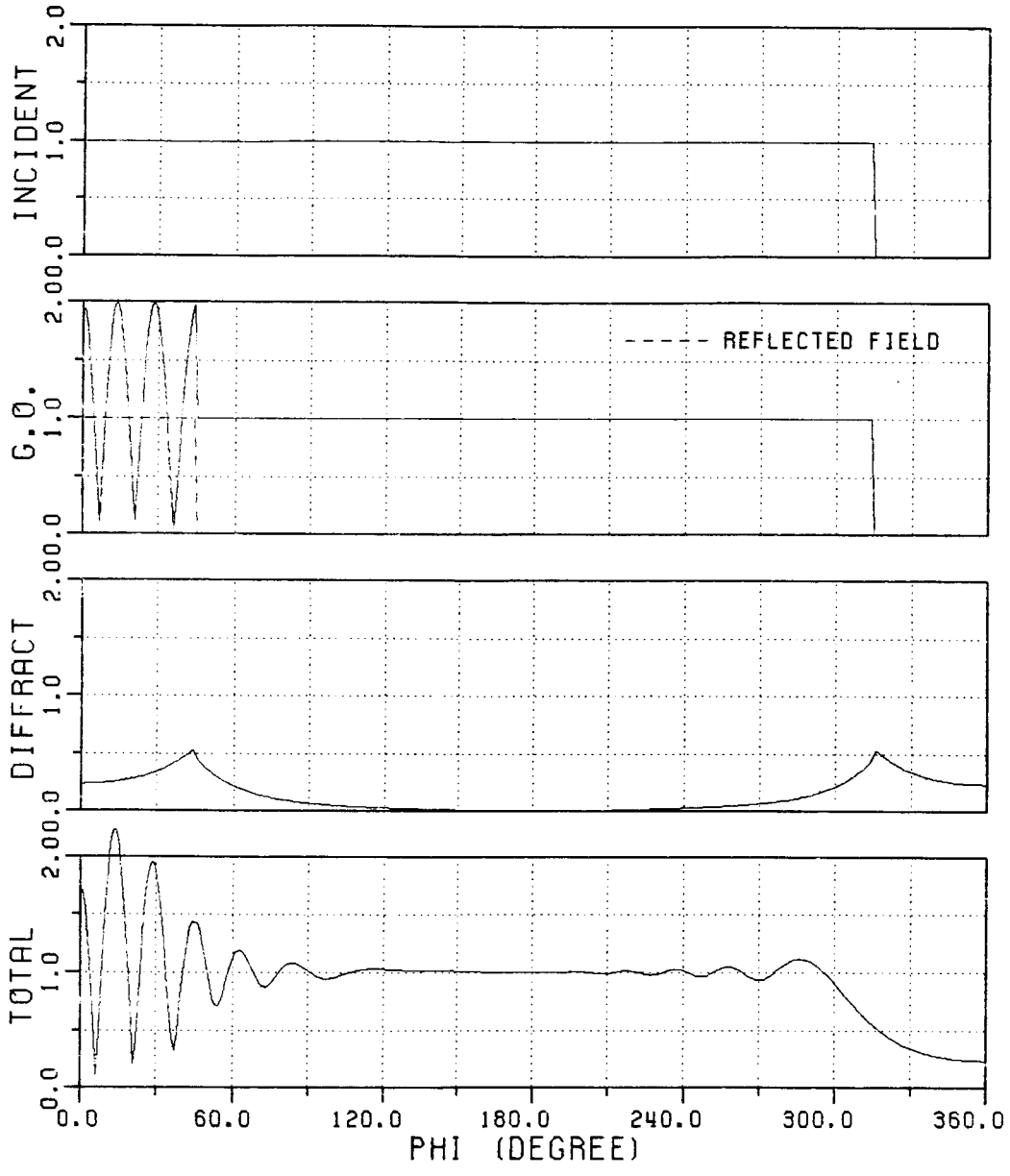

RS= 0.0 ϕ' = 135.0 (DEGREE)
XS= 0.0 R = 3.0 (LAMBDA)

Figure 34 Incident, reflected, diffracted and total field for a plane wave of unit strength which is polarized such that $\bar{H}^i = \hat{y}H_y^i$.

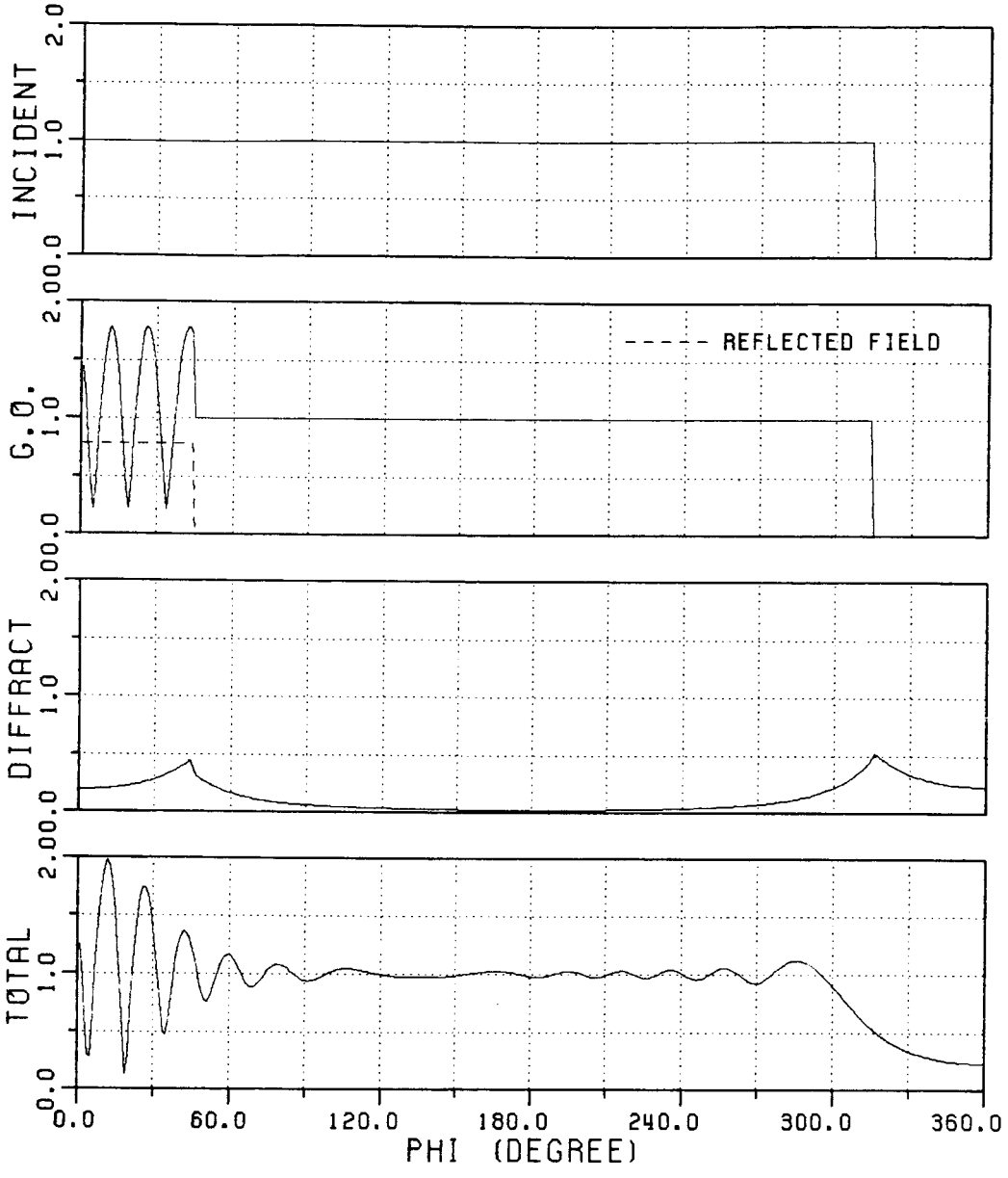

RS= 0.1 ϕ' = 135.0 (DEGREE)
XS= 0.3 R = 3.0 (LAMBDA)

Figure 35 Incident, reflected, diffracted and total field for a plane wave of unit strength which is polarized such that $\bar{H}^i = \hat{y}H_y^i$.

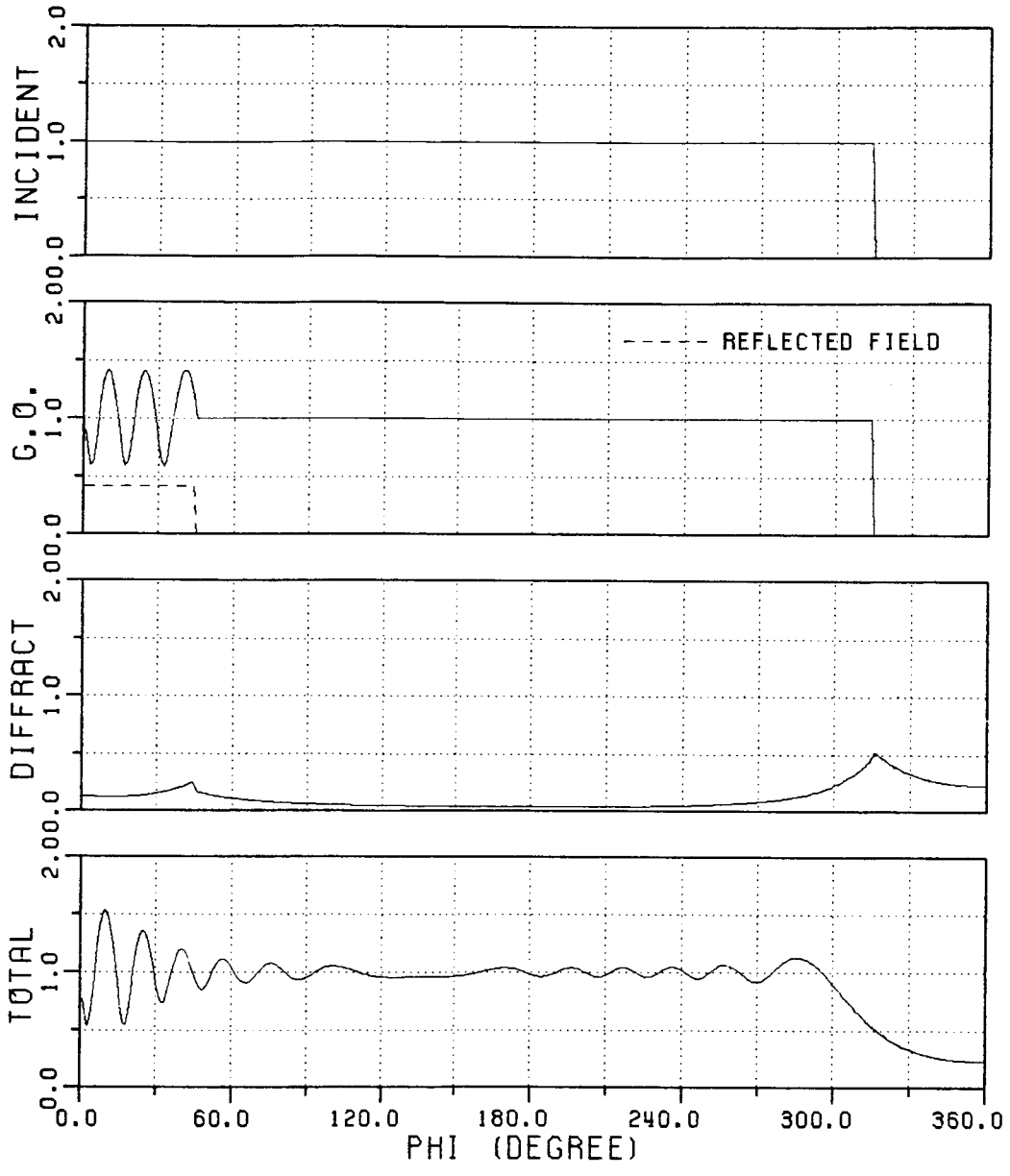

RS= 0.5 ϕ' = 135.0 (DEGREE)
XS= 0.5 R = 3.0 (LAMBDA)

Figure 36 Incident, reflected, diffracted and total field for a plane wave of unit strength which is polarized such that $\bar{H}^i = \hat{y}H_y^i$.

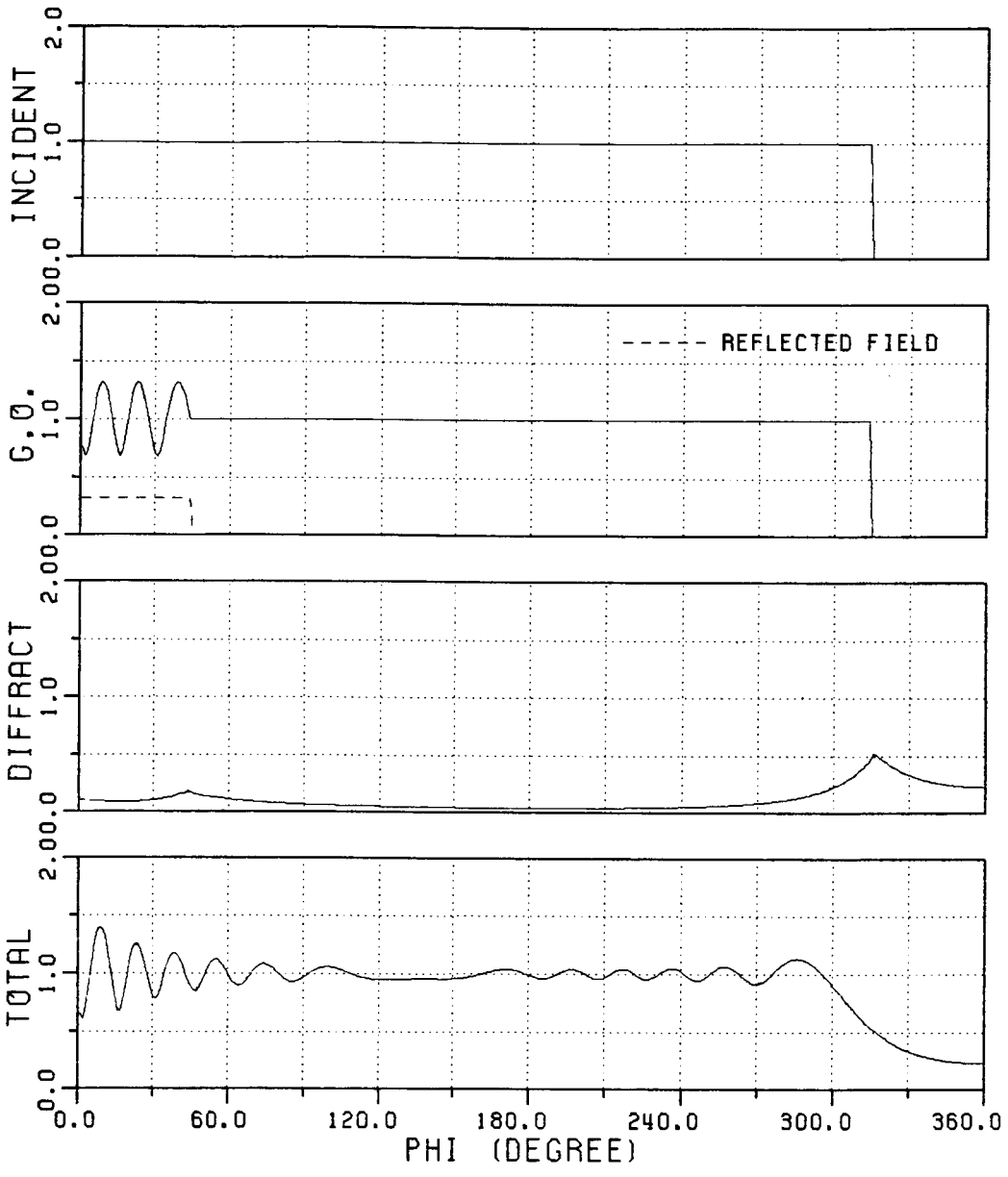

RS= 0.8 ϕ' = 135.0 (DEGREE)
XS= 0.5 R = 3.0 (LAMBDA)

Figure 37 Incident, reflected, diffracted and total field for a plane wave of unit strength which is polarized such that $\bar{H}^i = \hat{y}H_y^i$.

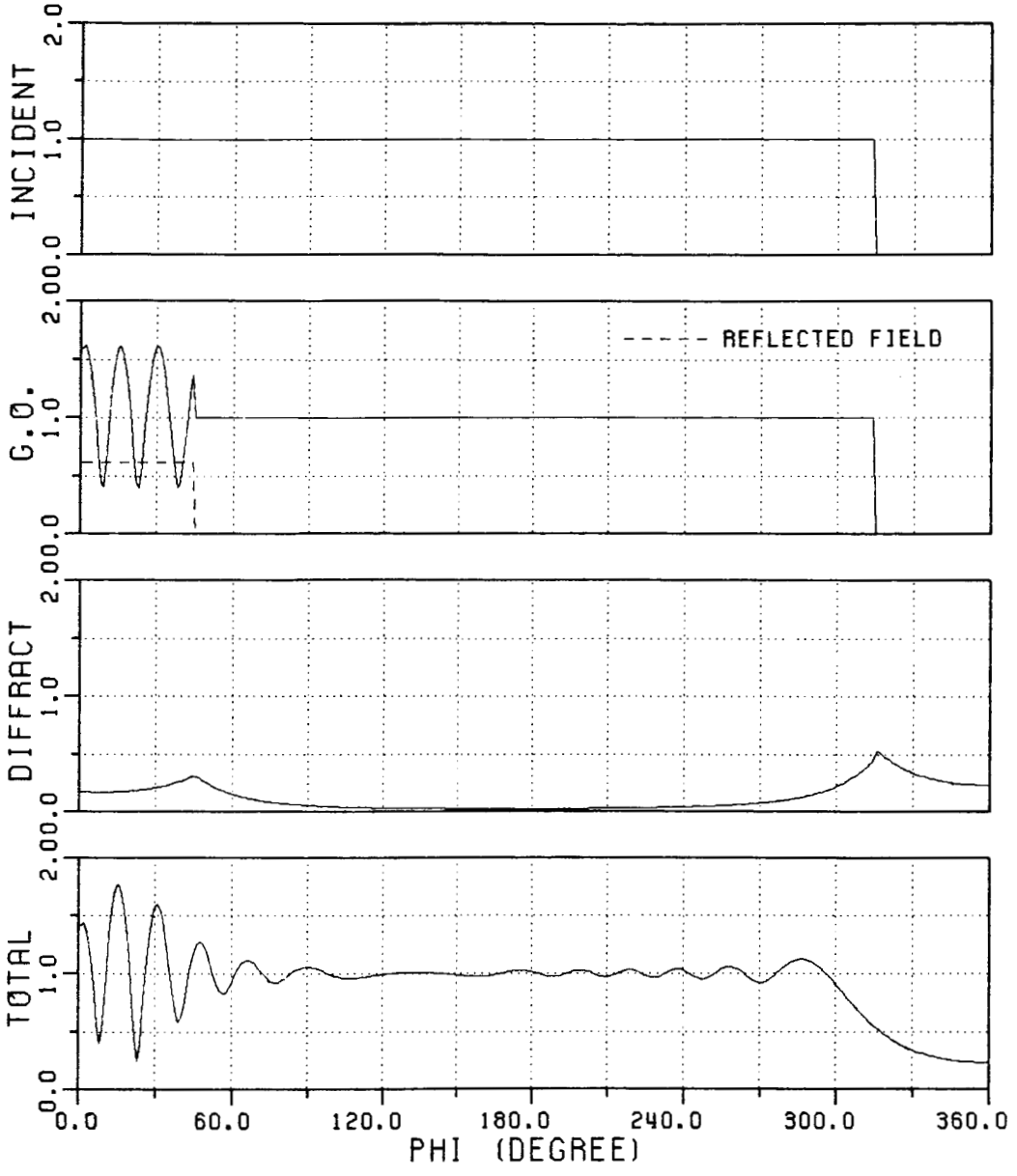

RS= 0.2 ϕ' = 135.0 (DEGREE)
XS= -0.3 R = 3.0 (LAMBDA)

Figure 38 Incident, reflected, diffracted and total field for a plane wave of unit strength which is polarized such that $\bar{H}^{i} = \hat{y}H_y^i$.

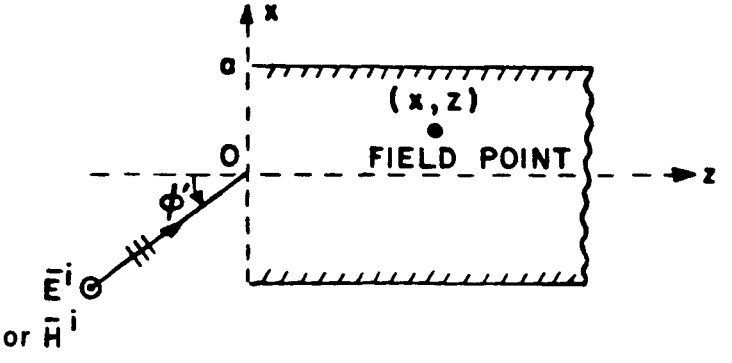

Figure 39. Semi-infinite parallel plate waveguide geometry showing the incident plane wave and the angle of incident.

from open end of the waveguide to the field point. Note that the backscattered field is entirely due to edge diffracted rays for the semi-infinite waveguide without any interior termination. These plots are repeated in Figures 55 and 56 as a function of the waveguide width for different wave polarizations.

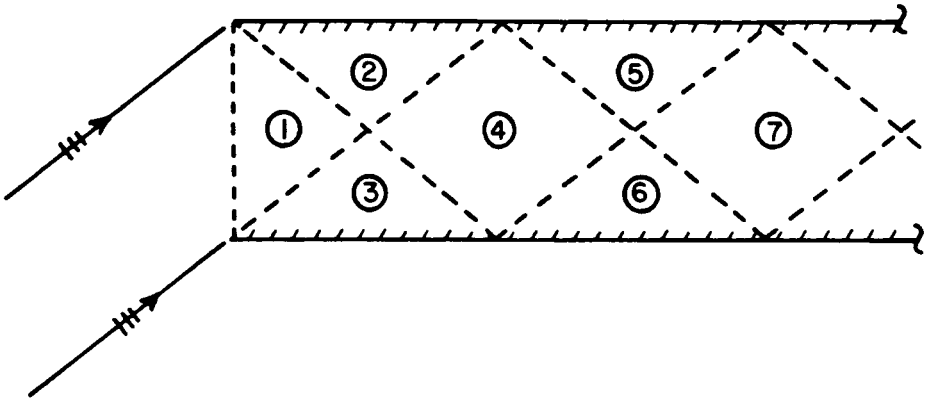

Region (1) Direct ray

(2) Direct and singly reflected rays

(3) None

(4) Singly reflected ray

(5) None

(6) Singly and doubly reflected rays

(7) Doubly reflected ray

Figure 40 Semi-infinite parallel plate wave guide showing different combinations of geometrical optical, direct, singly and multiply reflected rays in each region of the waveguide.

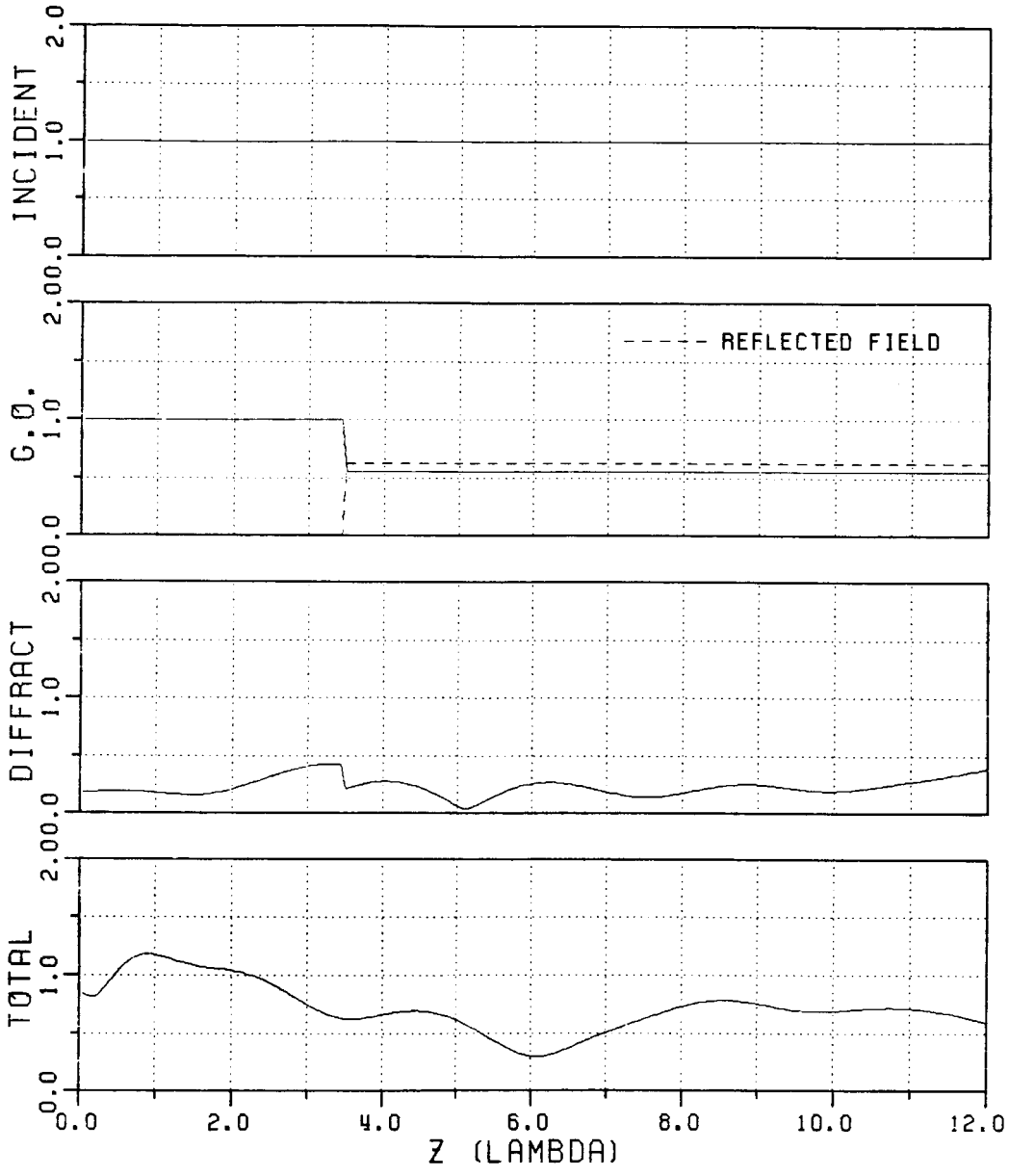

A = 5.0 (LAMBDA) RS = 0.5

X = 3.0 (LAMBDA) XS = 0.5

ϕ' = 30.0 (DEGREE)

Figure 41 Incident, reflected, diffracted and total fields as a function of the axial distance form open end to the field point for the plane wave with a parallel polarization (TM_y) case.

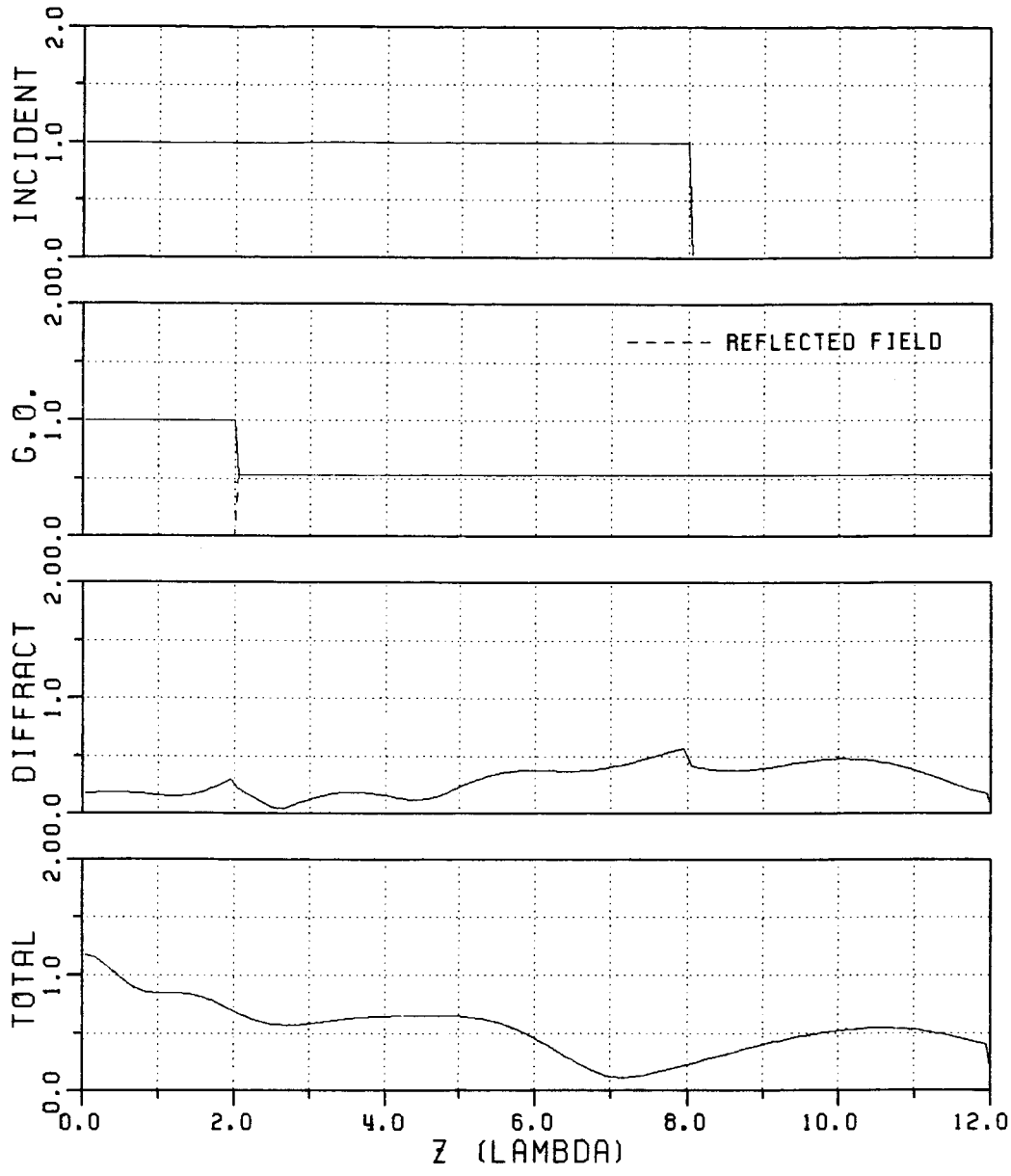

A = 5.0 (LAMBDA)
X = 3.0 (LAMBDA)
ϕ' = 45.0 (DEGREE)

RS = 0.5
XS = 0.5

Figure 42 Incident, reflected, diffracted and total fields as a function of the axial distance form open end to the field point for the plane wave with a parallel polarization (TM_y) case.

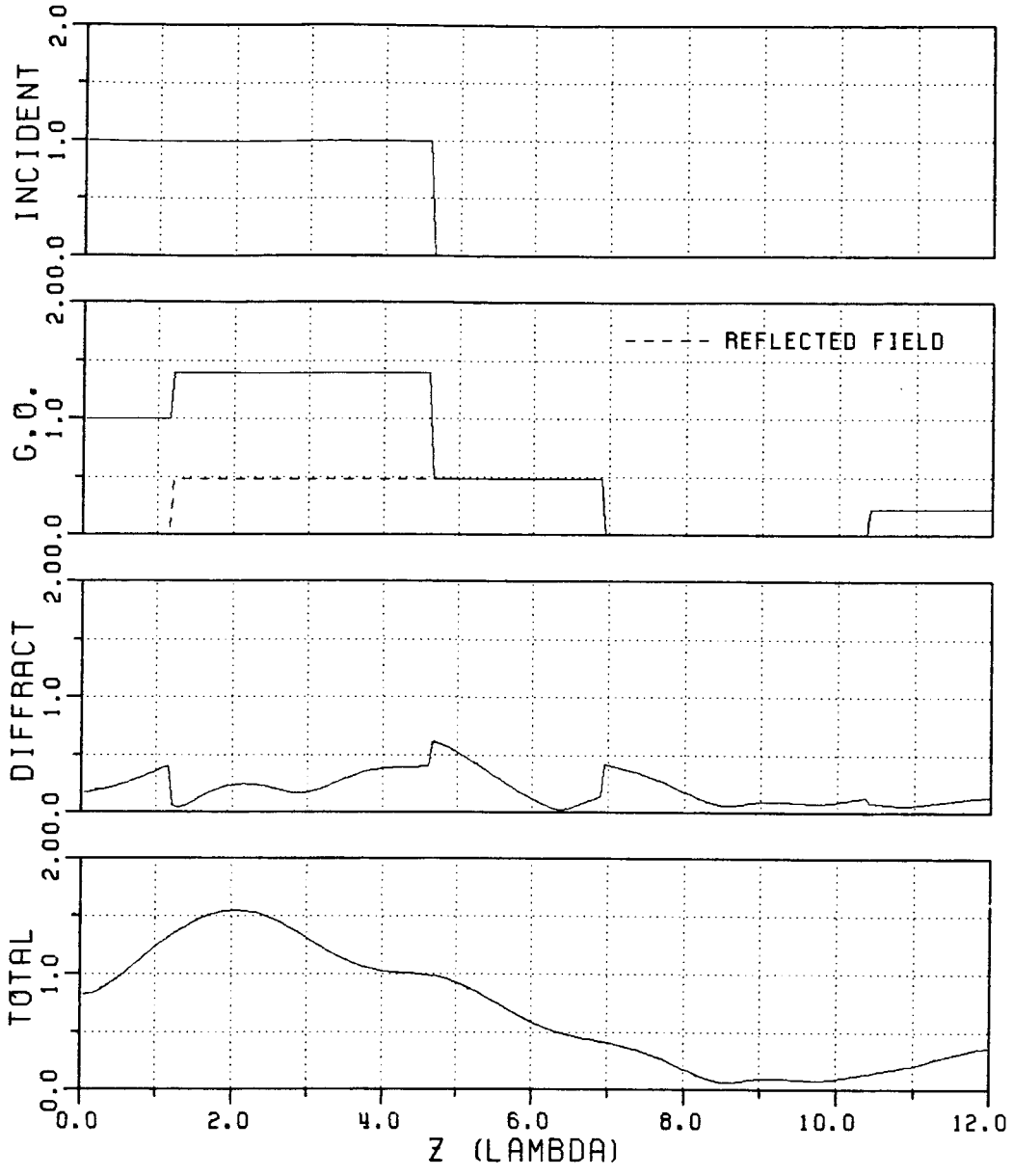

A = 5.0 (LAMBDA) RS = 0.5
X = 3.0 (LAMBDA) XS = 0.5
ϕ' = 60.0 (DEGREE)

Figure 43 Incident, reflected, diffracted and total fields as a function of the axial distance form open end to the field point for the plane wave with a parallel polarization (TM_y) case.

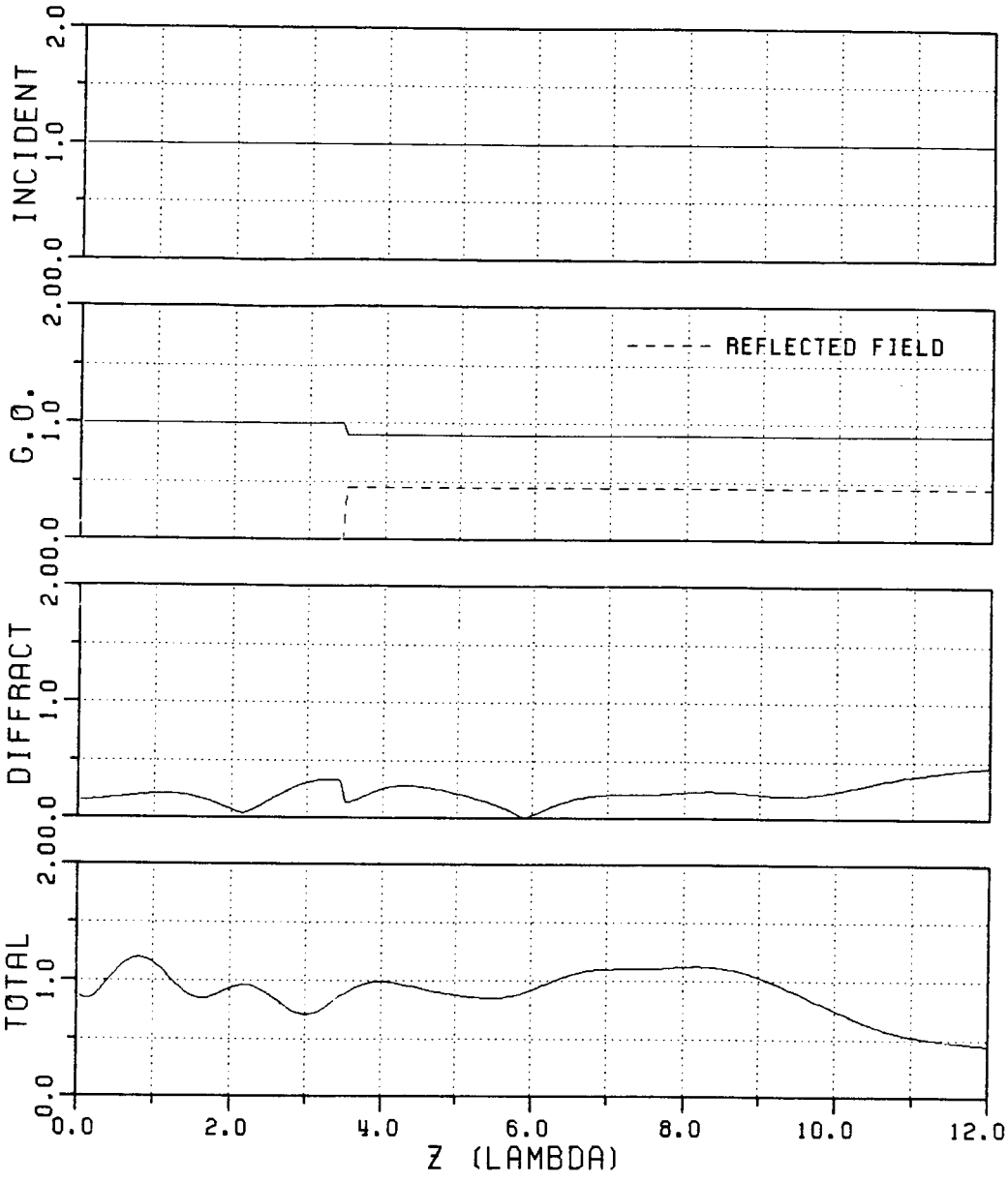

A = 5.0 (LAMBDA) RS = 0.5
X = 3.0 (LAMBDA) XS = 0.5
ϕ' = 30.0 (DEGREE)

Figure 44 Incident, reflected, diffracted and total fields as a function of the axial distance from open end to the field point for the plane wave with a perpendicular polarization (TE_y) case.

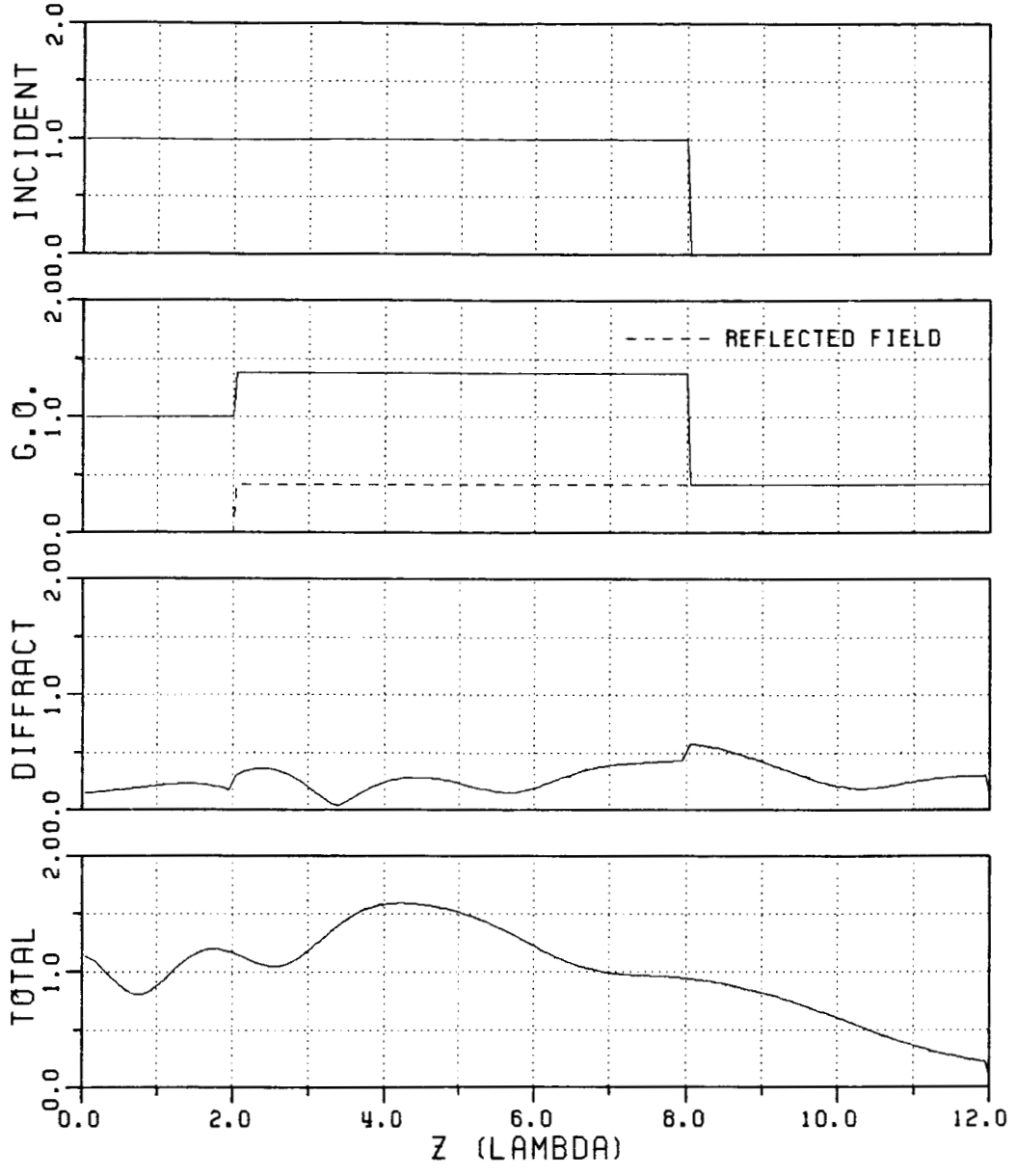

A = 5.0 (LAMBDA) RS = 0.5

X = 3.0 (LAMBDA) XS = 0.5

ϕ' = 45.0 (DEGREE)

Figure 45 Incident, reflected, diffracted and total fields as a function of the axial distance from open end to the field point for the plane wave with a perpendicular polarization (TE_y) case.

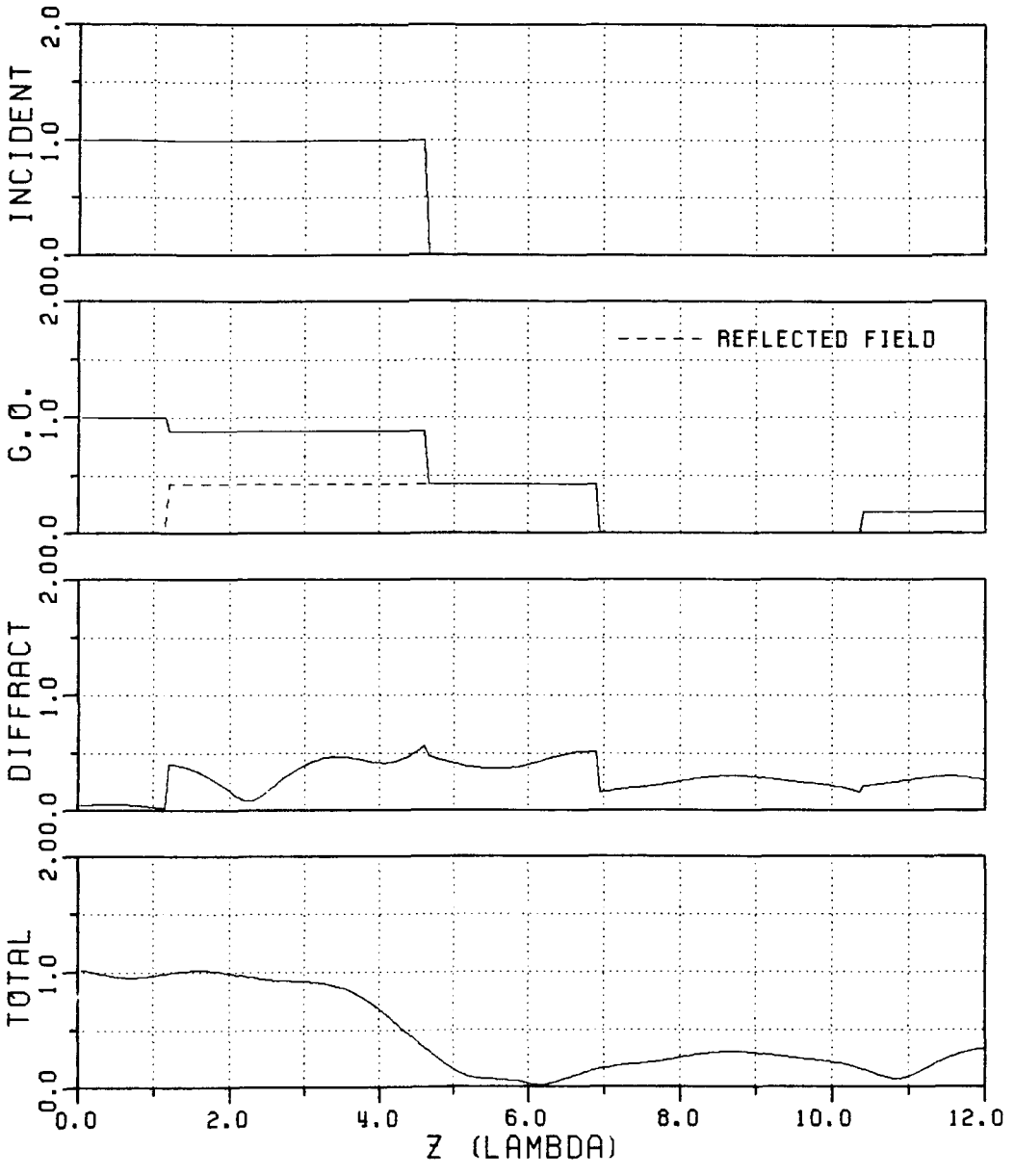

A = 5.0 (LAMBDA)
X = 3.0 (LAMBDA)
ϕ' = 60.0 (DEGREE)

RS = 0.5
XS = 0.5

Figure 46 Incident, reflected, diffracted and total fields as a function of the axial distance from open end to the field point for the plane wave with a perpendicular polarization (TE_y) case.

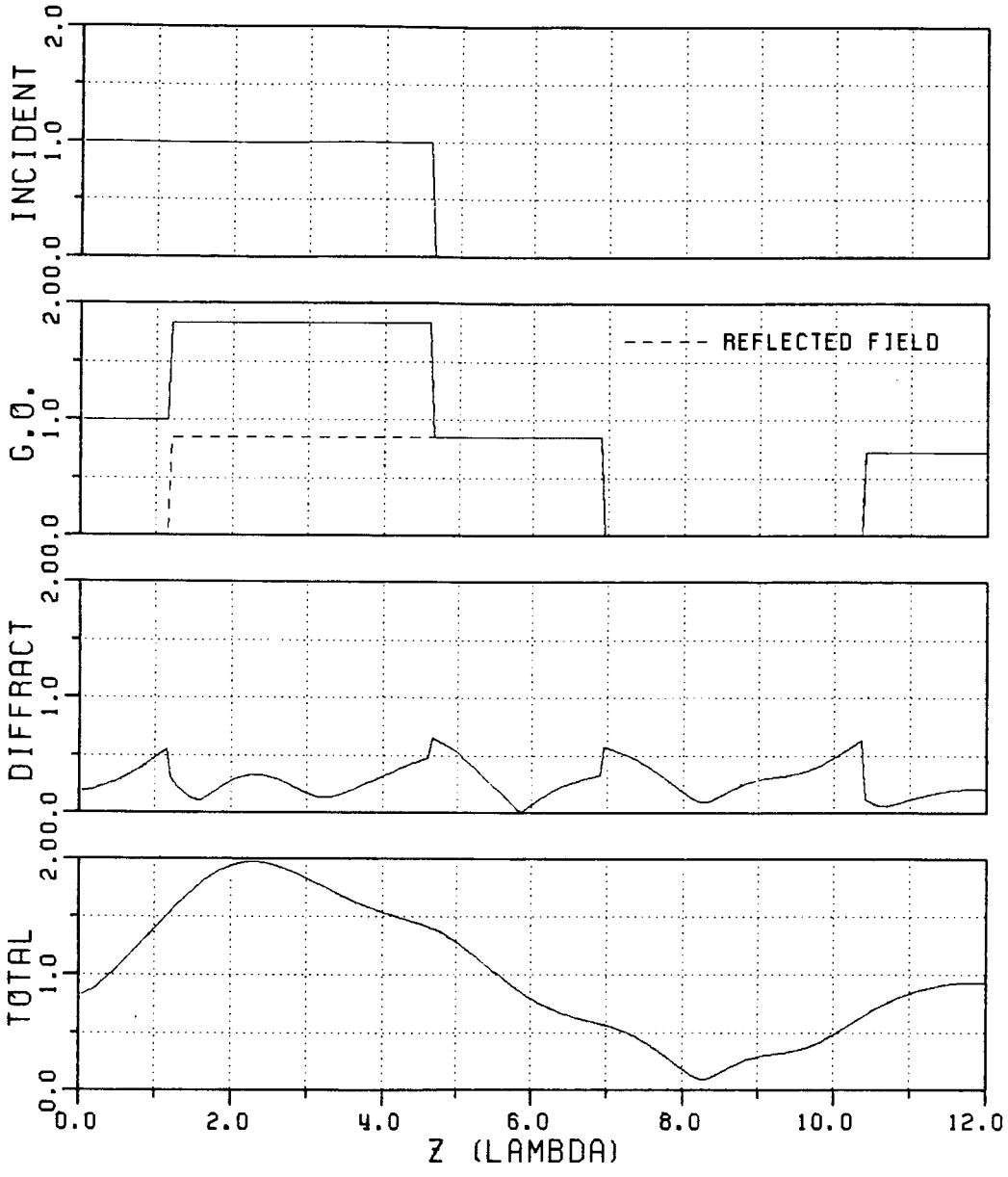

A = 5.0 (LAMBDA)
X = 3.0 (LAMBDA)
ϕ' = 60.0 (DEGREE)

RS = 0.1
XS = 0.3

Figure 47 Incident, reflected, diffracted and total fields as a function of the axial distance from open end to the field point for the plane wave with a parallel polarization (TM_y) case.

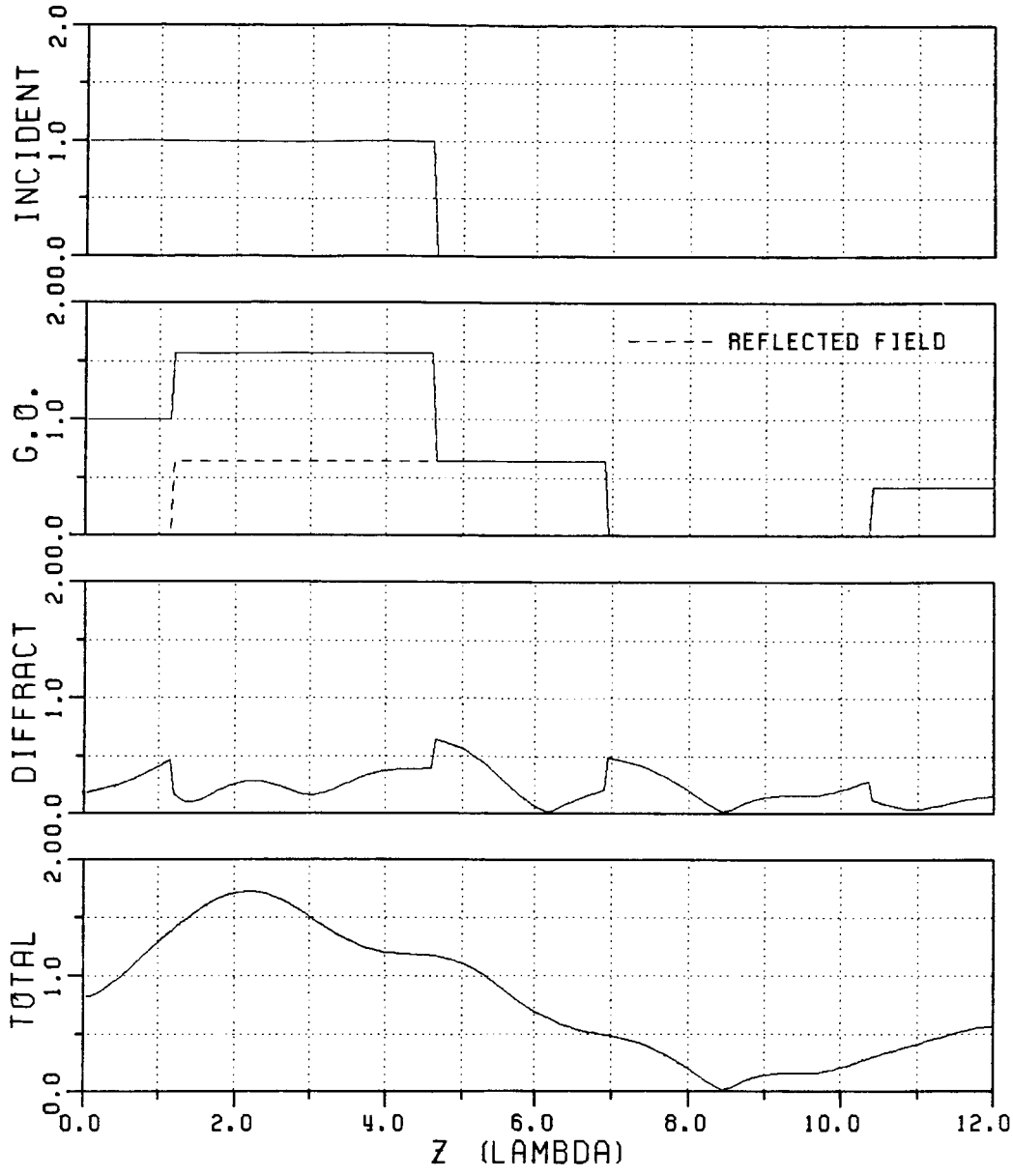

A = 5.0 (LAMBDA) RS = 0.3
X = 3.0 (LAMBDA) XS = 0.5
ϕ' = 60.0 (DEGREE)

Figure 48 Incident, reflected, diffracted and total fields as a function of the axial distance from open end to the field point for the plane wave with a parallel polarization (TM_y) case.

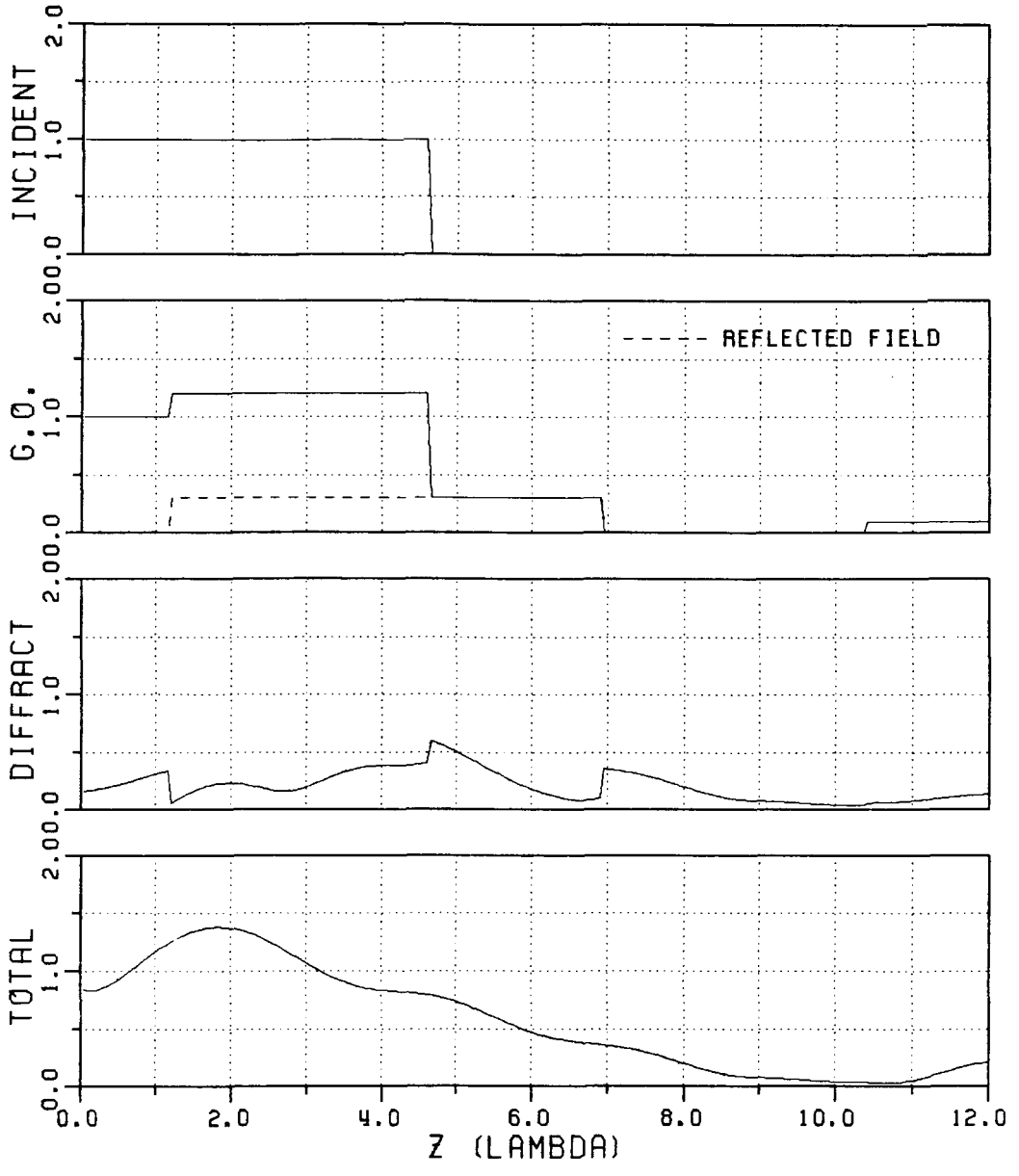

A = 5.0 (LAMBDA) RS = 0.8
X = 3.0 (LAMBDA) XS = 0.5
ϕ' = 60.0 (DEGREE)

Figure 49 Incident, reflected, diffracted and total fields as a function of the axial distance from open end to the field point for the plane wave with a parallel polarization (TM_y) case.

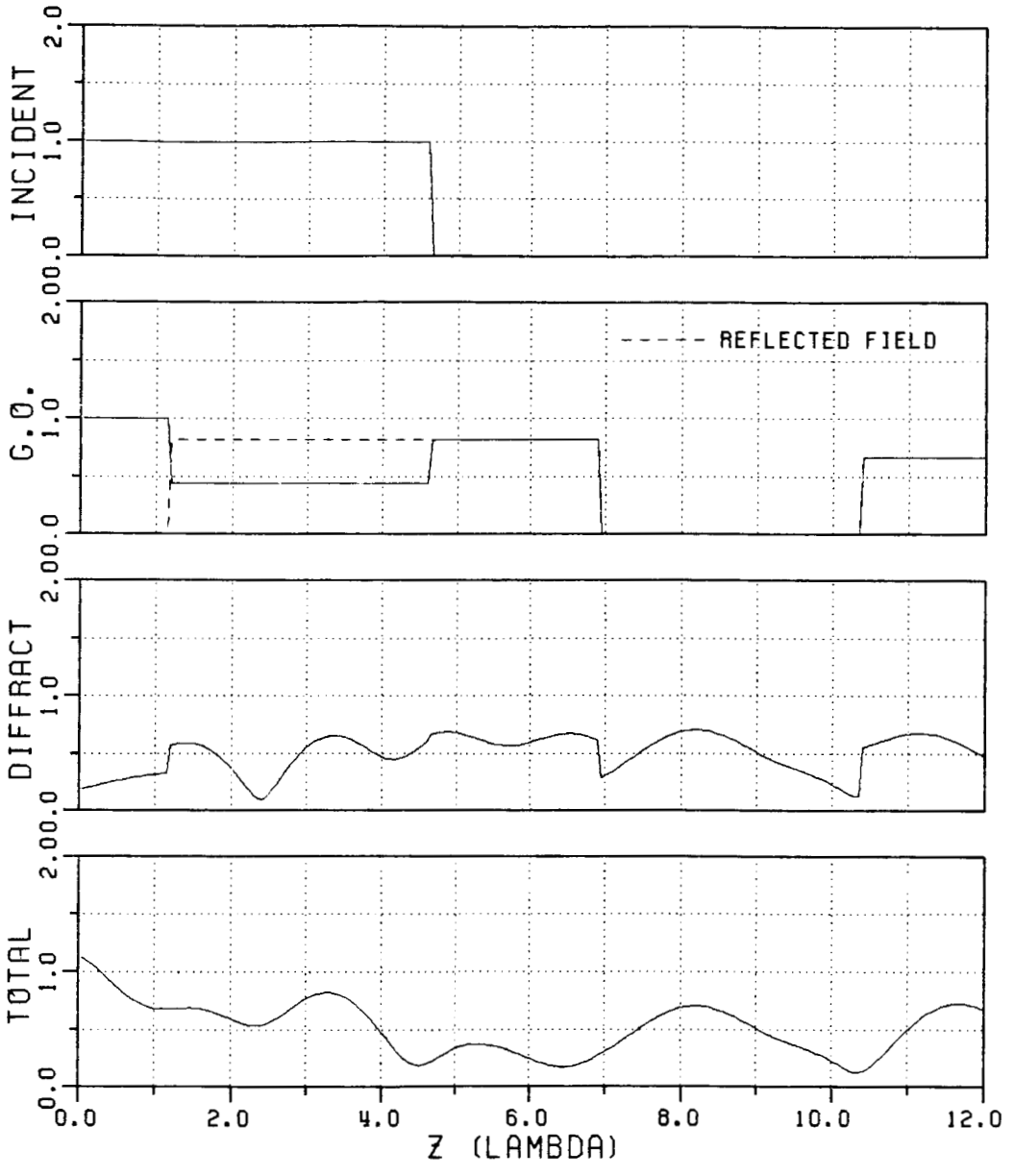

A = 5.0 (LAMBDA) RS = 0.1

X = 3.0 (LAMBDA) XS = 0.3

ϕ' = 60.0 (DEGREE)

Figure 50 Incident, reflected, diffracted and total fields as a function of the axial distance from open end to the field point for the plane wave with a perpendicular polarization (TE_y) case.

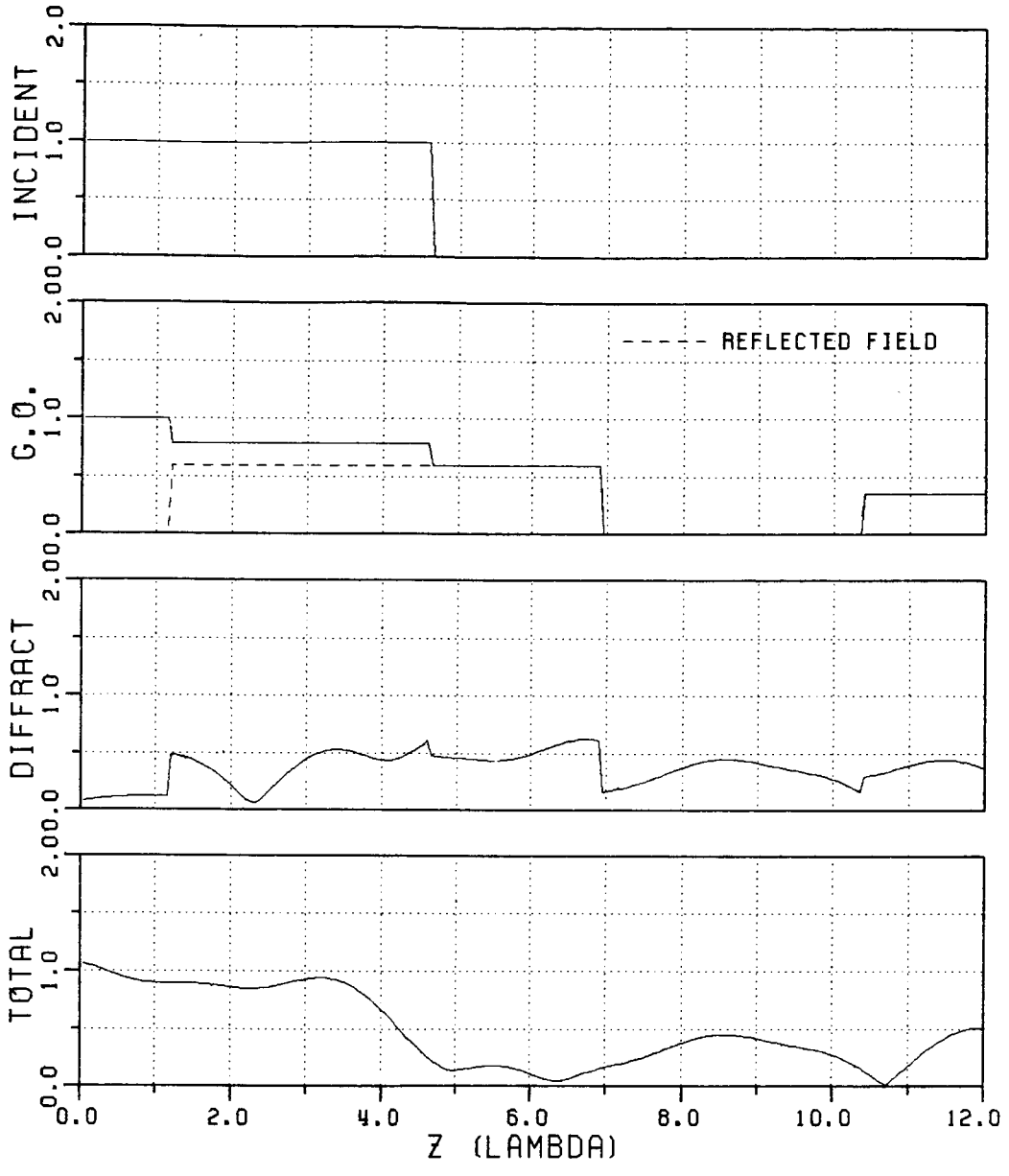

A = 5.0 (LAMBDA) RS = 0.3
X = 3.0 (LAMBDA) XS = 0.5
ϕ' = 60.0 (DEGREE)

Figure 51 Incident, reflected, diffracted and total fields as a function of the axial distance from open end to the field point for the plane wave with a perpendicular polarization (TE_y) case.

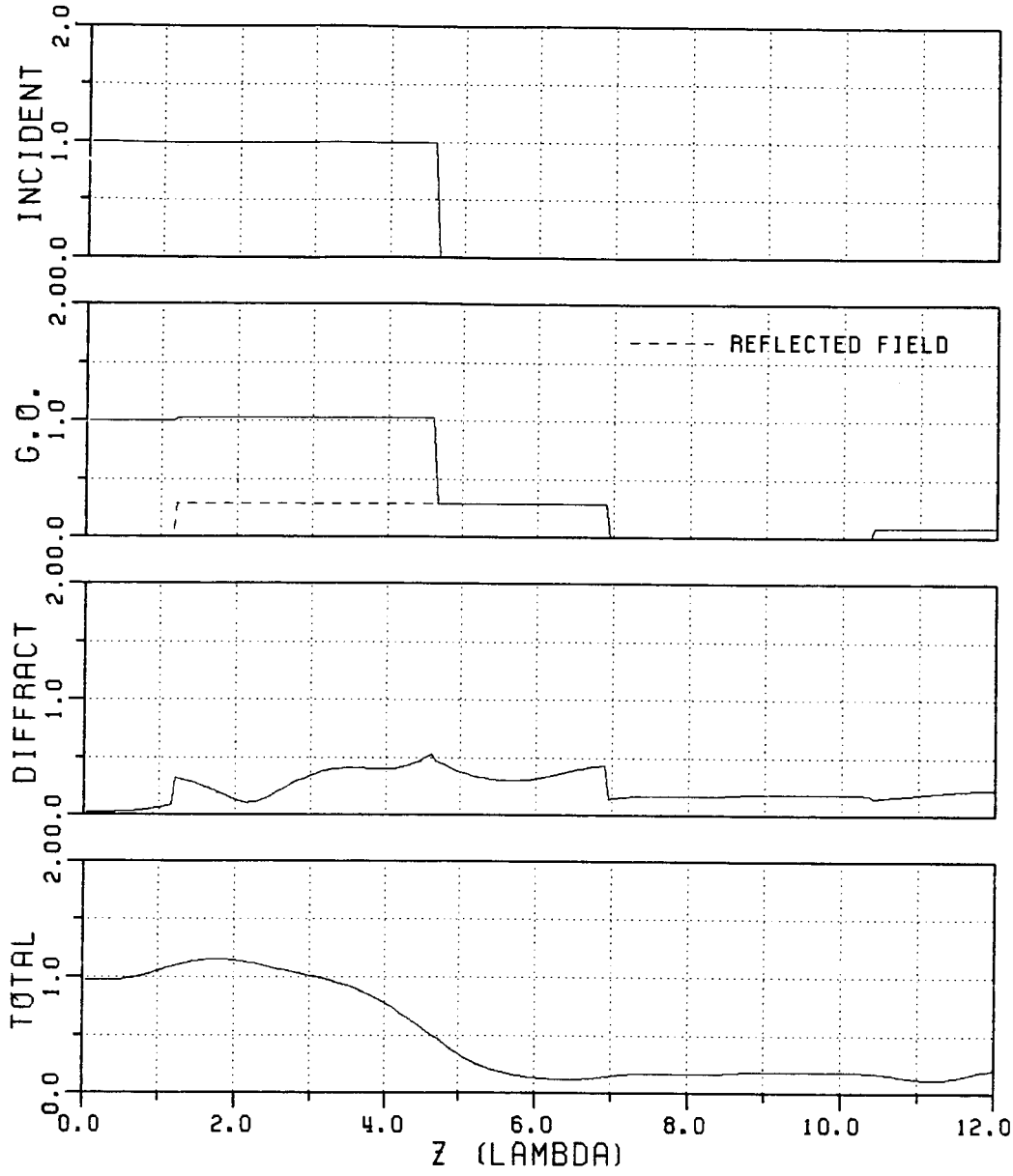

A = 5.0 (LAMBDA)
X = 3.0 (LAMBDA)
ϕ' = 60.0 (DEGREE)

RS = 0.8
XS = 0.5

Figure 52 Incident, reflected, diffracted and total fields as a function of the axial distance from open end to the field point for the plane wave with a perpendicular polarization (TE_y) case.

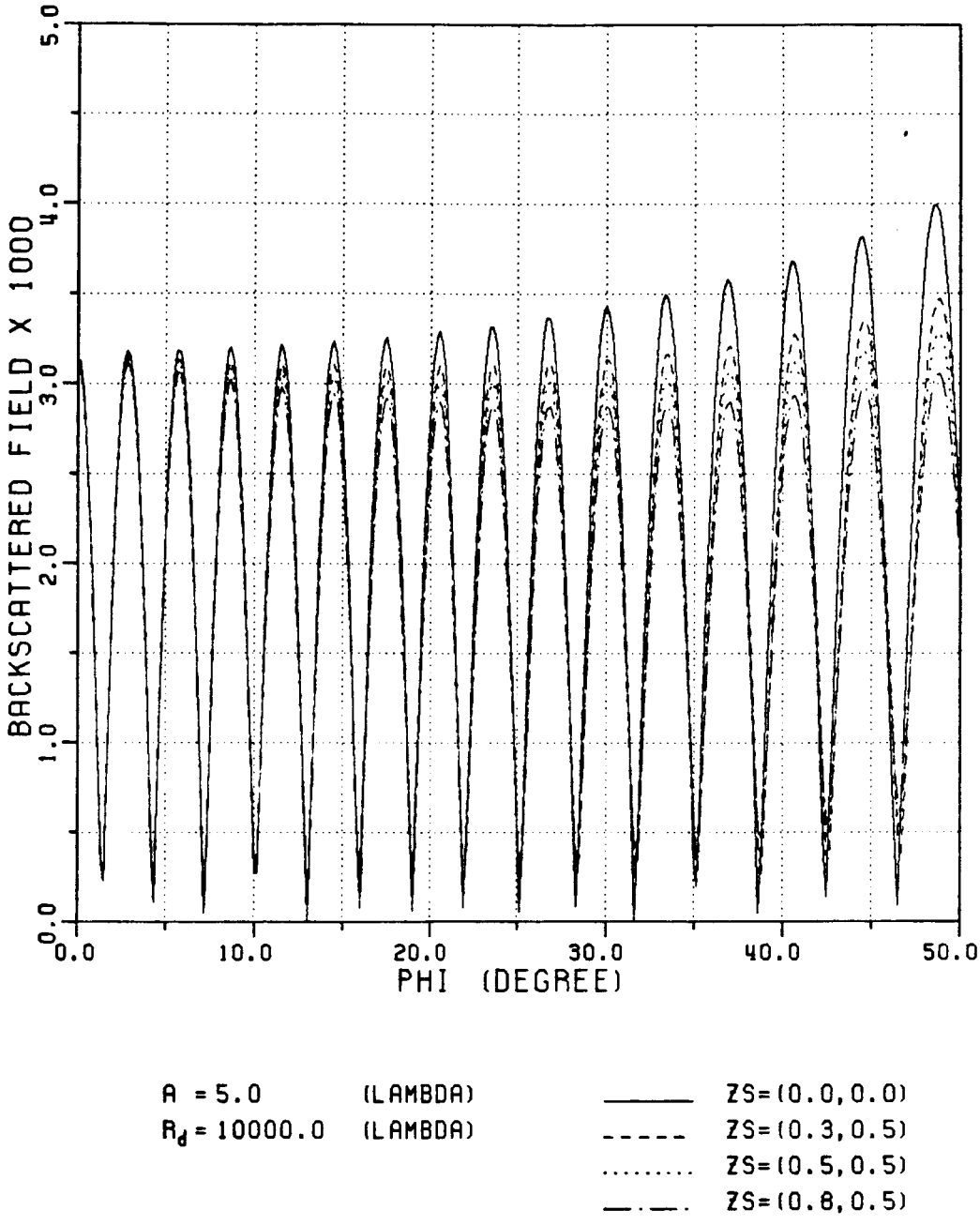

Figure 53 Backscattered field as a function of incident angle for a parallel polarization case.

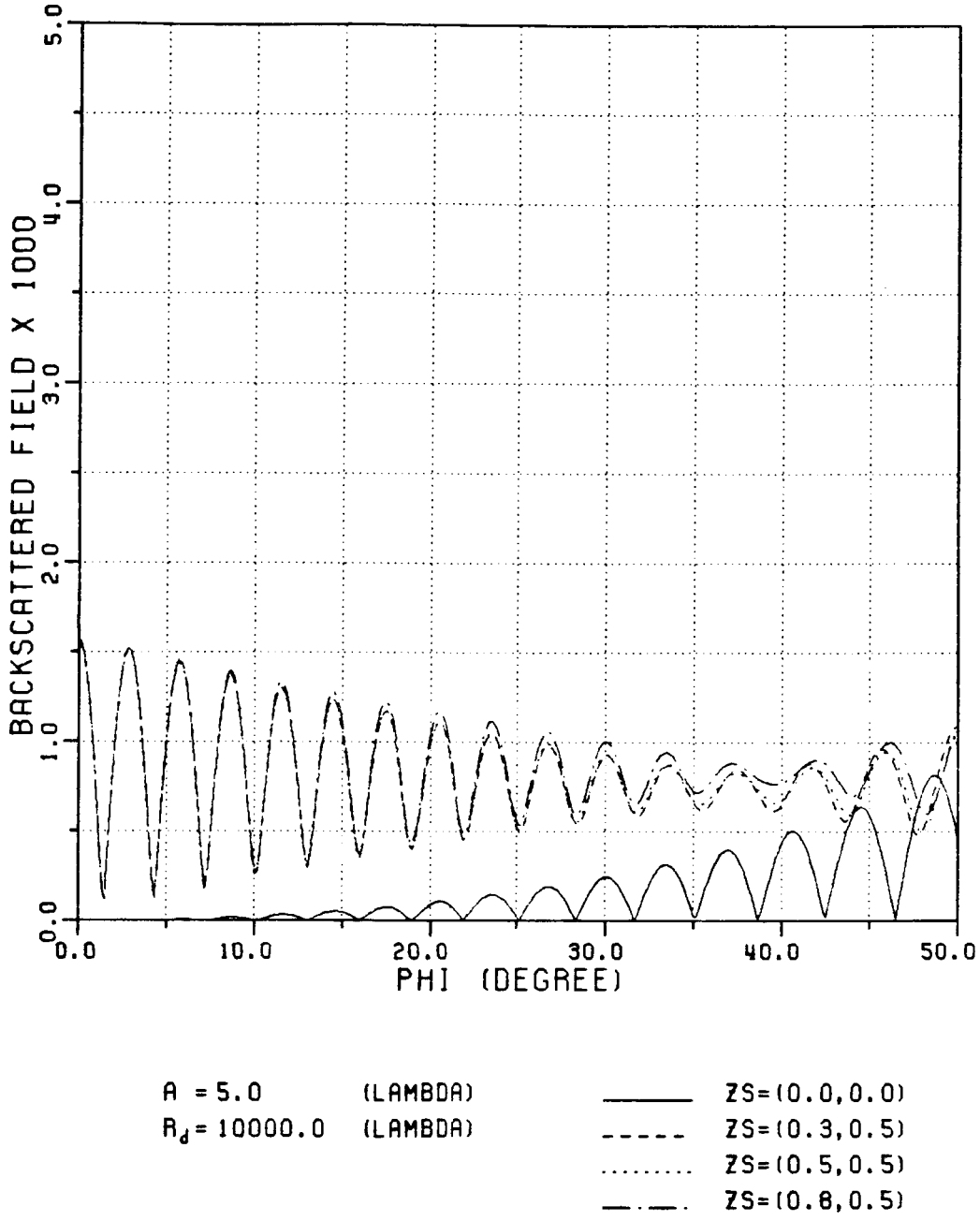

Figure 54 Backscattered field as a function of incident angle for a perpendicular polarization case.

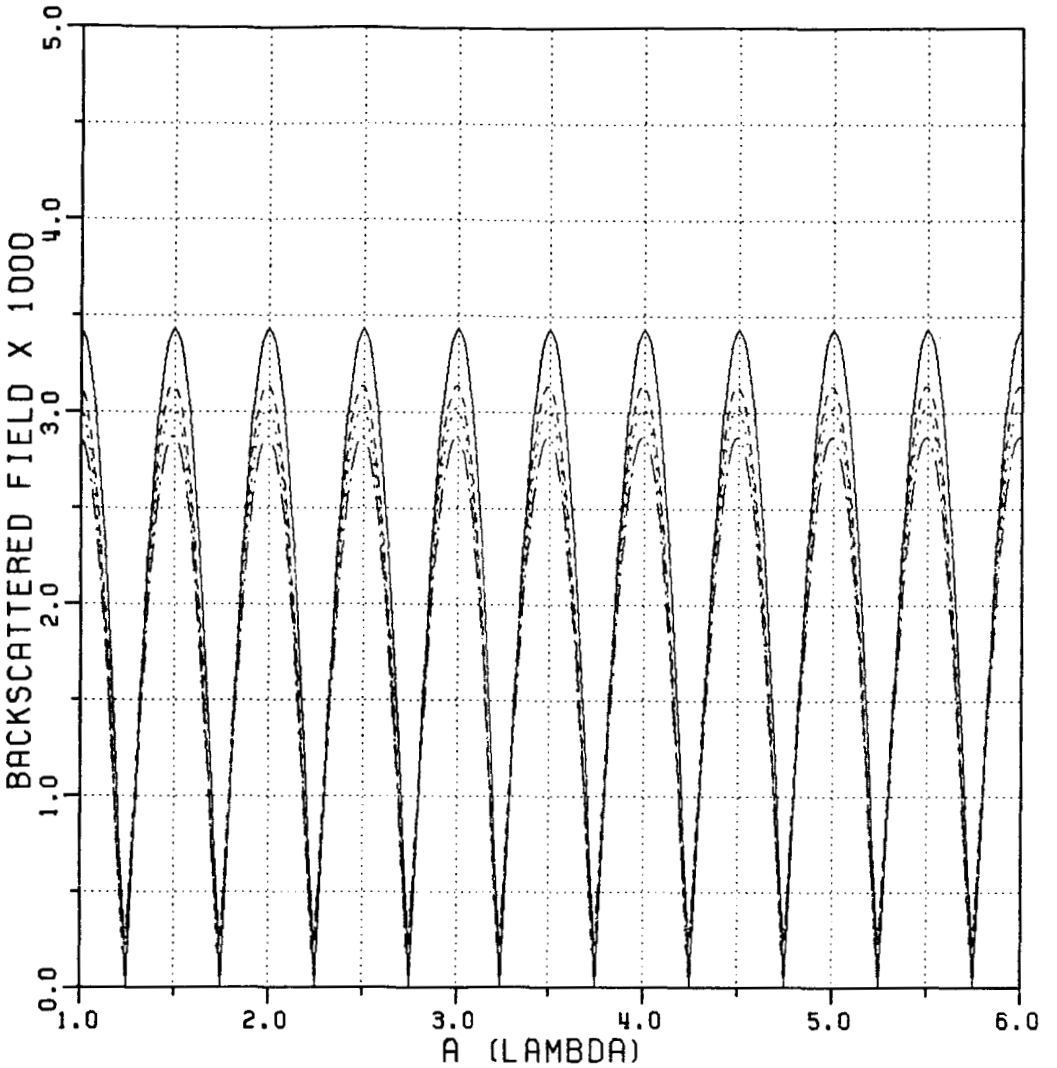

Figure 55 Backscattered field as a function of waveguide width for a parallel polarization case.

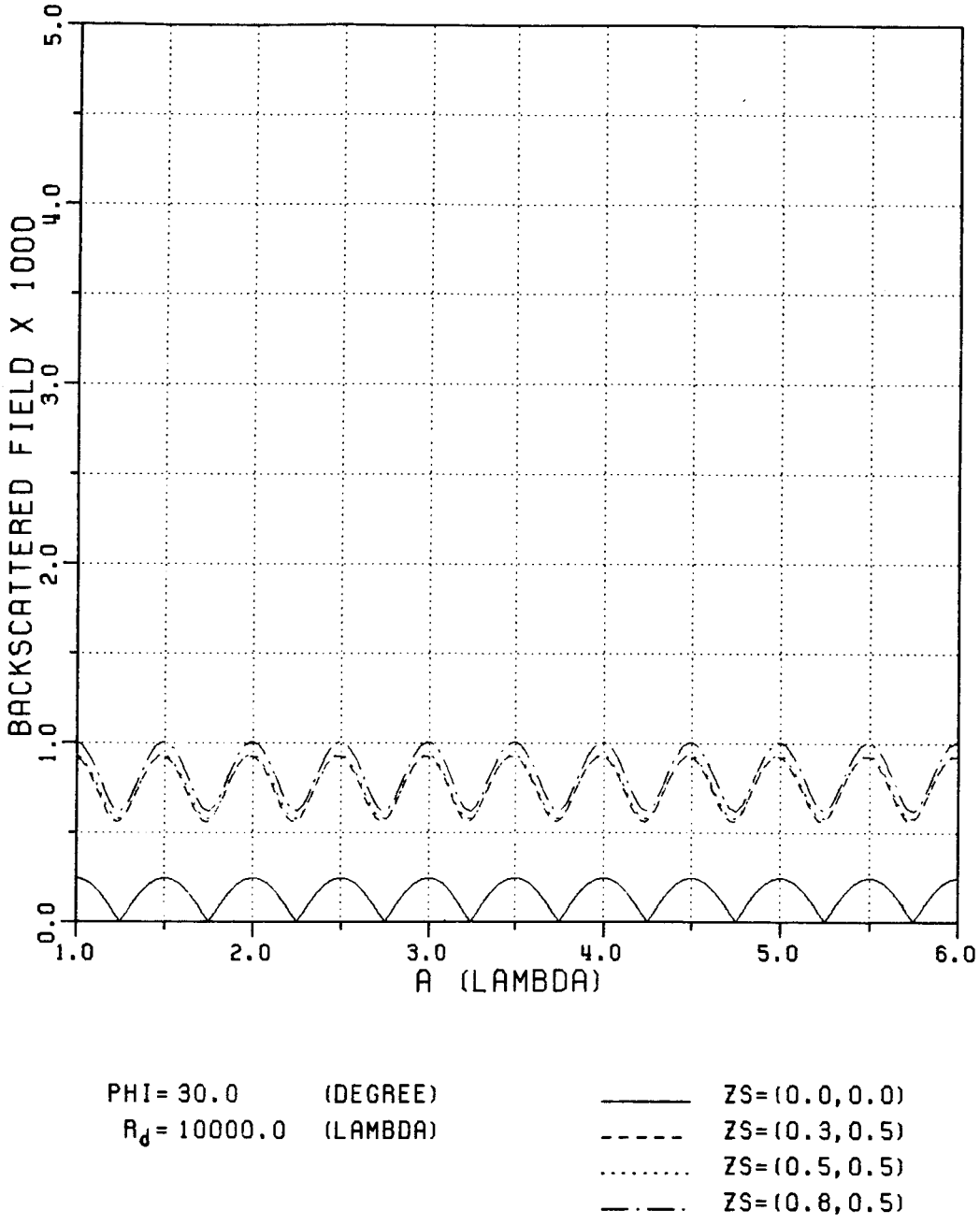

Figure 56 Backscattered field as a function of waveguide width for a perpendicular polarization case.

IV. SUMMARY AND DISCUSSION

Electromagnetic (EM) plane wave scattering by an open ended, perfectly-conducting, semi-infinite parallel plate waveguide with a thin, uniform layer of lossy material on its inner wall which is approximated by a surface impedance boundary condition is analyzed by the ray method. The ray method provides an approximate but sufficiently accurate analysis for this problem as long as the waveguide is large (in terms of the wavelength) to propagate the fields within. The numerical results from the ray method are compared with those obtained from the formally exact conventional modal solution for only the interior waveguide problem (involving an infinitely long waveguide) in order to check the accuracy of the interior ray solution. It is found that there is very good agreement between the two solutions.

Some of the advantages of the purely ray approach over the modal approach are that it does afford some physical insight into the scattering mechanisms particularly in connection with the coupling of the fields from the exterior to the interior regions in the case of the semi-infinite waveguide configuration, as well as into the effect of the wall impedance on the fields in the interior waveguide region. Also, the ray solution does not require one to evaluate the eigenvalues which are essential for the construction of the modal solution; these modal eigenvalues must be found numerically for different impedance values,

and for each mode, making the modal approach more inefficient as compared to the ray approach. Furthermore, it was found that, in general, the ray solution converged faster than the modal solution for the case of interest, namely, when the wall surface impedance contained loss. Furthermore, it was also found in this work that, in general, the rate of convergence of the modal solution did not improve significantly even with the presence of loss in the wall surface impedance.

The ray solution which has been developed for the 2-D semi-infinite parallel plate waveguide configuration of Figure 1 will be extended next to analyze the 3-D problem of EM plane wave scattering by a hollow, open-ended semi-infinite perfectly-conducting circular duct with a thin absorber coating on the inner wall. During the initial phase of this study, the absorber coating on the conducting circular waveguide walls will be approximated by a uniform surface impedance boundary condition. Subsequently, the impedance boundary condition will be relaxed in both the 2-D and 3-D cases to accommodate a moderately thin absorber coating. such as a lossy dielectric or ferrite coating of finite thickness (in which the thickness is electrically small). The effect on the interior waveguide fields due to variations in the electrical parameters and the thickness of the dielectric/ferrite wall coating would be of special interest in this study.

REFERENCES

[1] B. Friedman, Principles and Techniques of Applied Mathmatics, John Wiley and Sons, Inc., 1966.

[2] L.B. Felsen and N. Marcuvitz, Radiation and Scattering of Waves, Prentice Hall, Englewood Cliffs, New Jersey, 1973.

[3] G.D. Maliuzhinets, "Excitation, Reflection and Emission of Surface Waves from a Wedge with Given Fact Impedances," Soviet Phy. Dokl., Engl. Transl.,3, pp. 752-755.

[4] W.D. Burnside and K.W. Burgener, "High Frequency Scattering by a Thin Lossless Dielectric Slab," IEEE Trans. Antennas Propagat., vol. AP-31, no. 1, pp. 104-110, Jan. 1983.

[5] J.B. Keller, "Geometrical theory of diffraction." J. Opt. Soc. of Am., vol. 52, pp. 116-130, 1962.

[6] R.G. Kouyoumjian and P.H. Pathak, "A uniform geometrical theory of diffraction for an edge in a perfectly conducting surface," Proc. IEEE, vol. 62, pp. 1448-1461, 1974.

APPENDIX A

A METHOD OF THE NUMERICAL SOLUTION OF MODAL EIGENVALUES

The transcendental equation for solving the modal eigenvalues is obtained by setting the denominator of the integrand in Equation (6) equal to zero. Let this equation be written symbolically as $F(k_x) = 0$. This transcendental equation can be reexpressed in terms of any of its roots denoted by k_x as:

$$F(k_x) = (k_x+k\delta_0)(k_x+k\delta_a)e^{-j2k_xa} - (k_x-k\delta_0)(k_x-k\delta_a) \quad . \tag{A.1}$$

A popular method of finding the roots of a transcendental equation is the 'Newton-Raphson' method. The basic theory behind this method is that the function $F(x)$ is expanded in a Taylor series about some point x_0 which gives

$$F(x) = F(x_0) + (x-x_0)F'(x_0) + 1/2\ (x-x_0)^2\ F''(x_0) + \ldots \tag{A.2}$$

With the assumption that x is the root and x_0 is a good initial guess of the root, the series can be written approximately as

$$F(x) \approx F(x_0) + (x-x_0)F'(x_0) \quad . \tag{A.3}$$

since $(x-x_0)$ is small due to x being approximately equal to x_0 by a good initial guess.

Then the above equation can be rewritten as

$$x \approx x_0 - \frac{F(x_0)}{F'(x_0)} \quad , \tag{A.4}$$

which gives the iterative equation

$$x_{n+1} \approx x_n - \frac{F(x_n)}{F'(x_n)} \quad , \tag{A.5}$$

where x_n and x_{n+1} are the values of x after the n^{th} and $(n+1)^{th}$ iteration, respectively.

As seen from the above approximation, it is necessary to have a good initial guess when using the 'Newton-Raphson' method. This will allow rapid convergence to the proper root. The eigenvalues of the waveguide with perfectly-conducting inner walls are used as the initial guess in the modal analysis of the waveguide with impedance walls. The computer program stops iterating when the percent change in the magnitude of the root between successive iterations is less than 10^{-4}.

APPENDIX B

REFLECTION COEFFICIENT FOR AN IMPEDANCE BOUNDARY

Consider a plane wave obliquely incident on a surface impedance boundary, as shown in Figure B.1. The incident and reflected waves make angles of θ_i and θ_r with x axis, respectively, and Z_s is a normalized surface impedance. The field vectors shown in the figure are those corresponding to the TE_y case and thus $\bar{H}$ has only a y component.

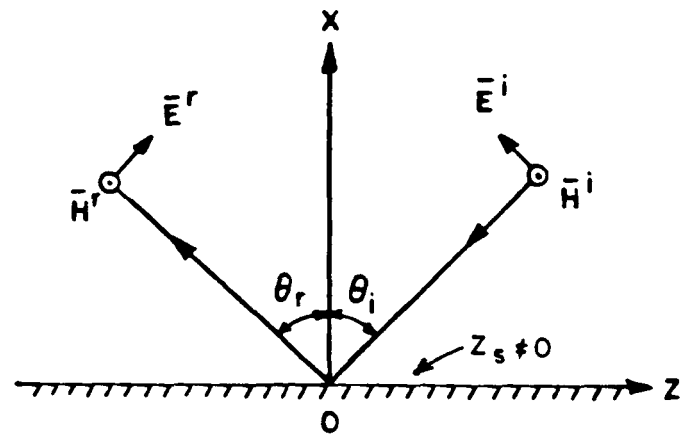

Figure B.1 A plane wave (TEy) obliquely incident on a surface impedance boundary.

The incident and reflected magnetic fields $\bar{H}^i$ and $\bar{H}^r$ in this TE_y are represented by

$$\bar{H}^i = \hat{y}H^i = \hat{y}\, e^{-jkz\sin\theta_i}\, e^{jkx\cos\theta_i} \tag{B.1}$$

and

$$\bar{H}^r = \hat{y}H^r = \hat{y}\, \tilde{R}e^{-jkz\sin\theta_r}\, e^{-jkx\cos\theta_r} \quad . \tag{B.2}$$

The total magnetic field H_y satisfies the following equation ont he impedgance boundary

$$\frac{\partial H_y}{\partial x} - jkZ_s H_y = 0 \qquad \text{at } x = 0 \quad . \tag{B.3}$$

Therefore, incorporating (B.1) and (B.2) into (B.3) gives

$$(jk\cos\theta_i - jkZ_s)e^{-jkz\sin\theta_i} - \tilde{R}(jk\cos\theta_r + jkZ_s)e^{-jkz\sin\theta_r} = 0 \quad . \tag{B.4}$$

From (B.4) one obtains the law of reflection ($\theta_i = \theta_r$) so that the fields can be phase matched at the boundary in order to satisfy (B.3). As a result, (B.4) reduces to:

$$\tilde{R}(Z_s + \cos\theta_i) + (Z_s - \cos\theta_i) = 0 \quad .$$

Hence the reflection coefficient for TE_y case is given by

$$\tilde{R}_{TE} = \frac{\cos\theta_i - Z_s}{\cos\theta_i + Z_s} \quad . \tag{B.5}$$

Likewise, the reflection coefficient for TM_y case is given by

$$\tilde{R}_{TM} = \frac{\cos\theta_i - Z_s^{-1}}{\cos\theta_i + Z_s^{-1}} \quad . \tag{B.6}$$

APPENDIX C

THE MAGNITUDE AND PHASE OF TRNSITION FUNCTION

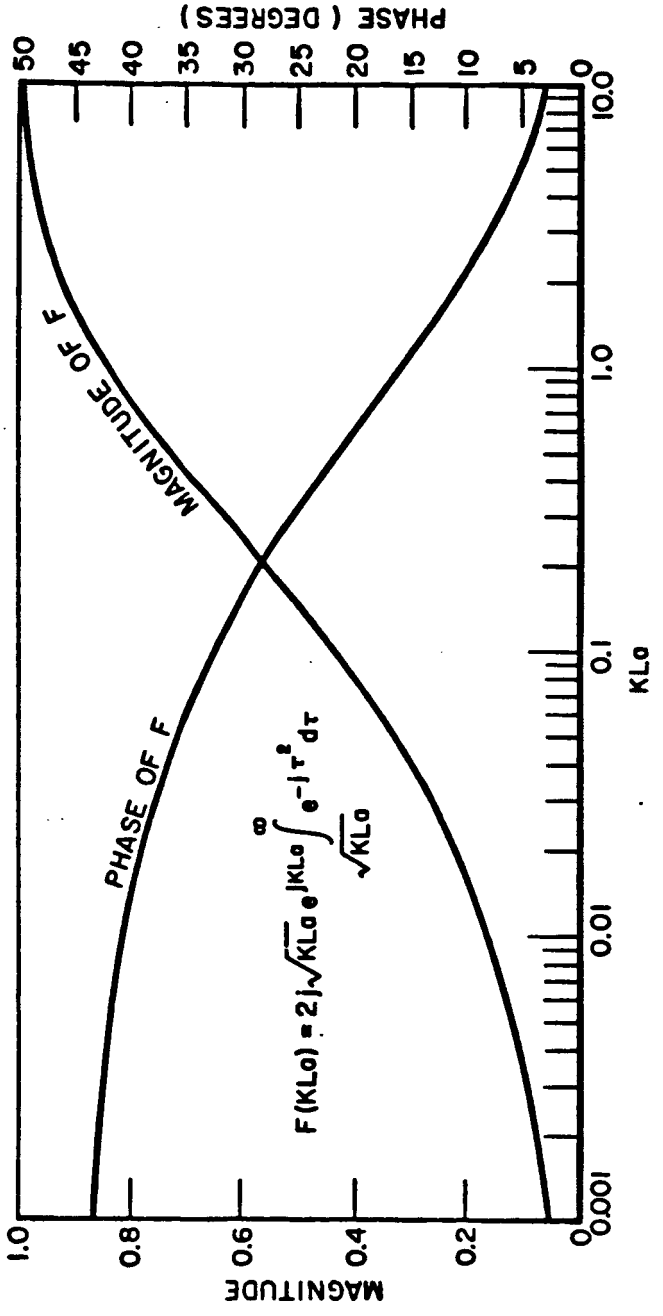

Figure C.1 The magnitude and phase of transition function.